THE ROLE OF $MGLU_7$ IN HIPPOCAMPALSYNAPTIC PLASTICITY: IMPLICATIONS FOR NOVEL THERAPEUTICS FOR RETT SYNDROME

By
Rebecca Klar

Dissertation

Submitted to the Faculty of the

Graduate School of Vanderbilt University

in partial fulfillment of the requirements

for the degree of

DOCTOR OF PHILOSOPHY

in Pharmacology

December, 2015

Nashville, TN

Professor P. Jeffrey Conn

Professor Colleen M. Niswender

Professor Carrie K. Jones

Professor Gregg D. Stanwood

Professor Danny G. Winder

Professor Jeremy Veenstra-VanderWeele

To my fiancé, Tim

and

To my family, Gary, Marj, and Leigh

ACKNOWLEDGEMENTS

First and foremost, I would like to extend my gratitude to my advisors, Dr. P. Jeffrey Conn and Dr. Colleen M. Niswender for allowing me to join their laboratories and perform my thesis work there. Dr. Conn has provided me with constant support and guidance throughout my time as a graduate student in his lab. He has allowed me to pursue science that is interesting to me and has guided me to reach beyond convention and explore novel biological mechanisms that could have an impact on human health and the treatment of CNS disorders. I am also eternally grateful to Dr. Conn for allowing me to learn brain slice electrophysiology in his lab. While the transition from bench biochemistry to electrophysiology has been challenging at times, I truly feel like I have found my passion in science and for that I am extremely thankful.

I also want to especially thank Dr. Niswender for being the best mentor I could have asked for over the past four years. She is a brilliant, creative scientist that isn't afraid of a crazy idea and she has been an excellent role model for me as a young, female scientist. She has also taught me to balance work and life and to keep a level head throughout the ups and downs that inevitably occur in science. Her passion for the unknown and her drive to make a real difference in the lives of people suffering from Rett syndrome and other CNS disorders is contagious. She is the type of scientist that I hope to be one day and I am so thankful I have had the opportunity to work with her.

I want to acknowledge my thesis committee members, Drs. Carrie Jones, Danny Winder, Gregg Stanwood, and Jeremy Veenstra-VanderWeele. They have provided wonderful guidance and suggestions over the years on how to make my science better. I thank them for useful discussions and for answering all of my questions. They have been

excellent resources for me and I could not have asked for a better group of brilliant scientists to guide me over the years.

There are many members of the Conn and Lindsley laboratories who have made significant contributions to my thesis work. First, I would like to thank the members of "Team Rett": Dr. Rocco Gogliotti, Rocio Zamorano, Nicole Fisher, Dr. Branden Stansley, and Dr. Colleen Niswender. I have truly enjoyed working as part of a like-minded team that has driven the science of Rett syndrome forward immeasurably in a very short amount of time. I look forward to seeing where this group goes in the future and I foresee big contributions to the field of Rett very soon. I would also like to acknowledge Dr. Hyekyung Plumley, who mentored me as a rotation student and then became one of my very best friends. She is a brilliant, hardworking scientist and has supported me throughout my time in the lab. Additionally, I would like to acknowledge Katrina Brewer and Drs. Jerri Rook, Zixiu Xiang, Hilary Nickols, Doug Sheffler, Kari Johnson, Shen Yin, and Greg Digby for providing scientific guidance and being good friends over the years. Dr. Darren Engers and Dr. Annie Blobaum have provided chemistry and DMPK guidance and collaboration over the years that have been essential to my project and I thank them for that. Finally, I would like to thank the ephys guys: Drs. Dan Foster, Adam Walker, Tristano Pancani, and Ayan Ghoshal for teaching me everything I know about doing electrophysiology, providing a judgement-free arena to bounce around scientific ideas, for creating the craziest, funniest, and most ridiculous work environment, and for being such great friends. They make sitting in a dark room with no windows every day worth it.

None of my thesis work would have been possible without my funding sources. Thank you to the Howard Hughes Medical Institute/Vanderbilt Program in Molecular Medicine for allowing me to expand my basic science research into the clinic and thank you to Autism Speaks and the Dennis G. Weatherstone Predoctoral Fellowship program for letting me pursue my interests and begin a life-long career in autism research.

In particular, I would like to thank two female scientists for shaping me over the years into the researcher and person I am today. First, thank you to my undergraduate mentor, Dr. Kari Heckman, for being OK with crazy ideas, for teaching me to love immunology, and for showing me that enjoying the lab environment is the most important thing. Without her guidance I would not have gone to graduate school. Thank you to Dr. Jana Shirey-Rice for being a scientific role model and a best friend. I cherished our time in lab together and thank her for teaching me to be a careful, determined scientist. She introduced me to the Conn lab and for that I am eternally grateful.

To all of the friends I have made at Vanderbilt over the years: Drs. Cody Wenthur, Brielle Wenthur, Patrick Gentry, Pedro Garica, Mike Schulte, Rachael Schulte, and Matt O'Reilly, thank you for the laughs and for the fun in and out of lab.

Finally, I would like to thank my parents, Gary and Marjorie Klar, for instilling in me a passion for knowledge. They have nurtured and guided me to pursue my interests and have always taught me that nothing is impossible. To my sister, Leigh, I thank you for being my best friend and for loving me unconditionally. I am so excited to see what the future holds for you as you pursue your true passions. To my fiancé, Tim Senter, I owe all of my success to you. You have stood by me and held me up at my lowest points

and have been there to celebrate all of my achievements. I am so thankful for our love and mutual interests in science; your passion for science drives me. Together, there is nothing that we can't achieve and I am so excited to see what the future holds for us.

TABLE OF CONTENTS

LIST OF TABLES

LIST OF FIGURES

LIST OF ABBREVIATIONS

aCSF	Artificial cerebrospinal fluid
ADX71743	$mGlu_7$ NAM
AKT	Protein kinase B
AMN082	$mGlu_7$ allosteric agonist
AMPAR	α-amino-3-hydroxy-5-methyl-4-isoxazolepropionic acid receptor
ANOVA	Analysis of variance test
AP5	NMDA receptor antagonist
A/T run	Sequence of DNA containing several A and T nucleotides
βAR	β adrenergic receptor
BCA	Bicinchoninic acid
BDNF	Brain derived neurotrophic factor
Bicuculline	$GABA_A$ receptor antagonist
cAMP	cyclic adenosine monophosphate
CA1	Cornus Ammonis 1
CA3	Cornus Ammonis 3
CB1	Cannabinoid receptor type 1
cDNA	Complementary DNA
cGMP	Cyclic guanosine monophosphate
ChIP	Chromatin immunoprecipitation
ChR2	Channelrhodopsin 2
CNQX	AMPA receptor antagonist
CNS	Central nervous system

CRD	Cysteine-rich domain
CREB	cAMP response element binding protein
Ct	Cycle threshold
DAG	Diacylglycerol
DCG-IV	Group II mGlu receptor agonist
DCPG	$mGlu_8$ agonist
DG	Dentate gyrus
DHPG	$mGlu_1$ and $mGlu_5$ agonist
DS	Double stranded
DSI	Depolarization-induced suppression of inhibition
$EAATs_{1-5}$	Excitatory amino acid transporter family, subtypes 1-5
eCBs	Endocannabinoids
EC_{50}	Concentration required for 50% of maximal receptor activation
ECL	Enhanced chemiluminescence
EDTA	Ethylenediaminetetraacetic acid
EGLU	Group II mGlu receptor antagonist
EPSCs	Excitatory post-synaptic currents
ERK	Extracellular signal-regulated kinase
ESI	Electronspray ionization
fEPSPs	Field excitatory post-synaptic potentials
F_u	Fraction unbound
GABA	γ-aminobutyric acid
$GABA_A$	GABA receptor, subtype A
$GABA_B$	GABA receptor, subtype B
GDP	Guanosine 5'-diphosphate

GIRK	G-protein inwardly rectifying potassium channel
GPCR	G-protein coupled receptor
GTP	Guanosine 5'-triphosphate
HFS	High frequency stimulation
HMGA1	High-mobility group protein 1
HPLC	High performance liquid chromatography
HRP	Horseradish peroxidase
IC_{50}	Concentration required for 50% inhibition of maximal receptor response
ICV	Intracerebroventricular
IGF-1	Insulin-like growth factor 1
I-LTD	Inhibitory LTD
i.p.	Intraperitoneal
IP_3	Inositol 1,4,5-triphosphate
IPSCs	Inhibitory post-synaptic currents
ISI	Inter-stimulus interval
ITI	Inter-train interval
KO	Knockout
KRH	Krebs-Ringer-HEPES buffer
L-AP4	Group III mGlu receptor agonist
LC/MS	Liquid chromatography/mass spectrometry
LFS	Low frequency stimulation
LSP4-2022	$mGlu_{4,\ 7\ and\ 8}$ agonist
LTD	Long-term depression
LTP	Long-term potentiation

LY341495	mGlu receptor antagonist
LY367385	$mGlu_1$ antagonist
MAPK	Mitogen-activated protein kinase
MBD	Methyl binding domain
MCCG	mGlu receptor antagonist
MECP2, Mecp2	Methyl CpG binding protein 2
Mecp2$^{-/y}$	Global Mecp2 knockout male mouse
Mecp2$^{+/-}$	Global Mecp2 heterozygous female mouse
mEPSCs	Spontaneous miniature excitatory post-synaptic currents
MF	Mossy fiber
MF-CA3	Mossy fiber-CA3 synapse in the hippocampus
mg/kg	milligrams per killogram
mGlu receptor	Metabotropic glutamate receptor
$mGlu_{1-8}$	mGlu receptor subtypes 1-8
MMPIP	$mGlu_7$ NAM
mOsm	Milliosmolar
MPEP	$mGlu_5$ NAM
mRNA	Messenger RNA
MSOP	Group III mGlu receptor antagonist
MSOPPE	Group II mGlu receptor antagonist
mTOR	Mammalian target of rapamycin
NAMs	Negative allosteric modulators
NMDAR	*N*-Methyl-D-aspartate receptor
NMDG	*N*-methyl-D-glucamine
NMR	Nuclear magnetic resonance

oIPSCs	Optically-induced IPSCs
PAMs	Positive allosteric modulators
PBS	Phosphate buffered saline
PCR	Polymerase chain reaction
PET	Positron emission tomography
PHCCC	$mGlu_4$ PAM
PIP_2	Phosphatidylinositol 4,5-bisphophate
PI3K	Phosphoinositide 3-kinase
PKC	Protein kinase C
PLC_β	Phospholipase C, variant β
PLD	Phospholipase D
PMI	Post-mortem interval
PPI	Paired pulse interval
PP-LFS	Paired-pulse low frequency stimulation
Ppm	Parts per million
PPR	Paired-pulse ratio
PSD-95	Postsynaptic density protein 95
PTP	Post-tetanic potentiation
PV	Parvalbumin
RAIGs	Retinoic acid-inducible orphan G protein coupled receptors
RIPA	Radioimmunoprecipitation buffer
RLU	Relative luciferase units
RT-qPCR	Quantitative real time PCR
SC	Schaffer collaterals
SC-CA1	Schaffer collateral-CA1 synapse in the hippocampus

SDS	Sodium dodecyl sulfate
SDS-PAGE	SDS Polyacrylamide gel electrophoresis
SEM	Standard error of the mean
sIPSCs	Spontaneous inhibitory post-synaptic currents
SLIN	Stratum lucidum interneuron
SNAP-25	Synaptosomal-associated protein 25
SNAT	Sodium-dependent neutral amino acid transporter
SST	Somatostatin
STP	Short-term plasticity
Sub-reg	Sub-region
TBS	Theta burst stimulation
TBS-T	Tris-buffered saline and Tween 20 buffer
TCA cycle	Tri-carboxylic acid cycle
TRD	Transcriptional regulation domain
TrkB	Tropomyosin receptor kinase B
TRPC1	Transient receptor potential channel 1
US	Unconditioned stimulus
VFT	Venus flytrap domain, N terminal domain of class C GPCRs
VGLUT	Vesicular glutamate transporter
VIP	Vasoactive polypeptide
VU0155094	Group III mGlu receptor PAM
VU0422288	Group III mGlu receptor PAM
VU-29	$mGlu_5$ PAM
XAP044	$mGlu_7$ antagonist
(1S,3S)-ACPD	Group II mGlu receptor agonist

4CPG	Group I and II mGlu receptor antagonist
7TM	7 transmembrane spanning
7TMRs	7 transmembrane spanning receptors
º C	Degrees Celsius
%XCI	Percent X chromosome inactivation

CHAPTER I

INTRODUCTION

Glutamatergic signaling in the brain

Glutamate is an amino acid and is the primary excitatory neurotransmitter in the central nervous system (CNS). Unlike other neurotransmitters, such as acetylcholine, dopamine, serotonin, and norepinephrine, which are produced uniquely in specific neurons, glutamate is produced as part of the tri-carboxylic acid cycle (TCA cycle) from α-ketoglutarate (Kandel et al., 1991). In neurons, glutamate is packaged into vesicles located within pre-synaptic terminals of axons via the actions of the vesicular glutamate transporter (VGLUT). VGLUT pumps glutamate into vesicles via a proton gradient driven by the actions of the Na^+-K^+ pump (Kandel et al., 1991).

Glutamate is released from vesicles into the synapse in a calcium-dependent manner, where it can bind and activate pre- and post-synaptic glutamate receptors. The duration of glutamate action within the synapse is regulated by the uptake and removal of glutamate from the synaptic cleft (Kandel et al., 1991). This is achieved by the actions of a second set of glutamate transporters, termed the excitatory amino acid transporters (EAATs). The EAAT family consists of 5 members ($EAAT_{1-5}$) (Jensen et al., 2015). $EAAT_{1 \text{ and } 2}$ are expressed on glia and are responsible for 90% of the uptake of glutamate. The other family members, with the exception of $EAAT_5$ which is retinally-restricted, are expressed on neuronal axon terminals, cell bodies, and dendrites and can also take up glutamate from the synapse (Jensen et al., 2015). Glutamate removed from the synapse is

converted into glutamine by an enzyme called glutamine synthase. The exchange of glutamine from glia and post-synaptic neurons to pre-synaptic terminals is accomplished by the sodium-dependent neutral amino acid (SNAT) transporter. Once inside pre-synaptic terminals, glutamine is converted back into glutamate by neuronal glutaminase enzymes, where it can be re-packaged into synaptic vesicles (**Figure 1**).

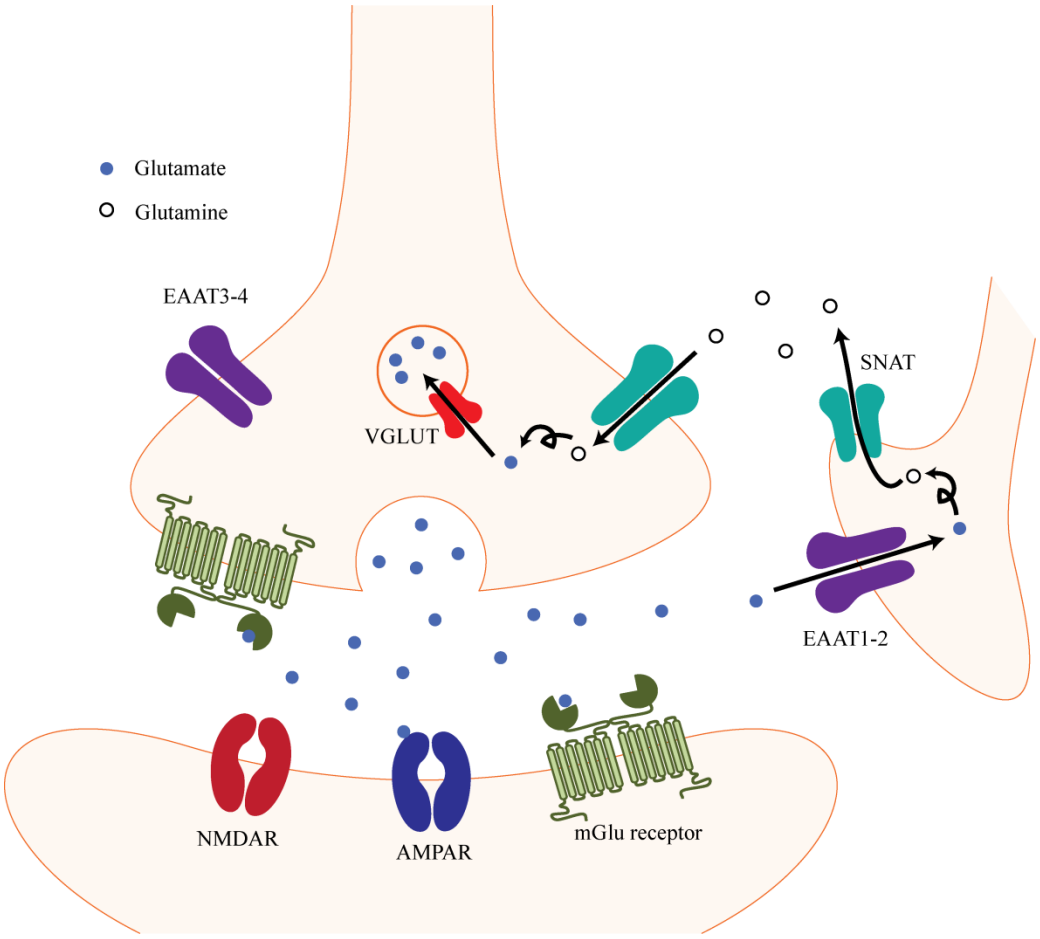

Figure 1. Schematic model of glutamatergic neurotransmission in the central nervous system. Glutamate is packaged into synaptic vesicles in the pre-synaptic nerve terminal by vesicular glutamate transporter (VGLUT) and is then released into the synaptic cleft. Upon release, glutamate is cleared from the synapse via the actions of glial and neuronal excitatory amino acid transporters (EAATs). $EAATs_{1 \text{ and } 2}$ are located on glia while $EAATs_{3 \text{ and } 4}$ are neuronally-restricted. In glia, glutamate is converted into the neutral molecule glutamine by glial glutamine synthase. Glutamine is removed from glia by the sodium-dependent neutral amino acid transporter (SNAT). A separate population of SNAT brings glutamine back into pre-synaptic terminals, where it is converted back into glutamate by neuronal glutaminase and re-packaged into synaptic vesicles.

Glutamate receptor classification and structure

Glutamate acts on two distinct types of receptors. The ionotropic glutamate receptors are ligand-gated ion channels responsible for fast synaptic transmission and consist of three family members: α-amino-3-hydroxy-5-methyl-4-isoxazoleproplionic acid (AMPA), N-methyl-D-aspartate (NMDA), and kainate receptors (Traynelis et al., 2010; Vyklicky et al., 2014). All three types of receptors are activated by glutamate binding and flux positively charged ions into the cell, resulting in depolarization. NMDA receptors are distinct from AMPA and kainate receptors due to the requirement for a co-incident relief of a Mg^{2+} block in response to depolarization for activation. As such, AMPA and kainate receptors tend to function primarily under basal transmission conditions, while NMDA receptors become active under strong synaptic activation.

The second group of glutamate receptors, termed the metabotropic glutamate receptors (mGlu receptors), are 7 transmembrane spanning (7TM), G-protein coupled receptors (GPCRs) that signal through second messenger systems and indirectly modulate ion channel gating activity. The mGlu receptors are members of the class C GPCRs, which also consists of the calcium-sensing receptors, the $GABA_B$ receptor, the taste receptors, the retinoic acid-inducible orphan G protein coupled receptors (RAIGs), and other orphan class C receptors (Yin and Niswender, 2014). All of the Class C family members are expressed both in the CNS and in the periphery. There are several distinct structural hallmarks that define class C GPCRs among the larger GPCR superfamily. These include a large, extracellular amino terminal domain called a Venus Flytrap domain (VFT), seven transmembrane-spanning domains with alternating intracellular and extracellular loops, and an intracellular carboxy terminus (Niswender and Conn, 2010).

In addition to these structural features, Class C GPCRs are unique from other classes of GPCRs in that they are expressed as obligate dimers (or oligomers) in the cell membrane.

The VFT domain is one of the most unique features of Class C GPCRs and, with the exception of some of the orphan receptors, forms the orthosteric binding site for the endogenous agonist(s) acting at each family member (Pin et al., 2003). Using homology models derived from the crystal structures of several bacterial periplasmic binding proteins (PBPs), which retain a small degree of sequence homology with the VFT of class C GPCRs, it was discovered that the VFT possesses a two-lobed clam shell-like structure that can switch between open and closed states (O'Hara et al., 1993). Agonist binding to the VFT is thought to stabilize the "closed" conformation, which results in a structural alteration transmitted through the 7TMs that allows for G protein activation and downstream signaling to occur (Bessis et al., 2002; Jingami et al., 2003). Indeed, for the VFT domains of mGlu 1, 3, and 7, the glutamate binding site is observed between the two lobes of the VFT (Kunishima et al., 2000; Tsuchiya et al., 2002; Muto et al., 2007).

The VFT domain and 7TMs are connected by a cysteine-rich domain (CRD). The CRD contains 9 cysteine residues; 8 of which form disulfide bonds to maintain the CRD structure (Niswender and Conn, 2010; Yin and Niswender, 2014). The 9^{th} forms a disulfide bond with the VFT and allows for transduction of agonist binding in the VFT to the 7TMs to facilitate G protein signaling. As mentioned above, Class C GPCRS are expressed as obligate dimers in the cell membrane. This is achieved via a single disulfide bond between two VFT's in the extracellular space.

Metabotropic glutamate receptor classification, signaling, and function

The diversity and complexity of metabotropic glutamatergic signaling is mediated by eight distinct receptor subtypes, $mGlu_{1-8}$, the genes for which were cloned in the 1990's (Masu et al., 1991; Abe et al., 1992; Tanabe et al., 1992; Nakajima et al., 1993; Saugstad et al., 1994; Saugstad et al., 1997). The mGlu receptor family can be further sub-divided into three major groups based on sequence homology and G protein coupling. Group I mGlu receptors consist of $mGlu_1$ and $mGlu_5$. Both of these receptors are coupled to the G_q subtype of G proteins. The activation of the receptors causes the exchange of GDP for GTP within the G protein, resulting in its disassociation from the receptor and the separation of α and βγ subunits which both activate downstream signaling cascades. The primary target of $G_q\alpha$ subunits is the activation of phospholipase C_β (PLC_β) and the hydrolysis of Phosphatidylinositol 4,5-bisphosphate (PIP_2) into Inositol 1,4,5-triposphate (IP_3) and Diacylglycerol (DAG) (Hermans and Challiss, 2001). IP_3 traditionally acts on IP_3 receptors located on the endoplasmic reticulum, resulting in the mobilization of intracellular Ca^{2+} stores and the activation of protein kinase C (PKC) (Sladeczek et al., 1985; Sugiyama et al., 1987; Abe et al., 1992; Schoepp et al., 1994; Toms et al., 1995; Schoepp et al., 1996). In addition to this classical signaling cascade, it is now appreciated that group I mGlu receptor stimulation can also lead to the activation of phospholipase D (PLD), the mitogen-activated protein kinase/extracellular receptor kinase (MAPK/ERK) pathway, and the Phosphoinositide 3-kinase (PI3K)/protein kinase B (AKT)/mammalian target of rapamycin (mTOR) pathway, among others (Hou and Klann, 2004; Page et al., 2006).

The group II mGlu receptors include $mGlu_2$ and $mGlu_3$, and the group III receptors consist of $mGlus_{4, 6, 7, and 8}$. Both group II and group III receptors couple to $G_{i/o}$ G proteins. Activation of these receptors leads to $G\alpha_{i/o}$-mediated reductions in cyclic adenosine monophosphate (cAMP) levels via the blockade of adenylyl cyclase activity. In addition to signaling mediated by Gα subunits, liberated Gβγ subunits can directly regulate the conductance of a variety of ion channels, such as N-type Ca^{2+} channels and G protein-coupled inwardly-rectifying potassium channels (GIRKs). Similar to what is seen for group I receptors, group II and group III receptors can also couple to various alternative downstream signaling pathways, including PI3K/AKT/mTOR and MAPK/ERK pathways (Iacovelli et al., 2002).

Pharmacological tool compounds used to study mGlu receptor function

The traditional approach to the development of tool compounds targeting mGlu receptors was to identify and optimize compounds that bind to the orthosteric site, or glutamate binding site, on the receptor. This strategy has been useful but has not provided many selective ligands for individual mGlu receptor subtypes due to the high conservation of the orthosteric site among all mGlu receptors (Mitri et al., 2004). Allosteric modulators, on the other hand, bind to a site on the receptor that is distinct from the orthosteric binding site; this has provided greater selectivity of compounds for one mGlu receptor subtype over other family members. There are several classes of allosteric modulators that have been developed, including both positive allosteric modulators (PAMs) and negative allosteric modulators (NAMs). PAMs bind to a receptor and potentiate the effect of the endogenous ligand whereas NAMs inhibit the

effects of the endogenous ligand in a non-competitive manner. The development and use of these compounds in pre-clinical animal models have been extremely successful (Niswender and Conn, 2010; Conn et al., 2014; Yin and Niswender, 2014). In the following sections, several selective and non-selective orthosteric and allosteric compounds targeting the mGlu receptors will be described; however, a specific description of the tool compounds used to manipulate $mGlu_7$ function will be described in the following section.

Specific tool compounds targeting $mGlu_7$

Among all of the group III mglu receptors, $mGlu_7$ has the lowest affinity for the endogenous orthosteric agonist, glutamate (Flor et al., 1996). As such, the use of glutamate in *in vitro* cell-based assays of receptor function is limited for $mGlu_7$ due to the need for extremely high concentrations of glutamate to elicit a response. Because of this, several other novel orthosteric agonists have been identified that activate $mGlu_7$ at lower concentrations (**Figure 2**). The most widely used orthosteric agonist is the glutamate analog L-2-amino-4-phosphonobutryic acid (L-AP4), which activates all of the group III mGlu receptors at varying potencies. The selectivity of L-AP4 for group III mGlu receptors over other family members is driven by the presence of a phosphonate functional group on L-AP4 that is not present in the structure of glutamate. The varying potencies at which L-AP4 activates the distinct group III receptor family members perhaps indicates that, although the group III receptors share 70-75% sequence homology, they have evolved to become activated in the brain under unique signaling environments. The rank order potency for L-AP4 at the group III receptors is $mGlu_4$ =

$mGlu_8$ > $mGlu_6$ >>> $mGlu_7$, with the actual potencies as determined by functional assays as 0.4 – 1 μM at $mGlu_{4\ and\ 8}$ (Hampson et al., 1999; Han and Hampson, 1999; Schoepp et al., 1999), 0.6 – 0.9 μM at $mGlu_6$ (Nakajima et al., 1993), and 160-800 μM at $mGlu_7$ (Okamoto et al., 1994; Shigemoto et al., 1996).

L-AP4 has been used in brain slice electrophysiology to investigate the effects of $mGlu_7$ activation in several instances (Gereau and Conn, 1995b; Bradley et al., 1998; Pelkey et al., 2005; Ayala et al., 2008; Kalinichev et al., 2013); however, the confounding effects of co-incident activation of the other group III receptors in addition to $mGlu_7$ considerably limits the use of L-AP4 to purely study $mGlu_7$ function. Since the discovery of L-AP4, a novel, orthosteric agonist has been developed with greater selectivity for $mGlu_7$ over $mGlu_8$ (Goudet et al., 2012). This compound, termed LSP4-2022, is the most potent $mGlu_7$ orthosteric agonist reported to date, with a rank potency order within the group III receptors of $mGlu_4$ > $mGlu_6$ > $mGlu_7$ > $mGlu_8$ (actual potencies are reported as 0.11 μM at $mGlu_4$, 4.4 μM at $mGlu_6$, 11.6 μM at $mGlu_7$, and 29.2 μM at $mGlu_8$) (Goudet et al., 2012). In addition to a large increase in potency at $mGlu_7$ over L-AP4, LSP4-2022 also provides the first instance of selectivity of an orthosteric agonist for $mGlu_7$ over $mGlu_8$. In addition, LSP4-2022, unlike L-AP4, is systemically active and exhibits behavioral efficacy is several rodent behavioral tasks such as the haloperidol-induced catalepsy task (Goudet et al., 2012).

In 2005, the first selective, allosteric agonist targeting $mGlu_7$ was reported, termed AMN082 (Mitsukawa et al., 2005) (**Figure 2**). In *in vitro* cellular assays, ANM082 leads to the activation of $mGlu_7$ without the need for binding of orthosteric agonists. Additionally, using mutant and chimeric $mGlu_7$ constructs, it was determined

that AMN082 binds to the transmembrane regions of the receptor, where it functions as an allosteric agonist with an EC_{50} of 64 nM (Mitsukawa et al., 2005). With the discovery of AMN082, a large number of studies were undertaken to investigate the effects of selective activation of $mGlu_7$ *in vivo.* One of the primary findings using AMN082 is that activation of $mGlu_7$ results in anti-depressant-like activity (O'Connor and Cryan, 2013; Palucha-Poniewiera et al., 2014). Despite initial enthusiasm for AMN082, it has since been discovered that the agonist activity of AMN082 is restricted to distinct *in vitro* assays and results in rapid internalization of the receptor (Pelkey et al., 2007). Additionally, *in vivo*, AMN082 is metabolized to a compound that modulates serotonergic activity, which could explain many of the reports published identifying $mGlu_7$ as a novel anti-depressant (Palucha et al., 2007; Sukoff Rizzo et al., 2011). Because of conflicting reports on the efficacy of AMN082 both *in vitro* and *in vivo*, our lab has chosen to limit studies to the use of L-AP4 and LSP4-2022 to activate $mGlu_7$.

In addition to agonists of $mGlu_7$, our lab has recently reported several non-selective group III PAMs that have activity at $mGlu_7$ (Jalan-Sakrikar et al., 2014) (**Figure 2**). VU0155094 was initially identified from a high throughput screen for $mGlu_8$-selective PAMs. While it has an EC_{50} at $mGlu_8$ of 1.6 μM, it also displays activity at all of the other group III receptors (EC_{50} at $mGlu_4$ = 3.2 μM, $mGlu_6$ = 900 nM, $mGlu_7$ = 1.5 μM), and, as such, was published as a pan-group III receptor PAM (Jalan-Sakrikar et al., 2014). In addition to VU0155094, VU0422288 was developed as part of a drug discovery effort within our laboratory to develop selective $mGlu_4$ PAMs. VU0422288 is also a pan-group III PAM (EC_{50} at $mGlu_8$ = 125 nM, $mGlu_7$ = 146 nM, $mGlu_4$ = 108

nM); however, it is more potent at $mGlu_{4,\ 7,\ and\ 8}$ than VU0155094, thus requiring lower concentrations to achieve potentiation of the receptors.

There are two reported orthosteric antagonists that block $mGlu_7$ function (**Figure 2**). The first, which was developed as a group II receptor antagonist, LY341495, exhibits potencies at the group III receptors of 22 μM at $mGlu_4$, 0.99 μM at $mGlu_7$, and 0.17 μM at $mGlu_8$ (Kingston et al., 1998). While dramatically more potent at the group II receptors, LY341495 is a useful orthosteric antagonist when used at appropriate concentrations. In addition to LY341495, a novel orthosteric antagonist, XAP044, as recently been reported (Gee et al., 2014). This compound blocks agonist activation of the receptor with an IC_{50} of 2.8 μM at $mGlu_7$ and is inactive at $mGlu_4$ and $mGlu_6$, although full selectivity at all of the other mGlu receptors has yet to be reported.

Finally, several NAMs of $mGlu_7$ exist, including MMPIP and ADX71743 (**Figure 2**). The first to be discovered, MMPIP, antagonizes $mGlu_7$ with an IC_{50} of 20 nM in Chinese Hamster Ovary (CHO) cells co-expressing $mGlu_7$ and a promiscuous G protein, Gα15 (Suzuki et al., 2007). While this compound is selective in cells lines for $mGlu_7$, it exhibits context-dependent pharmacology similar to that seen with AMN082, making its utility limited (Niswender et al., 2010). More recently, a novel $mGlu_7$ NAM has been reported, ADX71743, which displays both *in vitro* and *in vivo* efficacy (Kalinichev et al., 2013). ADX71743 has an IC_{50} at $mGlu_7$ of 50 nM and is not active at any of the other mGlu receptors, making it an ideal tool compound to investigate $mGlu_7$ activity in native systems (Kalinichev et al., 2013). As such, we have utilized this compound as a selective $mGlu_7$ NAM for the majority of our studies.

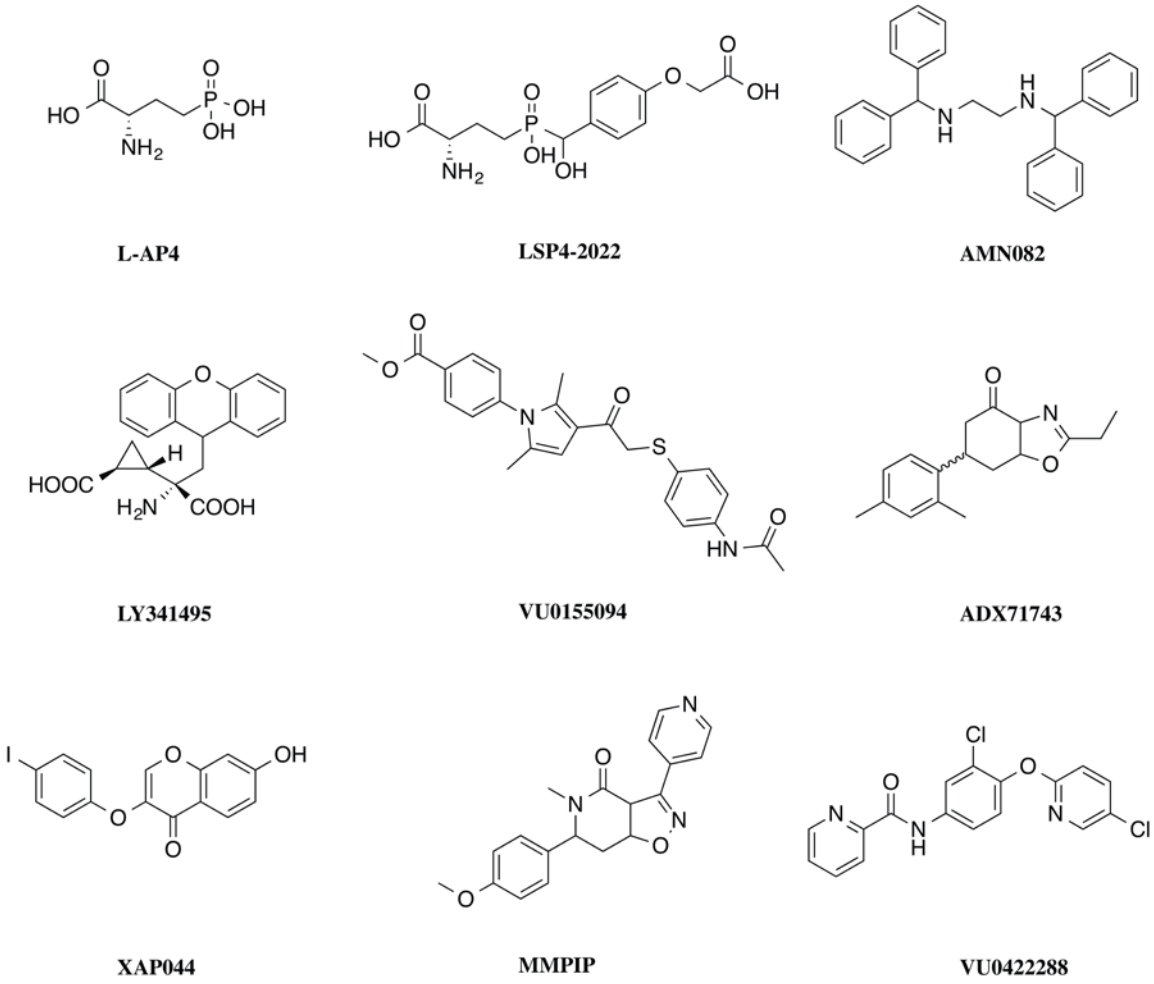

Figure 2. Tool compounds used to study $mGlu_7$ function. L-AP4 and LSP4-2022 are non-selective orthosteric agonists (Rosemond et al., 2004; Goudet et al., 2012), while AMN082 is a selective allosteric agonist (Mitsukawa et al., 2005). LY341495 and XAP044 are orthosteric antagonists, whereas MMPIP and ADX71743 are selective NAMs (Kingston et al., 1998; Suzuki et al., 2007; Kalinichev et al., 2013; Gee et al., 2014). VU0155094 and VU0422288 are pan-group III mGlu receptor PAMs (Jalan-Sakrikar et al., 2014).

Expression pattern of metabotropic glutamate receptor 7 in the brain

The mGlu receptors are primarily expressed throughout the CNS. The majority of studies investigating the expression of the various mGlu receptors have utilized both *in situ* hybridization and immunohistochemistry using subtype-specific antibodies in whole brain slices from either rat or mouse. $mGlu_7$ is expressed widely throughout the adult rodent brain. Expression is observed in the mitral and tufted cells of the olfactory bulb, several cortical regions, in pyramidal cells of areas CA1 and CA3 of the hippocampus, in granule cells of the DG, in the ventral pallidum, the substantia nigra pars reticulata, the amygdala, the hypothalamus, the locus coeruleus, and Purkinje cells of the cerebellum (Ohishi et al., 1995a; Bradley et al., 1996). $mGlu_7$ is predominantly expressed pre-synaptically on both glutamatergic and GABAergic terminals where it functions to negatively regulate neurotransmitter release (Ohishi et al., 1995b). This thesis will focus on the activity of $mGlu_7$ in area CA1 of the hippocampus. As such, the specific expression of $mGlu_7$ on distinct glutamatergic and GABAergic cells within this area will be discussed in detail below.

Circuitry within the hippocampus

The hippocampus has long been considered a primary brain region responsible for several important cognitive functions, such as learning and memory (Andersen, 2007; Schultz and Engelhardt, 2014). The hippocampal network is highly dynamic and has the capacity to undergo changes in synaptic efficacy in an activity-dependent manner. These forms of synaptic plasticity observed within the hippocampal circuitry are thought to be critical for many major functions of the hippocampus. Short-term plasticity (STP), long-

term potentiation (LTP), and long-term depression (LTD) are the most commonly investigated forms of synaptic plasticity within the hippocampus (Andersen, 2007).

The hippocampus can be divided into three anatomical sub regions referred to as the DG, CA1, and CA3 (Andersen, 2007; Schultz and Engelhardt, 2014) (**Figure 3**). Synaptic plasticity is most commonly studied in two major intra-hippocampal pathways. The mossy fiber (MF) pathway consists of projections from DG granule neurons to area CA3, while the projections from CA3 pyramidal neurons compose the Schaffer collaterals that innervate area CA1 pyramidal neurons (SC-CA1) (Cajal, 1894; Andersen, 2007). The SC-CA1 synapse is the most commonly studied synapse within the hippocampal circuit as it is readily assessable for studies in isolation in the intact brain as well as in acute brain slices.

The MF pathways are comprised of excitatory projections from the DG granule cells that synapse onto either CA3 pyramidal cells or inhibitory interneurons (Cajal, 1894). The name 'mossy' was coined by Ramón y Cajal in 1894 because of the numerous and characteristic projections these neurons make, giving a moss-like appearance (Cajal, 1894). Granule cell axons from the DG have more than one terminal type, forming both large mossy fiber boutons innervating the CA3 pyramidal neurons and small, filopodial extensions which emanate from these boutons that innervate the stratum lucidum interneurons of CA3 (Acsady et al., 1998; Henze et al., 2000; Nicoll and Schmitz, 2005). Unlike the SC-CA1 synapse, the MF synapses are less extensively characterized pathway owing to their overall complexity in anatomy as well as in physiology.

In addition to the intra-hippocampal connections described above, the hippocampus receives strong cortical input from the entorhinal cortex via the perforant

pathway (Witter, 2007). Traditionally, the perforant path connects most strongly to the DG via either the medial or lateral perforant path; however, there is also evidence that connections from the entorhinal cortex can project directly to areas CA3 and CA1 (Witter, 2007). The majority of connections arise from layer II of the entorhinal cortex, which have been shown to project both to the DG and area CA3; however, a small number of additional connections can also arise from the deep layers of the entorhinal cortex (Andersen, 2007). The most heavily studied projections, those from the entorhinal cortex to the DG, are known to undergo synaptic plasticity, which plays a critical role in regulating the strength and timing of perforant path connections (Poschel and Stanton, 2007; Witter, 2007). In addition, there is also evidence that connections from the entorhinal cortex to area CA3 can also undergo synaptic plasticity (Cosgrove et al., 2011). The focus of this thesis will be on synaptic plasticity at the SC-CA1 synapse, however, synaptic plasticity at both of these projections have been discussed in recent reviews (Poschel and Stanton, 2007; Witter, 2007; Cosgrove et al., 2011). It should be noted, however, that the contribution of the perforant path to general information flow through the hippocampus is critical and, additionally, that the ability of those connections to undergo synaptic plasticity is important for the overall strength and timing of entorhinal cortex input to the hippocampus.

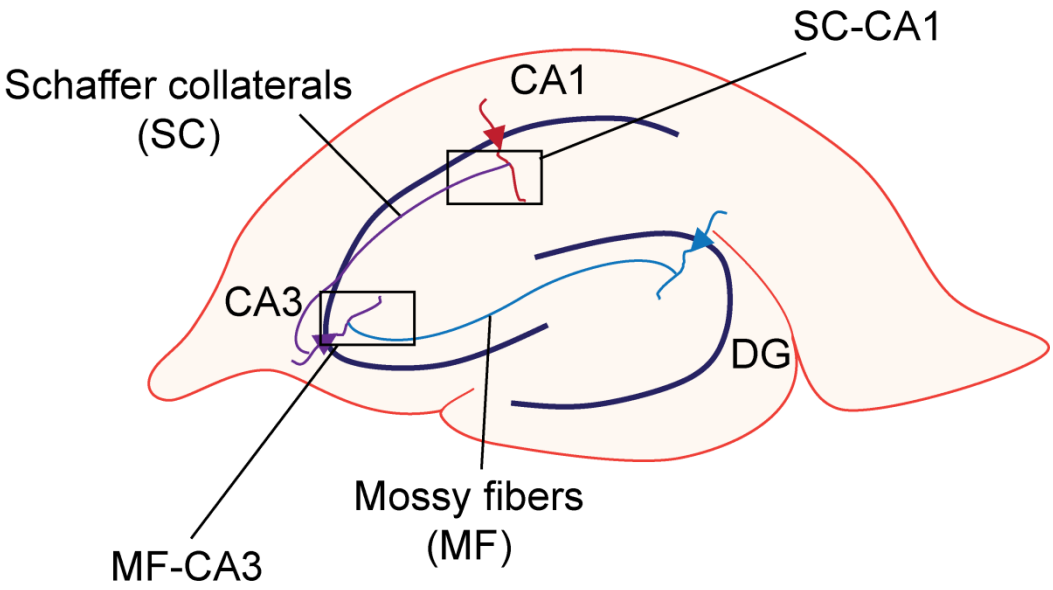

Figure 3. Diagram of the intra-hippocampal connections in the hippocampus. The majority of information enters the dentate gyrus (DG) via perforant pathway connections from layer II of the entorhinal cortex. DG granule cell axons make projections to CA3 pyramidal cells via a connection called the mossy fiber pathway (MF). This synapse is termed the MF-CA3 synapse. CA3 pyramidal neuron axons, termed Schaffer collaterals (SC), make synaptic connections onto CA1 pyramidal cells, thus forming the SC-CA1 synapse.

Localization of metabotropic glutamate receptors within the intra-hippocampal connections

The expression of the various mGlu receptors within the intra-hippocampal network is both spatially and developmentally restricted (**Figure 4**). At the SC-CA1 synapse, both $mGlu_1$ and $mGlu_5$ are expressed postsynaptically on CA1 pyramidal cells (Gereau and Conn, 1995a; Ferraguti et al., 1998). At the mossy fiber (MF)-CA3 synapse, $mGlu_1$ and $mGlu_5$ are expressed on the dendrites and dendritic spines of CA3 pyramidal cells. (Lujan et al., 1996). The expression of group II receptors is most prominent in the dentate gyrus and at the MF-CA3 synapse; however, there is evidence of $mGlu_3$ receptor expression on astrocytes within area CA1 (Ohishi et al., 1993b; Winder and Conn, 1996;

Winder et al., 1996). At the MF-CA3 synapse, $mGlu_2$ is the predominant group II receptor and is expressed on presynaptic MF boutons (Shigemoto et al., 1997). With the exception of retinally-restricted $mGlu_6$ (Nakajima et al., 1993), all of the other group III receptors are expressed at varying levels in the hippocampus. $mGlu_4$ is expressed axonally on CA3 afferents at extremely low levels but there is no functional evidence for its contribution to transmission at the CA3-CA1 (SC-CA1) synapse (Ferraguti and Shigemoto, 2006; Ayala et al., 2008; Jalan-Sakrikar et al., 2014). $mGlu_8$ is expressed presynaptically on CA3 afferents in neonatal animals; however, functional expression of the receptor disappears with age (Corti et al., 1998; Ayala et al., 2008). In contrast, $mGlu_7$ expression is low at SC-CA1 synapses in neonatal animals and increases with age (Bradley et al., 1998; Ayala et al., 2008). In adult animals, $mGlu_7$ is expressed presynaptically at asymmetrical glutamatergic synapses within the synaptic cleft in CA3 (Okamoto et al., 1994; Bradley et al., 1996). In addition, $mGlu_7$ is also expressed pre-synaptically on the terminals of GABAergic interneurons that express somatostatin (SST), vasoactive polypeptide (VIP) and parvalbumin (PV) (Somogyi et al., 2003). At MF synapses, $mGlu_7$ is also expressed presynaptically on MF afferents synapsing onto stratum lucidum inhibitory interneurons (Shigemoto et al., 1997).

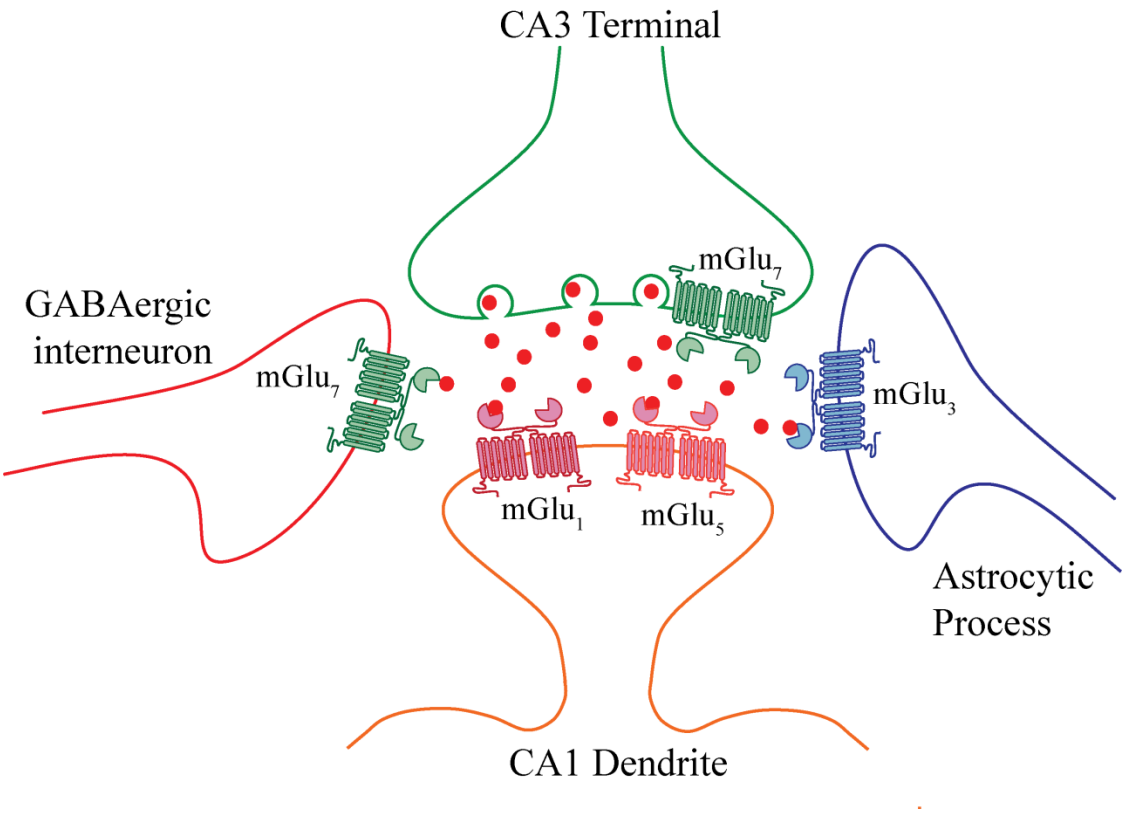

Figure 4. Summary of the expression of mGlu receptors at SC-CA1 synapses. Afferents projecting from CA3 pyramidal cells synapse onto the dendrites of CA1 pyramidal neurons. $mGlu_7$ is expressed presynaptically on both glutamatergic and GABAergic terminals. In contrast, both $mGlu_1$ and $mGlu_5$ are expressed postsynaptically on CA1 pyramidal neurons. $mGlu_3$ expression is restricted to astrocytes within area CA1.

mGlu receptor modulation of basal synaptic transmission at SC-CA1 synapses

Basal transmission at the SC-CA1 synapse can be modified by the activation of several mGlu receptors. For simplicity, basal synaptic transmission is defined as the stimulation of SC afferents at a frequency that does not induce synaptic plasticity and results in a stable response. Activation of group I mGlu receptors by bath application of DHPG causes an increase in intracellular Ca^{2+} both in the soma and dendrites of CA1 pyramidal cells and results in a strong inward current when cells are recorded in voltage-clamp (Abe et al., 1992; Bianchi et al., 1999; Mannaioni et al., 2001). These effects are

primarily mediated by the activation of $mGlu_1$, as antagonism of $mGlu_5$ using the NAM, MPEP, does not block the DHPG effects (Mannaioni et al., 2001). Additionally, $mGlu_1$ activation leads to the depolarization of CA1 pyramidal cells via the blockade of a potassium leak current (Mannaioni et al., 2001).

In addition to $mGlu_1$'s direct effects on CA1 cells, it can also alter CA1 cell excitability indirectly via manipulation of GABAergic transmission onto pyramidal cells. Indeed, activation of $mGlu_1$ leads to an increase in the frequency of spontaneous inhibitory post-synaptic currents (sIPSCs); however, it concomitantly leads to a reduction in the amplitude of evoked monosynaptic IPSCs that is also dependent upon $mGlu_5$ activation (Gereau and Conn, 1995a; Mannaioni et al., 2001). Taken together, these results indicate that activation of the group I mGlu receptors leads to an overall net increase in excitatory drive through the CA1 region of the hippocampus. However, despite these excitatory effects of DHPG on CA1 cells, activation of $mGlu_1$ also leads to a pre-synaptic decrease in evoked excitatory post-synaptic potentials (EPSCs) and a reduction in fEPSP slopes at low concentrations of DHPG (Gereau and Conn, 1995a; Mannaioni et al., 2001). At higher concentrations, this decrease in EPSCs can be converted form a transient depression into a form of long term depression which will be described in a later section.

As the primary localization of $mGlu_3$ is on astrocytes within area CA1 of the hippocampus and no $mGlu_2$ expression is observed in this region, the effects of group II mGlu receptor activation on basal synaptic transmission are minor. The selective group II orthosteric agonist, DCG-IV does not have any effect on fEPSPs recorded in area CA1, or any direct effects on the excitability of CA1 pyramidal cells, indicating that this group

of receptors does not play a large role in the modulation of basal responses in this region of the hippocampus (Gereau and Conn, 1995a). Group II receptors do, however, play an important role in a form of associative plasticity that requires co-incident activation of β adrenergic receptors (βAR) (Gereau and Conn, 1994; Gereau et al., 1995).

In contrast to the group II mGlu receptors, there are significant effects of group III mGlu receptor activation on basal transmission at SC-CA1 synapses. As described earlier, there is a distinct lack of $mGlu_4$ expression in this region and no electrophysiological effect of $mGlu_4$ agonists or PAMs on transmission at this synapse (Ayala et al., 2008; Jalan-Sakrikar et al., 2014). The primary effects of group III receptor activation are mediated independently by $mGlu_8$ and $mGlu_7$. $mGlu_8$ is the predominant group III mGlu receptor expressed at this synapse in neonatal animals (Corti et al., 1998; Ayala et al., 2008). Indeed, in neonatal (9-11 day-old) rat hippocampal slices, application of low concentrations of L-AP4 (50 μM) induces a dramatic reduction in the fEPSP slope with an IC_{50} of 25 μM, consistent with concentrations necessary to activate $mGlu_8$ (Ayala et al., 2008). In addition, application of the selective $mGlu_8$ orthosteric agonist, DCPG, mimicked the effects of 50 μM L-AP4 and results in a decrease in fEPSP slope, further confirming that $mGlu_8$ is the predominant group III mGlu receptor present in neonatal animals.

In adult animals (>80 day old rats and 6-week old mice), application of DCPG no longer affects fEPSP slopes (Ayala et al., 2008; Jalan-Sakrikar et al., 2014), indicating that there is no longer functional $mGlu_8$ present at this synapse. In contrast, in adult animals, much higher concentrations of L-AP4 (650 μM) are required to observe a reduction in fEPSP slope. Additionally, as will be described in a section below,

concentrations of LSP4-2022 that activate $mGlu_7$ also induce a decrease in fEPSP slope in adult animals (Jalan-Sakrikar et al., 2014). Application of both of these agonists, with and without co-application of two distinct group III mGlu receptor PAMs, VU0155094 and VU0422288, also results in an increase in the paired-pulse ratio (PPR), which is consistent with a pre-synaptic localization of the effect.

In addition to effects on fEPSP slopes, application of L-AP4 in adult rodent slices also results in a decrease in the frequency of spontaneous miniature EPSCs (mEPSCs) (Gereau and Conn, 1995b). As these events are known to occur independently of the activation of voltage-gated Ca^{2+} channels, it is thought that $mGlu_7$ may regulate pre-synaptic glutamate release via a mechanism independent of alterations in Ca^{2+} channel opening. Additionally, as will be described below, application of LSP4-2022 results in a decrease in monosynaptic IPSC amplitudes, suggesting that $mGlu_7$, in addition to its localization directly within the synaptic cleft on glutamatergic terminals, is also expressed pre-synaptically on GABAergic terminals that synapse onto CA1 pyramidal cells where it can alter GABA release.

Forms of long term potentiation at SC-CA1 synapses

Long term potentiation (LTP) is the process of experience-dependent strengthening of synaptic connections. The existence of LTP was first identified in the rabbit hippocampus by Bliss and Lomo in 1973 at the perforant path synapse within the dentate gyrus (Bliss and Lomo, 1973). In response to a high frequency stimulation (15 stimulations per second) of the perforant path from the entorhinal cortex, the population field excitatory postsynaptic potentials (fEPSPs) recorded from granule cells (at 0.5

stimulations per second) were significantly potentiated for several hours after the high frequency stimulation (Bliss and Lomo, 1973). Since this discovery, several forms of LTP have been described at the SC-CA1 synapse. The most commonly studied form of LTP at this synapse is a potentiation induced by applying high frequency stimulation (HFS) to the axon fibers from CA3 (Schwartzkroin and Wester, 1975). This results in a long-lasting form of LTP, which has been used as the basis for many studies to date. This form of LTP is known to be frequency-dependent, as stimulation of axon fibers at 100 Hz for 1 second leads to a robust LTP, whereas stimulation at 3 Hz results in a robust LTD, and stimulation at 10 Hz does not result in any change in synaptic strength (Dudek and Bear, 1992). HFS-induced LTP is dependent upon NMDA receptor activation, postsynaptic increases in intracellular calcium, and depolarization of CA1 pyramidal cells (Dunwiddie and Lynch, 1978; Collingridge et al., 1983; Malinow and Miller, 1986; Morris et al., 1986). After the discovery of HFS-induced LTP, a second form of LTP was identified, which is induced by theta burst stimulation (TBS) (Larson et al., 1986). This paradigm more closely mimics the oscillation patterns of firing CA3 neurons observed *in vivo* (Larson et al., 1986); thus, it may be more physiologically relevant compared to HFS paradigms. As many of the mechanisms underlying HFS and TBS-induced LTP overlap, they will be discussed together (Larson and Lynch, 1986, 1988).

Role of mGlu receptors in LTP at SC-CA1 synapses

The role of postsynaptic group I ($mGlu_1$ and $mGlu_5$) receptors in the induction and maintenance of both forms of LTP at the SC-CA1 synapse is controversial. To date, very few studies have been performed that directly investigate the contribution of $mGlu_1$

activation to LTP at this synapse (Aiba et al., 1994; Conquet et al., 1994; Neyman and Manahan-Vaughan, 2008); however, one study has found that application of the $mGlu_1$ antagonist, LY367385, prevented the induction of LTP at SC-CA1 synapses when the antagonist was applied prior to HFS, but not after HFS (three trains of 100 Hz stimulation) (Neyman and Manahan-Vaughan, 2008). Additionally, Aiba *et al.* reported that slices from $mGlu_1$ knockout mice respond with substantially reduced levels of LTP at SC-CA1 when stimulated using HFS (five trains of 100 Hz stimulation); this phenotype was accompanied by modest deficits in a contextual fear conditioning assay, a measure of hippocampal-mediated learning and memory (Aiba et al., 1994). However, a separate study failed to observe LTP deficits at SC-CA1 in $mGlu_1$ knockouts using HFS consisting of one train of 100 Hz stimulation (Conquet et al., 1994). *In vitro*, several studies indicate that $mGlu_1$ activation increases the number of functional NMDA receptors on the postsynaptic membrane (Lan et al., 2001; Skeberdis et al., 2001). In addition, in *Xenopus* oocytes, activation of $mGlu_1$ results in a Synaptosomal-associated Protein 25 (SNAP-25)-mediated exocytosis of NMDA receptors (Lan et al., 2001). $mGlu_1$ stimulation also leads to the activation of Transient Receptor Potential Channel 1 (TRPC1) cation channels, which are responsible for a slow, inward current present in cerebellar purkinje cells; a similar mechanism for the induction of LTP may also be at play in the hippocampus (Kim et al., 2003). $mGlu_1$ activation also leads to increases in intracellular calcium and depolarization of CA1 pyramidal cells, all of which could facilitate LTP induction (Mannaioni et al., 2001). Thus, taken together, these results suggest that, while $mGlu_1$ may participate in regulation of LTP, this receptor is not necessary for the induction or maintenance of LTP at SC-CA1.

The second member of the group I mGlu receptor family is $mGlu_5$, which has been extensively characterized as a major regulator of LTP at SC-CA1 (Balschun et al., 1999; Manahan-Vaughan and Braunewell, 2005). Genetic deletion of $mGlu_5$ (Lu et al., 1997; Jia et al., 1998) or application of the $mGlu_5$ selective antagonist MPEP (Manahan-Vaughan and Braunewell, 2005) can reduce induction of LTP (using both TBS and 3 trains of 100 Hz stimulation) at the SC-CA1 synapse (Francesconi et al., 2004; Shalin et al., 2006), while the $mGlu_{1/5}$ agonist DHPG primes LTP induction using either one train of 100 Hz stimulation or a sub-maximal TBS induction paradigm (5 bursts of 100 Hz, 200 ms inter-burst interval) (Cohen and Abraham, 1996; Raymond et al., 2000). $mGlu_5$ activation leads to potentiation of NMDA receptor currents due to a coupling mechanism that involves scaffolding through both postsynaptic density protein 95 (PSD-95) and Homer (Hermans and Challiss, 2001; Mannaioni et al., 2001). This may contribute to the regulation of LTP by $mGlu_5$. In addition, recent studies suggest that TBS-induced activation of $mGlu_5$ can induce a form of "metaplasticity" that is mediated by release of endocannabinoids (eCBs) from CA1 pyramidal cells and eCB activation of CB1 receptors to induce depression of transmission at inhibitory synapses onto CA1 pyramidal cells (Chevaleyre and Castillo, 2003; Younts et al., 2013; Xu et al., 2014). This disinhibition, combined with the ability of $mGlu_5$ to potentiate NMDA receptor currents, could be a major component of the role of $mGlu_5$ in "priming" SC-CA1 synapses for induction of LTP reported in earlier studies (Cohen and Abraham, 1996; Raymond et al., 2000).

The persistent portion of LTP is dependent upon *de novo* protein synthesis (Stanton and Sarvey, 1984; Deadwyler et al., 1987; Frey et al., 1988) and is also

regulated by activation of $mGlu_5$ (Francesconi et al., 2004). Therefore, activation of $mGlu_5$ potentiates both the induction and maintenance of LTP at SC-CA1 synapses. Indeed, a threshold-level of LTP induced with one train of TBS can be significantly potentiated when slices are pre-treated with $mGlu_5$ PAMs (Ayala et al., 2009; Noetzel et al., 2013). This pre-treatment results in an increase in short term plasticity, termed post-tetanic potentiation (PTP), as well as the induction of LTP (Ayala et al., 2009). Taken together, $mGlu_5$ plays an important role in regulating both the induction and maintenance of LTP at SC-CA1, and compounds that potentiate $mGlu_5$ function may also help to restore LTP in settings where SC-CA1 plasticity is compromised.

The expression of group II receptors at SC-CA1 is extremely low (Ohishi et al., 1993a, b; Ohshima et al., 1996). There is a distinct lack of $mGlu_2$ expression at the SC-CA1 synapse and $mGlu_3$ expression is restricted to astrocytes in area CA1 (Ohishi et al., 1993a, b). Antagonism of $mGlu_2$ and $mGlu_3$ using the orthosteric antagonist, MCCG, does not block LTP (induced using eight trains of 200 Hz stimulation) at this synapse, suggesting that activation of these receptors is not necessary for induction of LTP (Breakwell et al., 1998). In contrast, agonism of $mGlu_2$ and $mGlu_3$ using the orthosteric agonist, (1S,3S)-ACPD, prevents the formation of LTP but retains much of the PTP using the same induction paradigm listed above (Breakwell et al., 1998). The authors suggest that activation of group II mGlu receptors may increase the threshold for LTP induction by reducing presynaptic glutamate release; however, this hypothesis has not been directly tested at the SC-CA1 synapse (Breakwell et al., 1998). Additionally, activation of group II mGlu receptors with concentrations of the group II agonist, DCG-IV, that are selective for these receptors does not affect basal excitatory transmission at SC-CA1, and the direct

effects of DCG-IV on LTP induction has not been investigated (Gereau and Conn, 1995b). However, when group II mGlu receptors are co-activated with a G_s coupled-receptor, such as a β-adrenergic receptor (βAR), a profound depression of synaptic transmission results (Gereau and Conn, 1994; Gereau et al., 1995). These effects are due to synergistic signaling of group II mGlu receptors and βARs on astrocytes, resulting in release of adenosine and subsequent activation of A_1 adenosine receptors on SC terminals (Winder et al., 1996). This mechanism is thought to be mediated by $mGlu_3$, as it is the only group II mGlu receptor subtype localized on astrocytes throughout the brain, including in CA1 (Ohishi et al., 1993a). Given the recent evidence indicating that astrocytes play an important role in neuronal network function, including the induction of LTP (Ota et al., 2013), $mGlu_3$ may play an important role in this unique form of associative plasticity at this synapse.

The group III receptors, which consist of $mGlu_4$, $mGlu_6$, $mGlu_7$, and $mGlu_8$, are also presynaptic $G_{i/o}$-coupled receptors that traditionally function as autoreceptors to decrease neurotransmitter release (Losonczy et al., 2003). Among these receptors, $mGlu_7$ and $mGlu_8$ are the only members of this group that have been shown to be functional at SC-CA1 synapses (Ayala et al., 2008; Jalan-Sakrikar et al., 2014). $mGlu_6$ is expressed almost exclusively in the retina (Nakajima et al., 1993) and evidence for expression of functional $mGlu_4$ at SC-CA1 synapses has not been found (Kristensen et al., 1993; Tanabe et al., 1993; Ayala et al., 2008; Jalan-Sakrikar et al., 2014). Group III receptors are expressed presynaptically on synaptic terminals from CA3 where their activation results in a reduction in glutamatergic transmission (Gereau and Conn, 1995b; Ayala et al., 2008; Niswender et al., 2010; Kalinichev et al., 2013; Jalan-Sakrikar et al., 2014).

Reductions in transmission have primarily been shown using the group III orthosteric agonist, L-AP4. When concentrations of L-AP4 are used that should selectively activate $mGlu_4$, no reduction in glutamatergic transmission is observed (Ayala et al., 2008). Additionally, the $mGlu_4$-selective PAM, PHCCC, fails to potentiate the effects of L-AP4 at this synapse (Ayala et al., 2008). In neonatal animals, there is strong evidence that $mGlu_8$ is the only group III receptor subtype present at SC-CA1 synapses; however, there is a developmental switch that occurs where $mGlu_7$ expression replaces $mGlu_8$ in adulthood (Baskys and Malenka, 1991; Ayala et al., 2008). Due to this change in receptor expression, there have been no studies to date that have investigated the role of $mGlu_8$ in LTP in adult animals. It will be interesting, however, to determine if perhaps it plays a role in LTP early in development.

Finally, $mGlu_7$ is expressed presynaptically at SC-CA1 synapses in adult animals, and several studies have directly investigated the role of this receptor in LTP (Bradley et al., 1996; Shigemoto et al., 1996; Bushell et al., 2002; Klar et al., 2015). One study in $mGlu_7$ knockout mice demonstrated that there was a deficit in PTP and short-term potentiation (STP), but no effect on LTP (induced using one train of 100 Hz stimulation) (Bushell et al., 2002). This could be due to compensatory changes that might occur due to life-long genetic deletion of $mGlu_7$. It is possible that the developmental switch that normally occurs between $mGlu_8$ and $mGlu_7$ expression does not occur when $mGlu_7$ is genetically deleted, thus perhaps $mGlu_8$ takes over for the role of $mGlu_7$ in this instance. As will be described in a future chapter of this thesis, we have determined using pharmacological antagonists that activation of $mGlu_7$ is necessary for the induction of

LTP at SC-CA1 synapses via a mechanism reliant on disinhibition of CA1 pyramidal cells (Klar et al., 2015).

There have also been numerous studies *in vivo* indicating that $mGlu_7$ knockout mice or mice treated with a selective $mGlu_7$ NAM, MMPIP, show deficits in behavioral tasks that rely on proper hippocampal plasticity (Holscher et al., 2004, 2005; Callaerts-Vegh et al., 2006; Goddyn et al., 2008; Hikichi et al., 2010). Loss of $mGlu_7$ has been attributed to deficits in working memory (Holscher et al., 2004, 2005) and fear learning (Callaerts-Vegh et al., 2006; Goddyn et al., 2008). Specifically, these studies found deficits in a 4-arm maze working memory task, where $mGlu_7$ KO mice accumulated more errors than wild-type controls. Additionally, the same deficit was found in the 8-arm maze task as well, with no deficits in perception of acoustic stimuli, vision, motor activity, or motivation. There are also impairments in contextual fear conditioning, where animals spend less time freezing compared to controls on test day of the task (Goddyn et al., 2008). All these data point towards a role for $mGlu_7$ in modulating learning in memory associated with the hippocampus.

Forms of long term depression at SC-CA1 synapses

There are three distinct forms of mGlu receptor-modulated LTD that are commonly studied at SC-CA1 synapses. The first is a chemical LTD which is induced by application of the group I orthosteric agonist, DHPG (Fitzjohn et al., 1999; Huber et al., 2000; Huber et al., 2001). DHPG-LTD is NMDA receptor-independent; however, it relies on rapid extracellular signal-regulated kinase (ERK)-dependent dendritic messenger RNA (mRNA) translation without new transcription (Palmer et al., 1997;

Huber et al., 2000; Huber et al., 2001; Ayala et al., 2009). Several studies suggest that this mechanism of LTD involves changes in both post and presynaptic function. Indeed, DHPG application results in a lasting reduction in postsynaptic AMPA receptor expression (Snyder et al., 2001) as well as a reduction in presynaptic glutamate release (Fitzjohn et al., 2001).

The second form of LTD is mediated by synaptically-released glutamate and is induced by applying a low-frequency stimulation (900 stimuli delivered at 1 Hz, LFS) (Dudek and Bear, 1992). This LTD is developmentally regulated, as a robust form of LTD is observed in young rats (aged 12-20 days), whereas this LTD is absent in adult animals (Kemp et al., 2000) and is also dependent upon *de novo* postsynaptic protein synthesis (Neyman and Manahan-Vaughan, 2008). Additionally, a third form of LTD can be induced by applying 900 paired stimulations at 1 Hz (PP-LFS) (Kemp and Bashir, 1997, 1999; Huber et al., 2000). This LTD persists at all ages; however, the requirement for NMDA receptor activation seems to change with age. In young animals (younger than 50 day old rats), NMDA receptor antagonists prevent induction of LTD; in contrast, LTD can still be induced even in the presence of the NMDA receptor antagonist, AP5, in adult animals (rats aged 12-15 weeks) (Kemp et al., 2000). There is, however, a form of PP-LFS that is still NMDA receptor-dependent in adult animals. This can be achieved by adjusting the paired-pulse interval (PPI) from 50 to 200 ms. Additionally, these separate forms of LTD (LFS, PP-LFS) occur via different downstream mechanisms, as the induction of one cannot be occluded by prior saturation of the other (Kemp et al., 2000).

Role of mGlu receptors in LTD at SC-CA1 synapses

There is strong evidence that the different forms of LTD present at SC-CA1 synapses are differentially regulated by group I mGlu receptors (Huber et al., 2001; Neyman and Manahan-Vaughan, 2008; Ayala et al., 2009) (**Figure 5**). There is evidence that $mGlu_1$ and $mGlu_5$ play distinct roles in the regulation of CA1 cell excitability (Mannaioni et al., 2001). $mGlu_1$ activation is responsible for increasing postsynaptic intracellular Ca^{2+} concentrations and depolarization of CA1 cells, whereas $mGlu_5$ activation results in the suppression of a Ca^{2+}-activated potassium current and direct potentiation of NMDA receptors (Mannaioni et al., 2001). In addition, there are clear differences in the roles of these receptors in regulation of LTD at SC-CA1 synapses (Neyman and Manahan-Vaughan, 2008). For example, antagonism of $mGlu_1$ using LY367385 prior to induction of LTD using LFS results in a complete blockade of LTD (Neyman and Manahan-Vaughan, 2008). This effect of $mGlu_1$ antagonism was specific to the induction phase of LTD, as application of an $mGlu_1$ antagonist after LFS does not prevent LTD (Neyman and Manahan-Vaughan, 2008). This finding points to a specific role for $mGlu_1$ in regulating the induction, rather than the maintenance, of LFS-LTD. In contrast, selective antagonism of $mGlu_5$ with MPEP results in blockade of LFS-LTD regardless of whether the NAM is applied before or after LFS (Neyman and Manahan-Vaughan, 2008), indicating that there is a mechanistic difference in the ability of $mGlu_1$ and $mGlu_5$ to activate downstream signaling pathways necessary for LFS-LTD. It is interesting to note, however, that application of the $mGlu_5$ PAM, VU-29, does not potentiate LFS-LTD (Ayala et al., 2009). One explanation for this phenomenon could be that LFS induction requires saturating recruitment of $mGlu_5$ for induction, such that a

PAM provides no further efficacy of LTD induction. In contrast to LFS-LTD, application of VU-29 results in a potentiation of PP-LFS LTD and DHPG-LTD when a sub-maximal concentration of DHPG (25 µM) is used and (Ayala et al., 2009). These results suggest that $mGlu_5$ PAMs maintain the proper form and direction of specific forms of synaptic plasticity depending upon the stimulation paradigm.

Few studies to date have found evidence for a direct role of group II receptors at SC-CA1 synapses using subtype-selective compounds in the modulation of LTD (Manahan-Vaughan, 1997; Santschi et al., 2006) (**Figure 5**). One study found that the non-selective group I/II mGlu receptor antagonist, 4CPG, and the group II antagonists MSOPPE and EGLU, blocked LFS-LTD induced *in vivo* in awake, behaving rats (Manahan-Vaughan, 1997). Additionally, activation of group II receptors using 5 µM DCG-IV, along with concomitant elevations in cyclic guanosine monophosphate (cGMP), leads to a weak LTD at SC-CA1 synapses (Santschi et al., 2006). However, the requirement for the use of 5 µM DCG-IV to observe this effect does not rule out off-target activity at other receptors, as this concentration is sufficient to activate NMDA receptors (Wilsch et al., 1994; Uyama et al., 1997). Specific involvement of group II receptors in common forms of LTD discussed earlier has not been directly studied and both $mGlu_2$ and $mGlu_3$ have been shown to be involved in the induction of LTD in other brain regions (Otani et al., 2002; Johnson et al., 2011; Lodge et al., 2013; Walker et al., 2015). Thus, it will be important to investigate the involvement of these receptors in various forms of LTD using newer generation, selective antagonists of these receptors.

As described earlier, the primary group III receptor expressed at SC-CA1 synapses in adult animals is $mGlu_7$ (Baskys and Malenka, 1991; Ayala et al., 2008; Jalan-

Sakrikar et al., 2014). Due to the lack of sub-type selective compounds, direct investigation of $mGlu_7$ in LTD has not been performed (**Figure 5**). There are several reports, however, indicating that antagonism of group III mGlu receptors blocks LTD at SC-CA1 synapses (Altinbilek and Manahan-Vaughan, 2007). When considered with anatomical expression patterns and functional studies at SC-CA1, it is possible that these effects can be attributed to $mGlu_7$ (Okamoto et al., 1994; Bradley et al., 1996; Ayala et al., 2008; Niswender et al., 2010; Kalinichev et al., 2013; Jalan-Sakrikar et al., 2014). Additionally, one study found that intracerebroventricular (ICV) injection of L-AP4 resulted in a slow-onset chemically-induced LTD observed *in vivo* in area CA1 (Naie et al., 2006). However, despite these studies, direct investigation using selective compounds targeting $mGlu_7$ have not been performed and, as such, the precise involvement of $mGlu_7$ in the regulation of LTD has not been determined.

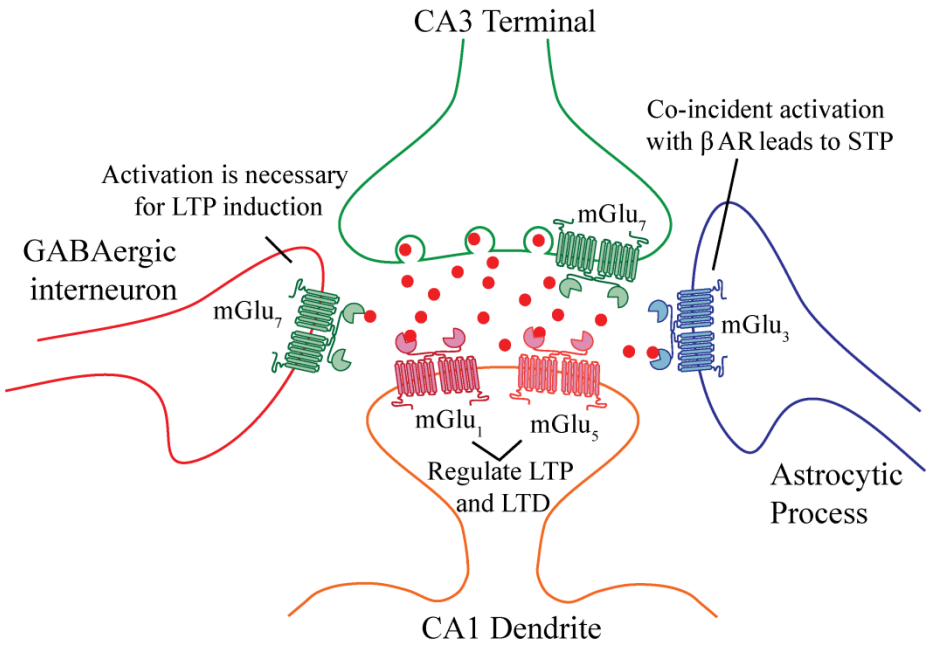

Figure 5. Roles of mGlu receptors in synaptic plasticity at SC-CA1 synapses. $mGlu_7$ is expressed presynaptically on both glutamatergic and GABAergic terminals and its activation on GABAergic terminals is necessary for the induction of LTP. Both $mGlu_1$ and $mGlu_5$ are known to regulate both LTP and LTD. $mGlu_3$ is involved in the induction of a short term depression also reliant on co-incident activation of β adrenergic receptors.

Role of mGlu receptors in hippocampal transmission: conclusions

As has been described in previous sections, many of the mGlu receptors can contribute to the overall output of area CA1. Importantly, many of these changes are due to alterations in synaptic efficacy (i.e. the induction of either LTP or LTD). Although it has been shown that agonism of $mGlu_{1,\ 5,\ 7,\ and\ 8}$ results in decreases in transmission at the SC-CA1 synapse, all of these effects require the exogenous application of agonist to brain slices. Therefore, under basal transmission conditions, it is unclear what, if any, role these receptors play in the modulation of transmission. The more useful and biologically relevant way to understand the role of these receptors basally would be to investigate whether the receptors are active tonically with the use of antagonists. Indeed, there have

been several studies investigating this. Application of the group I antagonists, LY367385 or MPEP, has no effect on the basal fEPSP response when SC fibers are stimulated at a frequency of 0.025-0.05 Hz (Neyman and Manahan-Vaughan, 2008). This indicates that, under these basal conditions, neither $mGlu_1$ nor $mGlu_5$ is tonically active. Additionally, the same is true for $mGlu_7$ and $mGlu_8$. Indeed, application of the orthosteric antagonist, LY341495, at several concentrations that should antagonize all of the mGlu receptors does not alter basal fEPSPs slopes (Ayala et al., 2008). Additionally, application of the $mGlu_7$ NAM, ADX71743, also has no effect on basal fEPSP slopes (Kalinichev et al., 2013). Taken together, these findings indicate that none of the mGlu receptors expressed at the SC-CA1 synapse seem to be tonically active to regulate glutamate release.

There is strong evidence, however, that the mGlu receptors can become active under specific synaptic firing patterns to regulate the induction of both LTP and LTD. Indeed, while not specifically required for the induction of LTP, activation of $mGlu_5$ can potentiate LTP induced with 100 Hz HFS and TBS induction paradigms (Ayala et al., 2009). Additionally, antagonism of $mGlu_1$ or $mGlu_7$ can block the induction of LTP at this synapse, indicating that there are mechanisms by which synaptically evoked glutamate can result in the endogenous activation of mGlu receptors (Neyman and Manahan-Vaughan, 2008; Klar et al., 2015). Additionally, while chemically-induced LTD is reliant on the direct activation of group I mGlu receptors, several of the synaptically evoked forms of LTD are reliant on mGlu receptor activation as well (Altinbilek and Manahan-Vaughan, 2007). Taken together, these results indicate that the major function of mGlu receptors endogenously is to modify and regulate long-lasting changes in synaptic strength. These effects seem to be mediated both by receptors that

are required for the induction of these forms of synaptic plasticity and by receptors whose activation can fine-tune the level of potentiation or depression that occurs in response to a given stimuli.

Rett syndrome is a Neurodevelopmental Disorder

Rett syndrome is a postnatal neurological disorder that was first described by Dr. Andreas Rett in 1954. Patients with Rett syndrome develop relatively normally for the first 6-18 months of life, after which they undergo a severe, rapid developmental regression phase. This regression is characterized by growth arrest, the deterioration of higher brain functions, including loss of purposeful hand movements, speech and communication skills, motor and cognitive abilities, the development of autism-like symptoms, periods of apneas, dementia, and microcephaly (Hagberg et al., 1983). After this developmental regression phase, patients enter a stable, plateau phase that can last for decades. During this plateau phase, many patients develop epilepsy and eventually a Parkinsonian-like phenotype. Interestingly, despite undergoing a marked developmental regression, there is no evidence that patients experience neurodegeneration (Hagberg, 1985; Chahrour et al., 2008).

One of the hallmarks of early descriptions of patients with Rett syndrome was that the disorder seemed to predominantly affect females. Because of this unique finding, it was initially hypothesized that Rett syndrome had a genetic etiology and that the causative gene of the disorder was located on the X chromosome. Indeed, many of this work was done investigating a small population of patients in which the disorder was familial (Hagberg et al., 1983; Zoghbi, 1988; Zoghbi et al., 1990; Ellison et al., 1992;

Schanen et al., 1997; Schanen and Francke, 1998). These studies suggested that the inheritance pattern was through maternal lines, providing further evidence that Rett syndrome was an X-linked disorder that was lethal in males, thus explaining the almost exclusively female patient population with an incidence of 1:10,000 females (Hagberg et al., 1983; Zoghbi, 1988; Zoghbi et al., 1990; Ellison et al., 1992; Schanen et al., 1997; Schanen and Francke, 1998).

In 1999, Huda Zoghbi's laboratory at Baylor College of Medicine mapped the causative gene for Rett syndrome to a location on the X chromosome (Xq28) encoding a gene called Methyl CpG Binding Protein 2, *MECP2* (Amir et al., 1999), which had previously been identified by Dr. Adrian Bird's lab as a transcription factor (Lewis et al., 1992). Mutations in *MECP2* account for 95% of classical Rett syndrome cases (Wan et al., 1999; Trappe et al., 2001). Interestingly, during the initial studies of *MECP2* mutations, it was discovered that the majority of Rett syndrome cases were the result of sporadic, *de novo* mutations, not due to familial inheritance. These mutations most commonly occur in the paternal germline and often involve a change from C to T at CpG dinucleotides (Wan et al., 1999; Trappe et al., 2001). These changes result in missense, nonsense, frame shift, and early stop codon mutations that have a variety of effects on MECP2 protein function (Christodoulou et al., 2003; Chahrour and Zoghbi, 2007; Baker et al., 2013).

In addition to clinical variability due to random *de novo MECP2* mutations, another source of phenotypic variation comes from random X chromosome inactivation. Because females only express one copy of the X chromosome in each cell, and the choice of which X chromosome is expressed is usually random, the severity of Rett syndrome

can vary greatly based on the percentage of cells expressing the mutant copy of MECP2 protein versus the wild-type copy. Despite this random X chromosome inactivation, there is strong evidence that many Rett syndrome patients do not in fact express 50% mutant MECP2, but rather have a more favorable skewing of the X chromosome inactivation in favor of the wild-type copy of the protein. This is thought to be due to the viability of cells expressing mutant *MECP2*, which might be weaker and less sustainable than their wild-type counterparts. Indeed, cells expressing wild-type MECP2 divide faster than those expressing mutant MECP2. In humans, the case for skewing of X chromosome inactivation is best represented by studies of monozygotic twins with MECP2 mutations where one twin presents with a much milder phenotype than her genetically identical sister (Dragich et al., 2000). In addition, X chromosome skewing has also been observed in the brains of animal models of Rett syndrome where favorable skewing in one brain region correlates with milder symptom severity and the expression of mutant MECP2 is associated with more severe symptomology (Young and Zoghbi, 2004).

MECP2 protein structure, function, and disease-causing mutations

The MECP2 protein consists of several functional domains: an N-terminal methyl CpG binding domain (MBD), a C-terminal transcriptional regulation domain (TRD), and three A/T Hook binding domains (Guy et al., 2011). In addition, MECP2 contains a well-characterized nuclear localization signal (Nan et al., 1996). Although MECP2 is expressed throughout the mammalian body, it is most highly expressed in the brain (Skene et al., 2010) in a sub-nuclear compartment (Klose et al., 2005). In addition,

MECP2 expression is low early in development and increases dramatically with age (Skene et al., 2010). This increase in MECP2 expression seems to also correlate with the process of synaptogenesis in neurons (Guy et al., 2011).

MECP2 was initially identified as a repressor of gene transcription. MECP2 interacts with methylated CG dinucleotides through its MDB. In addition, MECP2 has been shown to recruit proteins such as histone deacetylase and Sin3A, which together silence gene transcription (Nan et al., 1996; Jones et al., 1998). It has now been appreciated, however, that in addition to its function as a transcriptional repressor, MECP2 can also function as a transcriptional activator. This has been best shown by large-scale microarrays, where many genes actually decrease in expression when MECP2 is lost (Traynor et al., 2002; Tudor et al., 2002; Chahrour et al., 2008). Indeed, MECP2 has been shown to interact with the transcriptional activator, cAMP response element binding protein (CREB) at the promoter of activated, but not repressed, genes (Chahrour et al., 2008), which could provide a mechanism by which MECP2 binding can lead to transcriptional activation of specific genes.

When MECP2 was initially characterized, it was determined that its MBD preferentially interacts with methylated CG dinucleotides. This interaction, however, is necessary but insufficient to completely direct MECP2 binding. In addition to CG dinucleotide binding, MECP2 binding is enriched at sites containing a run of A and T nucleotides (Klose et al., 2005). This was determined using Methyl-SELEX approaches where small fragments of methylated, double-stranded DNA were generated and tested for MECP2 binding *in vitro.* Using this technique, it was observed that MECP2 preferentially bound to fragments containing an A/T run of at least 4 base pairs located

adjacent (within 1-3 or 6-9 base pairs) to a CG dinucleotide (Klose et al., 2005). Interestingly, despite the sequence similarity between A/T runs preferential for MECP2 binding with the "RGR" motif present in many A/T hook-binding proteins (such as high-mobility group protein (HMGA1)), the ability for MECP2 to bind to A/T runs adjacent to CG dinucleotides only requires the MBD, not the A/T hook domains (Klose et al., 2005; Baker et al., 2013). Instead, the A/T hook domains are thought to be important for long-range DNA contacts that support chromatin remodeling (Horike et al., 2005; Baker et al., 2013). In addition to MECP2 binding to methylated CG dinucleotides, it is now appreciated that MECP2 can also interact with other cytosine moieties in the DNA, such as methyl-CH, hydroxymethyl-CH, and methyl-CA dinucleotides, adding further complexity and specificity to MECP2 binding and regulation of transcription (Chen et al., 2015; Kinde et al., 2015).

Disease-causing mutations have been identified throughout the entire MECP2 protein. Several of the most common mutations include Arg106Trp, Arg133Cys, Thr158Met, Arg168X, Arg255X, Arg270X, Arg294X, and Arg306Cys (Bienvenu and Chelly, 2006; Lawson-Yuen et al., 2007; Baker et al., 2013). Overall, the Arg168X mutation makes up the majority of the mutations found in females with Rett syndrome (11.5%), with all of the other mutations varying in prevalence between 5-9% (**Figure 6**). The primary location of most of these mutations is either in the MBD or the TRD (Bienvenu and Chelly, 2006) and the clinical severity of each of these mutations varies greatly. Additionally, for several of these mutations, mouse models where a point mutation has been made in MECP2 exist and will be discussed below.

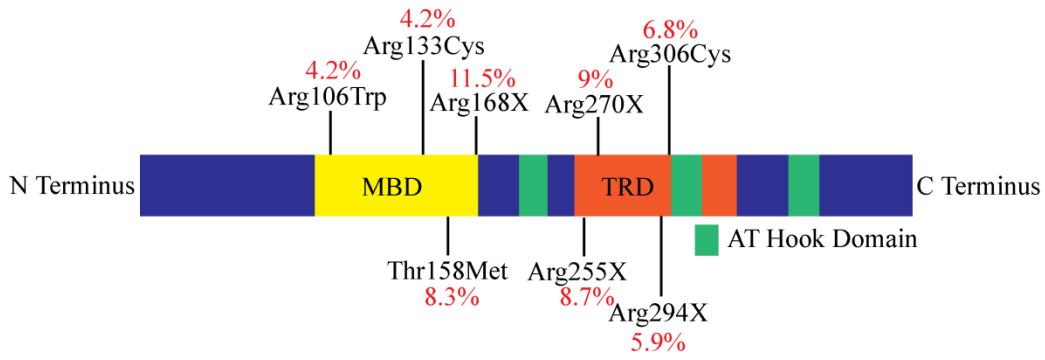

Figure 6. MECP2 protein structure and common mutations observed in Rett syndrome patients. MECP2 contains a methyl binding domain (MBD), a transcriptional regulation domain (TRD), and three AT Hook domains. Several of the most common mutations (denoted as the three letter abbreviation of the natural amino acid, the amino acid number, and the new amino acid abbreviation or "X" for a stop codon) found in patients are highlighted on the linear protein structure, with the majority of mutations occurring either in the MBD or the TRD. The prevalence of each mutation within the human Rett syndrome patient population is denoted in red as a percentage.

Animal models of Rett syndrome

The first animal model of Rett syndrome was developed in Dr. Adrian Bird's laboratory in 2001 (Guy et al., 2001). This mouse model was generated by replacing exons 3 and 4 of the mouse *Mecp2* gene with the same exons flanked by *loxP* sites. These animals were then crossed with mice expressing Cre ubiquitously, thus generating global *Mecp2*-null male mice ($Mecp2^{-/y}$) and Mecp2 heterozygous females ($Mecp2^{-/+}$). Similar to the patient phenotype, both $Mecp2^{-/y}$ males and $Mecp2^{-/+}$ females do not display any overt symptoms of Rett syndrome at birth. They develop symptoms, however, between 4-6 weeks (in males) or 12-18 weeks (in females). This includes the development of an uncoordinated gait and motor abnormalities, hind-limb clasping, tremors, and apneas (Guy et al., 2001). Additionally, female heterozygous mice display a wide range of symptom severity, most likely due to random X chromosome inactivation, thus making this population of mice difficult to study.

As many of the symptoms associated with Rett syndrome seem to be neurologic in origin, a second mouse model was generated where the *loxP*-flanked exons 3 and 4 mouse was crossed with a mouse expressing Cre under the control of the *nestin* promoter in order to genetically delete Mecp2 only from neuronal and glial cells (Guy et al., 2001). Interestingly, all of the phenotypes observed in the global Mecp2 knockout mouse were recapitulated in the neuronal- and glia-specific knockout mice, indicating that the majority of Mecp2 functions occur in the CNS (Guy et al., 2001). Excitingly, almost all of the symptoms of Rett syndrome can be reversed if Mecp2 is re-expressed in post-mitotic neurons, indicating that the damage caused by loss of Mecp2 may be reversible (Guy et al., 2007) .

Mouse models harboring point mutations in Mecp2

Once both the global and neuronal KO of Mecp2 was achieved in mice, several groups developed mice harboring unique point mutations in Mecp2 to better understand the role of the different functional domains in Mecp2 and the consequences of specific point mutations found in the patient populations on Mecp2 function *in vivo*. The first of these models to be developed was a truncating mutation engineered at amino acid 308 within the mouse Mecp2 protein (Shahbazian et al., 2002). This mutation was chosen because it occurs in a region surrounded by mutations found in male patients with severe neonatal encephalopathy and death or severe mental retardation, seizures, and ataxia. Truncation at amino acid 308 ($Mecp2^{308}$) retains the function of the MBD and TRD; however, it removes the C terminal domain, thus providing a model to understand the unique functions of this region of Mecp2. Male $Mecp2^{308}$ mice develop symptoms that

are milder compared to the global or neuronal KO animals. These symptoms begin with slight tremors at around 6 weeks of age, which eventually develop into more severe tremors at around 4 months. Coinciding with the development of tremors, myoclonic seizures are also apparent at 4 months. In addition, male Mecp2^{308} mice display mild motor impairments as evidenced by reduced time spent on an accelerating rotarod, decreased time spent on a hanging wire grid test, and more falling episodes in a horizontal dowel walk assay (Shahbazian et al., 2002). Mecp2^{308} mice also display enhanced anxiety and repetitive movement of the forelimbs. In one study, no deficits in social interaction, conditioned fear learning, and spatial learning were observed, indicating that the C terminal region of Mecp2 is not important for these functions (Shahbazian et al., 2002). However, in a second study, Moretti *et al.* observed a significant deficit in freezing behavior in the contextual fear conditioning assay and deficits in spatial learning via the Morris water maze task (Moretti et al., 2006). There are several explanations for the differences observed in these two studies. First, each study was performed using Mecp2^{308} mice on different genetic backgrounds. The Shahbazian *et al.* study utilized mixed 129/SvEv X C57BL/6 mice, whereas the Moretti *et al.* study used mice on a pure 129/SvEv background. Additionally, different training paradigm intensities were used that could also explain these differences. Moretti *et al.* utilized less intense paradigms, which seem to be more sensitive to differences in learning and memory that are lost when more intense paradigms are used.

In 2007, a second mouse model harboring a truncating mutation in Mecp2 was generated. This mouse, containing the Arg168X mutation, display similar phenotypes to the global KO; however, they have a slightly longer average lifespan of 85 days

(Lawson-Yuen et al., 2007). Arg168X is the most common mutation found in Rett syndrome patients and, as it is located within the MBD, most likely results in loss of MBD function. Arg168X mice display many of the characteristic features of Rett syndrome, such as hind limb clasping, apneas, and motor abnormalities (Lawson-Yuen et al., 2007; Schaevitz et al., 2013; Wegener et al., 2014). In addition, these mice display enhanced anxiety and deficits in cognitive function (Schaevitz et al., 2013; Wegener et al., 2014). These cognitive deficits include impaired novel object recognition and decreased time freezing in both a contextual and cued fear conditioning assay (Schaevitz et al., 2013). Taken together, these data indicate that many of the symptoms observed in Rett syndrome patients can be recapitulated if the protein is truncated at amino acid 168. As amino acid 168 is located within the MBD, this also perhaps indicates that function of both the MBD and TRD are necessary for proper Mecp2 function.

Additionally, a third mutant mouse model of Rett syndrome has been developed in which mice harbor a point mutation at amino acid 140 (Ala140Val) (Jentarra et al., 2010). Ala140Val is a less common point mutation, accounting for only 0.6% of all reported MECP2 mutations, which results in a very mild form of mental retardation in females. Ala140Val mice display no overt phenotypic abnormalities, however, they display increased cellular density in the hippocampal regions CA1 and the DG (Jentarra et al., 2010). They also display several electrophysiological phenotypes associated with altered hippocampal function, which will be discussed in detail in a later section (Ma et al., 2014).

Finally, there is strong evidence from male patients with MECP2 mutations that symptom onset and clinical severity can be influenced by mutation location (Baker et al.,

2013). This phenomenon has specifically been observed for mutations within amino acids 270-273. Mutations at amino acid 270, such as Arg270X, result in truncation of the protein prior to the first AT hook functional domain and manifests in severe neonatal encephalopathy and death. Mutations three amino acids later in the protein, such as at amino acid 273 (Gly273X), retain AT hook function and result in a milder phenotype characterized by survival and minor neurological deficits. These clinical findings indicate that the proper function of the AT hook domain in Mecp2 is critical to determining symptom severity and clinical outcome. As such, Baker *et al.* generated two mouse models harboring either the Arg270X or the Gly270X mutations and investigated their survival and phenotypic outcomes. Consistent with the human phenotype, Gly273X mice have a delayed disease progression and survive longer than Arg270X mice (Baker et al., 2013). These differences are attributable to an inability of Arg270X mice to maintain normal chromatin structure, despite normal MBD binding to DNA. As such, this indicates that, while MBD mutations determine whether a patient will develop Rett syndrome, dysfunction of the AT hook domain can alter clinical severity.

Genetic deletion of Mecp2 from unique subsets of neurons

In order to understand the contribution of Mecp2 to the wide range of symptoms present in Rett syndrome patients, many different mouse models have been developed where Mecp2 has been genetically deleted from specific subsets of neuronal populations. Because so many mouse models exist, only the overt phenotypes of these models will be discussed. When Mecp2 is knocked out from neurons in the forebrain, hippocampus, and brain stem, this resulted in a delayed, less severe, progression of the disease (Chen et al.,

2001). These mice displayed characteristic hind limb clasping, decreased time spent on the rotarod, increased anxiety behaviors, impaired cued fear conditioning, and deficits in social interaction (Gemelli et al., 2006). Taken together, these data suggest that many of the main functions of Mecp2 occur via actions in the forebrain, hippocampus, and brainstem.

An interesting finding is that GABAergic interneurons express two times as much Mecp2 compared to all other neuronal subtypes, perhaps indicating that Mecp2 plays an important role in the function of these neurons (Chao et al., 2010). Chao *et al.* generated a mouse model in which Mecp2 was genetically deleted from all GABAergic interneurons. Excitingly, these mice display almost all of the same phenotypes present in the global KO. These mice display a similar disease progression to global KO mice in that they develop symptoms at around 5 weeks of age and have 50% lethality by 26 weeks of age (Chao et al., 2010). This progression is associated with the development of hind limb clasping, apneas, and cognitive and motor impairments. Additionally, they display severe respiratory apneas, cortical seizures, and deficits in hippocampal synaptic plasticity. Interestingly, these mice also display several symptoms that were not present in the global Mecp2 KO mice, including strong, repetitive grooming, and enhanced pre-pulse inhibition (PPI) indicative of deficits in sensorimotor gating and obsessive-compulsive-like behaviors (Chao et al., 2010).

Additionally, when Mecp2 was genetically removed from a subset of forebrain GABAergic interneurons, the breathing abnormalities were abolished. Many of the phenotypes observed in the global GABAergic interneuron Mecp2 KO, however, were retained, indicating that many of these behaviors are mediated by forebrain structures

(Chao et al., 2010). This is also in agreement with the genetic deletion of Mecp2 from all forebrain neurons (Chen et al., 2001; Gemelli et al., 2006; Chao et al., 2010), which suggests that Mecp2 is critical to the proper function of these brain structures.

Mecp2 has also been genetically deleted from several other neuronal populations, including serotonergic, dopaminergic, and noradrenergic neurons and neurons in the hypothalamus (Fyffe et al., 2008; Samaco et al., 2009). When Mecp2 is removed from serotonergic neurons, mice display increased aggression and hyperactivity but maintain a normal lifespan and display no alterations in motor function, anxiety, obsessive-compulsive behaviors, or breathing patterns (Samaco et al., 2009). Additionally, the levels of brain serotonin as well as its metabolites are reduced (Samaco et al., 2009). In contrast, when Mecp2 is removed from dopaminergic and noradrenergic neurons, this results in motor dysfunction and decreases in dopamine and norepinephrine levels, but no other overt phenotypes (Samaco et al., 2009). When Mecp2 is removed selectively from neurons within the hypothalamus using a specific *Sim1* promoter, this results in an enhanced stress response and dysfunction in social and feeding behavior (Fyffe et al., 2008). Interestingly, these results indicate that removal of Mecp2 from each of these populations individually contributes to unique behavioral outcomes and also indicates that Mecp2 has a cell-autonomous function to regulate the level of these biogenic amines.

Animal models of Rett syndrome: conclusions

Once the causative gene for Rett syndrome was identified, a large effort in the field was undertaken to model the disorder properly in rodents. After a decade of research, it is clear that Rett syndrome is a disorder of the CNS and, in particular, a

disorder associated most closely with neuronal dysfunction. Excitingly, almost all of the symptoms of Rett syndrome can be reversed if Mecp2 is re-expressed in post-mitotic neurons, indicating that the damage is reversible. This is especially promising because it indicates that many of the phenotypes could potentially be reversed by therapeutic intervention.

By incorporating all of the mouse models harboring various point mutations in Mecp2, it is clear that truncation mutations result in the most severe phenotypes. Additionally, many of the symptoms found in the global Mecp2 KO can be recapitulated when the function of the MBD is disrupted, thus indicating that mutations in this domain are causative of Rett syndrome. Interestingly, while MBD dysfunction is necessary for Rett syndrome, the clinical course and symptom severity of the disease are influenced greatly by the function of the AT hook domain. As such, it seems that both the direct regulation of specific gene transcription and more global chromatin structure regulation by Mecp2 can contribute to the pathology of the disease.

Finally, many in-depth studies of the effect of Mecp2 KO in discrete neuronal populations and from distinct brain regions have shed light on the contribution of specific neurons in precise structures to the unique phenotypes observed in global Mecp2 KO mice. Forebrain GABAergic neurons play a large role in the manifestation of many of the motor, breathing, repetitive behavior, and cognitive abnormalities, whereas serotonergic neurons play a role in social behavior and aggression. Additionally, when Mecp2 is deleted from the hypothalamus, an abnormal stress response is observed which is not prominent in the global Mecp2 KO. The development of novel phenotypes in these subtype-selective KO models is interesting, because it could indicate that these

phenotypes are either compensated for in the global KO or are the result of unique genetic backgrounds used to generate these mice. It will be interesting in the future to understand the role of other neuronal populations, such as cholinergic and glutamatergic neurons specifically, to get a complete understanding of how each of these neuronal populations contributes to the etiology of the disease. Additionally, these studies could potentially shed light on novel therapeutic mechanisms to treat specific phenotypes in Rett syndrome.

Evidence for hippocampal dysfunction and cognitive impairments in Rett syndrome

One of the most common reported findings from the study of several mouse models of Rett syndrome is the presence of alterations in hippocampal neuronal architecture and synaptic transmission. Indeed, there is strong evidence from postmortem studies of Rett syndrome patients that hippocampal spine density and dendritic arborization and branching of CA1 pyramidal cells are reduced (Armstrong, 2001). Additionally, neuronal cell size is also reduced (Hagberg et al., 2001). These findings have been recapitulated in mouse models of Rett syndrome, indicating that Mecp2 is important for either developing or maintaining proper neuronal architecture (Chen et al., 2001). These structural alterations can be hypothesized to affect both basal transmission properties and the ability of synapses to undergo long-lasting changes in synaptic strength. As such, the changes observed in both basal transmission and synaptic plasticity will be discussed below.

Alterations in hippocampal basal synaptic transmission and network excitability

Associated with the observed changes in synaptic connectivity, there are also corresponding alterations in synaptic transmission in the hippocampus of Rett syndrome model mice (Na et al., 2013). One such finding is the observation that loss of Mecp2 results in changes in presynaptic function (Moretti et al., 2006; Nelson et al., 2011). The most common mechanism to study changes in presynaptic function, such as alterations in presynaptic neurotransmitter release probability, is the assessment of paired pulse stimulation of fEPSPs at the SC-CA1 synapse. In this paradigm, two stimulations are delivered at varying amount of time apart and a paired pulse ratio is calculated (by comparing the slope of the second response to the slope of the first response). In wild-type brain slices, SC-CA1 synapses normally display paired pulse facilitation, which is indicative of a low neurotransmitter release probability (Moretti et al., 2006; Nelson et al., 2011). When the same paradigm is used in Mecp2 KO or mutant brain slices, the paired pulse ratio is reduced due to an enhanced first response (Moretti et al., 2006; Nelson et al., 2011). This indicates that the probability of neurotransmitter release, and thus evoked glutamatergic transmission, is enhanced in Mecp2-null animals.

This enhanced glutamatergic transmission results in an alteration in the balance between excitation and inhibition in favor of excitation. This is consistent with several key studies demonstrating that area CA1 of the hippocampus is hyper-excitable (Zhang et al., 2008; Calfa et al., 2011; Nelson et al., 2011; McLeod et al., 2013; Ma et al., 2014; Calfa et al., 2015). Interestingly, the enhanced excitability of CA1 neurons is thought to originate in area CA3, where increased spontaneous firing and reduced inhibitory rhythmic activity have been observed (Zhang et al., 2008; Calfa et al., 2011; Calfa et al.,

2015). Nevertheless, these alterations lead to a net increase in excitation over inhibition, which could explain the seizure phenotype described in both Rett syndrome patients and Mecp2 KO or mutant mouse lines. Indeed, Mecp2-null mice display higher seizure scores with a more rapid onset than wild-type littermate controls when challenged with the pro-convulsant, kainic acid (McLeod et al., 2013). This also resulted in higher gamma frequency field potentials recorded from hippocampal slices (McLeod et al., 2013). Additionally, hippocampal slices challenged with the $GABA_A$ receptor blocker, bicuculline, showed enhanced epileptiform activity (McLeod et al., 2013). Taken together, these data indicate that loss of Mecp2 results in enhanced glutamatergic transmission and network oscillations that may underlie the seizure phenotype observed in mouse models of Rett syndrome.

Alterations in hippocampal long term synaptic plasticity

In addition to changes associated with basal evoked transmission in the hippocampus, there have also been several reports of alterations in long-term synaptic plasticity in mouse models of Rett syndrome. Moretti *et al.* investigated hippocampal synaptic plasticity changes in the $Mecp2^{308}$ mouse model and observed a significant deficit in the induction of LTP using two different induction stimulation paradigms (two trains of 100 Hz stimulation or TBS) compared to wild-type controls (Moretti et al., 2006). Additionally, these findings have been recapitulated in the *Mecp2*$^{-/y}$ global KO mouse model using two trains of 100 Hz stimulation to induce LTP as well (Asaka et al., 2006; Weng et al., 2011). LTP induced in *Mecp2*$^{-/y}$ mice is also saturated compared to wild-type slices, as additional applications of HFS do not result in an increase in the level

of LTP as observed in wild-type slices (Weng et al., 2011). Interestingly, these deficits in LTP are only observed in symptomatic Mecp2-null mice. When the same stimulation paradigms are used in pre-symptomatic *Mecp2*$^{-/y}$ mice, no deficit in LTP is observed, indicating that the development of synaptic plasticity deficits correlates with the developmental onset of Rett syndrome (Asaka et al., 2006; Weng et al., 2011). Additionally, Chao *et al.* observed a similar deficit in LTP when Mecp2 was exclusively removed from GABAergic interneurons (Chao et al., 2010). This finding is particularly intriguing because it suggests that the primary location mediating the deficit in LTP is in GABAergic neurons, not glutamatergic neurons as would be expected.

Loss of Mecp2 function also results in deficits in LTD. Mecp2^{308} mice display a significant deficit in LTD induced using PP-LFS, an induction paradigm known to be reliant on the activation of mGlu receptors (Moretti et al., 2006). Additionally, *Mecp2*$^{-/y}$ mice also display a deficit in LTD induced using LFS (Weng et al., 2011). No deficit, however, was observed using DHPG-induced LTD in Mecp2^{308} mice, perhaps indicating that a shared mechanism between some, but not all, forms of LTD is dysfunctional when Mecp2 function is lost (Moretti et al., 2006).

Evidence for cognitive impairments in Rett syndrome

Both LTP and LTD are thought to be the molecular mechanisms underlying learning and memory. It is not surprising, therefore, that loss of Mecp2 results in cognitive impairments. Specifically, many of these cognitive impairments occur in tasks that are known to be reliant on proper hippocampal function, which suggests that perhaps the deficits observed in LTP and LTD at the SC-CA1 synapse may underlie the observed

behavioral impairments. Indeed, global Mecp2 null mice display severe deficits in contextual fear conditioning, a task that requires the hippocampus (Stearns et al., 2007; McGraw et al., 2011). Several other mouse models of Rett syndrome also display robust deficits in contextual fear conditioning, indicating that this phenotype is reproducible and not solely dependent on specific point mutations in Mecp2 (Shahbazian et al., 2002; Moretti et al., 2006; Goffin et al., 2012).

In the hidden platform version of the Morris water maze, $Mecp2^{308}$ and wild-type male mice were trained in eight consecutive trials to find a hidden platform located in one of four quadrants of a water maze. $Mecp2^{308}$ mice consistently take longer to learn the task compared to wild-type controls, indicating they have a deficit in spatial learning (Moretti et al., 2006). Additionally, when tested in a probe trial in which mice were placed back into the water maze without the hidden platform, $Mecp2^{308}$ mice spend significantly less time in the quadrant previously containing the hidden platform (Moretti et al., 2006). $Mecp2^{308}$ mice also display a significant deficit in long-term social recognition, which are both tasks that also rely on proper hippocampal function (Moretti et al., 2006). Arg168X mice also display behavioral deficits in learning and memory paradigms (Schaevitz et al., 2013). They display deficits in both contextual fear memory and in the ability to distinguish between a novel and familiar object (Schaevitz et al., 2013). Interestingly, the cognitive impairments have also been recapitulated when Mecp2 is removed from GABAergic neurons exclusively. Chao *et al.* found a deficit in the ability of mice to remember the location of the hidden platform in a probe trial of the Morris water maze only in animals that did not express Mecp2 in GABAergic neurons,

thus providing further evidence that the cognitive impairments arise from alterations in GABAergic transmission in the hippocampus (Chao et al., 2010).

Evidence for hippocampal dysfunction and cognitive impairments in Rett syndrome: conclusions

Loss of Mecp2 function results both in alterations in basal hippocampal synaptic transmission and in the ability of synapses to undergo changes in activity-induced synaptic strength (Na et al., 2013). While both of these phenomena occur at glutamatergic synapses, they may be caused by very different mechanisms. Indeed, there is strong evidence that loss of Mecp2 results in hyperactivity of CA3 pyramidal neurons, as evidenced by increased synaptic firing, which is thought to contribute to the enhanced glutamatergic transmission in area CA1 (Calfa et al., 2011; Calfa et al., 2015). Alternatively, deficits in LTP induction at the SC-CA1 synapse can be recapitulated when Mecp2 is only functionally lost from GABAergic neurons, indicating that, for LTP, the underlying deficit may be GABAergic in nature (Chao et al., 2010). Excitingly, there has been one report showing that application of the weak NMDA receptor blocker, memantine, can partially reverse some of the LTP deficits, which suggests that these deficits can be pharmacologically manipulated (Weng et al., 2011). This is particularly encouraging owing to the need for the development of novel therapeutic compounds, especially to treat the cognitive disorders associated with Rett syndrome, and indicates that these deficits may not be permanent.

There is strong literature evidence that the loss of Mecp2 results in reliable, reproducible deficits in cognition (Shahbazian et al., 2002; Moretti et al., 2006; Stearns et

al., 2007; McGraw et al., 2011; Goffin et al., 2012). In particular, many of the deficits are observed in tasks that are known to rely on proper hippocampal function. The contextual fear conditioning assay is a robust measure of hippocampal learning and memory and it is hypothesized that performance on the task requires either LTP or LTD in the hippocampus to occur. These ideas fit nicely with the findings from many investigators in the field that, regardless of whether Mecp2 is globally removed or its function is diminished by the introduction of a point mutation or a stop codon, mice display a severe deficit in their ability to perform this task. Additionally, these deficits can be recapitulated when Mecp2 is removed from GABAergic neurons in the forebrain, thus providing further evidence that both the LTP and contextual fear conditioning impairments arise from GABAergic transmission dysfunction. As the hippocampal-mediated cognitive impairments are one of the most reproducible findings in the Rett syndrome literature, developing novel strategies to treat these impairments is an extremely important avenue for basic science research.

Current treatment options and ongoing clinical trials

Currently, there are no pharmacological treatments specifically approved for the treatment of Rett syndrome (Pozzo-Miller et al., 2015). As such, there is a great need to identify novel therapeutic targets and develop new pharmacological compounds to treat the symptoms of Rett syndrome. The primary treatment options for patients include occupational and physical therapy to improve motor function, medications to prevent or control seizures and heartrate abnormalities, and dietary assistance to improve weight gain and overall health.

Despite the current lack of pharmacological therapies, several clinical trials are in progress to test novel therapeutics for the treatment of Rett syndrome (Pozzo-Miller et al., 2015). One of the most promising therapeutic avenues thus far is compounds that boost brain derived neurotrophic factor (BDNF) levels (Chen et al., 2003; Martinowich et al., 2003; Katz, 2014). BDNF is a growth factor that was one of the first genes to be identified as being specifically regulated by MECP2. BDNF is critical for neuronal growth and synapse formation through its interactions with the tropomyosin receptor kinase B (TrkB) receptor. Additionally, Mecp2 positively regulates BDNF levels through several complex interactions and BDNF levels and signaling are reduced in Mecp2 KO mice (Katz, 2014). As such, compounds that boost BDNF function are thought to be efficacious in reversing some symptoms of Rett syndrome (Katz, 2014). Direct treatment with BDNF, however, is not feasible due to the low permeability of BDNF through the blood brain barrier. Because of this, researchers have developed several novel mechanisms to boost signaling pathways mediated by BDNF. These include treatment with insulin-like growth factor-1 (IGF-1), which activates many of the same signaling cascades as BDNF, and Copaxone, which is an immunomodulatory agent that boosts BDNF levels. Both of these molecules are currently in clinical trials (Pozzo-Miller et al., 2015).

Several other agents are currently being tested in Rett syndrome patients or animal models, such as NMDA receptor antagonists, norepinephrine reuptake inhibitors, and gene therapy methods re-activate Mecp2 expression; however, the efficacy of all of these mechanisms have yet to be definitively determined (Pozzo-Miller et al., 2015). Despite these exciting and promising clinical and pre-clinical studies, there is still a need

for the discovery of new drug targets and the development of novel therapeutic mechanisms to treat specific symptoms of Rett syndrome.

CHAPTER II

METHODS

Compounds

(-) bicuculline methobromide, D-AP5, and LY341495 were purchased from Abcam Biochemicals. CNQX was purchased from R&D Systems. LSP4-2022, VU0422288, and VU0155094 were synthesized in-house according to previously published methodology (Selvam et al., 2010; Jalan-Sakrikar et al., 2014). (+)-6-(2,4-dimethylphenyl)-2-ethyl-6,7-dihydrobenzo[d]oxazol-4(5H)-one (ADX71743) was synthesized in-house according to the methods below. All drugs used for electrophysiology experiments were diluted in artificial cerebrospinal fluid, and drugs used for behavioral experiments were diluted in 10% Tween 80.

General procedure for the chemical synthesis of ADX71743

All NMR spectra were recorded on a 400 MHz FT-NMR DRX-400 FT-NMR spectrometer or 500 MHz Bruker DRX-500 FT-NMR spectrometer. ^{1}H chemical shifts are reported in δ values in ppm downfield with the deuterated solvent as the internal standard. Data are reported as follows: chemical shift, multiplicity (s = singlet, d = doublet, t = triplet, q = quartet, br = broad, m = multiplet), integration, coupling constant (Hz). Low resolution mass spectra were obtained on an Agilent 1200 series 6130 mass spectrometer with electrospray ionization. High resolution mass spectra were recorded on a Waters Q-TOF API-US plus Acquity system with electrospray ionization.

Analytical thin layer chromatography was performed on EM Reagent 0.25 mm silica gel 60-F plates. Analytical HPLC was performed on an Agilent 1200 series with UV detection at 215 nm and 254 nm along with ELSD detection. LC/MS: (Phenomenex-C18, 2.1 X 30 mm, 1.5 min gradient, 7%[0.1%TFA/CH3CN]:93%[0.1%TFA/H2O] to 95% [0.1%TFA/CH3CN]. Preparative purification was performed on a custom HP1100 purification system (reference 16) with collection triggered by mass detection. Solvents for extraction, washing and chromatography were HPLC grade. All reagents were purchased from Aldrich Chemical Co. and were used without purification.

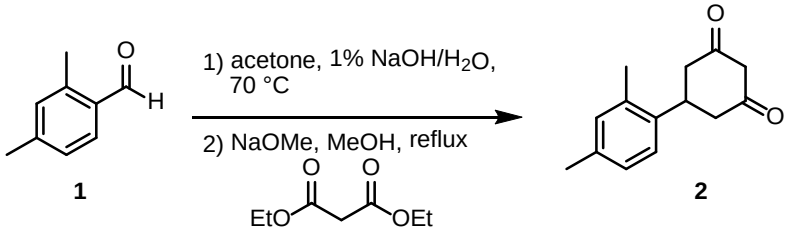

5-(2,4-dimethylphenyl)cyclohexane-1,3-dione (2). (Reference: WO 2011/062964 A1) To a suspension of 2,4-dimethylbenzaldehyde, 90 % technical grade, (**1**) (5.96 g, 40.0 mmol, 1.0 eq) in acetone (6.0 mL) and H_2O (8 mL) was added a 1% aqueous solution of NaOH (5 mL) dropwise. The reaction was heated to 70 °C. After 4 hours at 70 °C, the reaction was cooled to room temperature and poured into H_2O (100 mL). The mixture was extracted with $CHCl_3$ (3 x 50 mL) and the collected organic layers were concentrated.

To a solution of NaOMe (0.5M in MeOH, 84 mL, 1.05 eq) in MeOH (75 mL) was added diethyl malonate (6.2 mL, 40.0 mmol, 1.0 eq), dropwise to maintain temperature between 15-20 °C. The previously isolated residue in MeOH (5 mL) was then added to the reaction at 60 °C. The reaction was refluxed for 12 hours. To the reaction was added

a solution of NaOH (17.6 g) in H_2O (70 mL). The reaction was heated to reflux for an additional hour. To the reaction was added concentrated HCl (15 mL) dropwise. After removing the reaction from the heat, EtOAc (200 mL) was added and the organic layer was separated, washed with H_2O (2 x 80 mL), Brine (50 mL) and dried ($MgSO_4$). The mixture was filtered and the solvent removed under reduced pressure. The material was taken forward without further purification.

LCMS: RT = 0.873 min, >92% @ 215 nM, m/z = 217.0 [M + H]+.

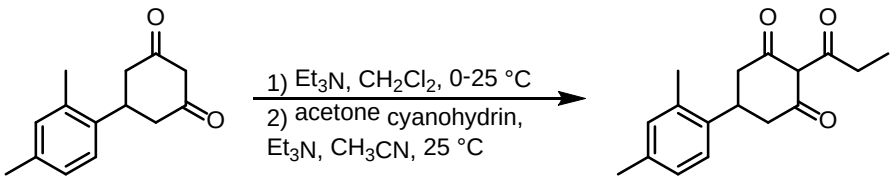

2 **3**

5-(2,4-dimethylphenyl)-2-propionylcyclohexane-1,3-dione (3). (Reference: WO 2011/062964 A1) To a solution of 5-(2,4-dimethylphenyl)cyclohexane-1,3-dione (**2**) (40.0 mmol, 1.0 eq) in DCM (100 mL) at 0 °C was added propionyl chloride (3.85 mL, 44.0 mmol, 1.1 eq), followed by Et_3N (6.7 mL, 48.0 mmol, 1.2 eq). After 15 minutes, the cold bath was removed. Following 3 hours at room temperature, the reaction was evaporated to dryness. The brown residue was re-dissolved in acetonitrile (50 mL) and acetone cyanohydrin (1 mL) and Et_3N (1 mL) were added. After 18 hours at room temperature, the reaction was concentrated and the residue was purified by reverse-phase HPLC (30-90% acetonitrile: H_2O w/ 0.1% TFA) to afford 3 (15-20% over 3 steps).

LCMS: RT = 1.211 min, >98% @ 215 and 254 nM, m/z = 272.8 [M + H]+;

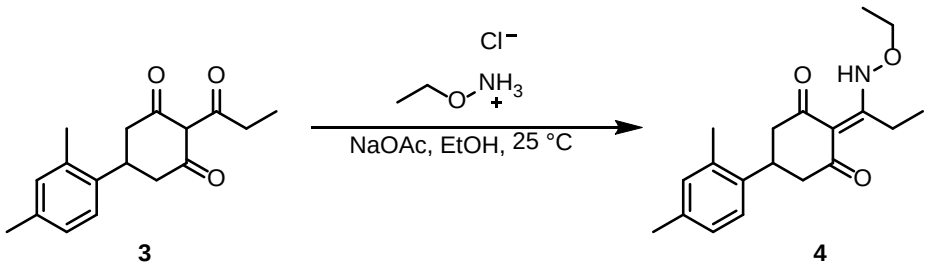

3 4

5-(2,4-dimethylphenyl)-2-(1-(ethoxyamino)propylidene)cyclohexane-1,3-dione (4). To a solution of 5-(2,4-dimethylphenyl)-2-propionylcyclohexane-1,3-dione (**3**) (210 mg, 0.77 mmol, 1.0 eq) in EtOH (8 mL) at room temperature was added O-ethylhydroxylamine • HCl (79 mg, 0.81 mmol, 1.05 eq), followed by NaOAc (70 mg, 0.85 mmol, 1.1 eq). The heterogeneous yellow reaction was stirred for 16 hours at room temperature. After the solvent was removed under vacuo, the residue was re-dissolved in DCM:H_2O (100 mL, 1:1) and the organic layer was separated using a hydrophobic phase separator. After the solvent was removed, the material was taken on without further purification.

LCMS: RT = 1.269min, >98% @ 215 and 254 nM, m/z = 315.8 [M + H]+.

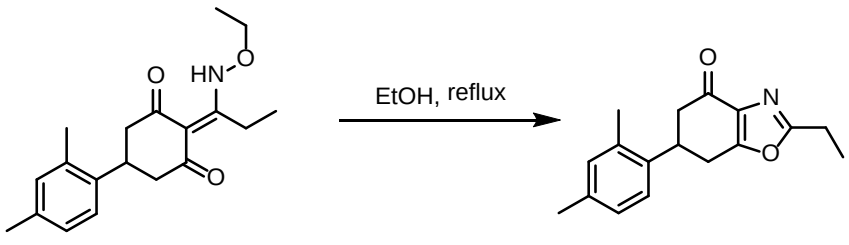

4 5

6-(2,4-dimethylphenyl)-2-ethyl-6,7-dihydrobenzo[*d*]oxazol-4(5*H*)-one (5). A solution of 5-(2,4-dimethylphenyl)-2-(1-(ethoxyamino)propylidene)cyclohexane-1,3-dione (**4**) (0.77 mmol, 1.0 eq) in EtOH (50 mL) was heated to reflux. After 24 hours at reflux, the

reaction was concentrated and the residue was purified by reverse-phase HPLC (20-75% acetonitrile: H_2O w/ 0.1% TFA) to afford **5** (96.4 mg, 47% over 2 steps).

LCMS: RT = 1.065 min, >98% @ 215 and 254 nM, m/z = 269.8 [M + H]+;

HRMS, calculated for $C_{17}H_{20}NO_2$, 270.1494 $[M + H]^+$, found 270.1496.

^{1}H NMR (400 MHz, CDCl3): δ 7.20 (d, J = 7.9 Hz, 1H), 7.06 (d, J = 7.3 Hz, 1H), 7.06 (s, 1H), 3.83 (m, 1H), 3.15-3.05 (m, 2H), 2.88-2.80 (m, 3H), 2.72 (dd, J = 16.48, 3.8 Hz, 1H), 2.35 (s, 3H), 2.33 (s, 3H), 1.40 (t, J = 7.6 Hz, 3H).

13C NMR (125 MHz, CDCl3): δ 190.4, 166.4, 163.3, 137.0, 136.8, 135.2, 134.1, 131.8, 127.2, 125.4, 44.7, 36.7, 29.3, 21.7, 20.9, 19.3, 10.9.

Animals: Chapters III and IV

All of the animals used in the present studies were group housed with food and water available *ad libitum*. Animals were kept under a 12 h light/dark cycle with lights on from 6:00 AM to 6:00 PM and were tested during the light phase. All of the experimental procedures were approved by the Vanderbilt University Animal Care and Use committee and followed the guidelines set forth by the *Guide for the Care and Use of Laboratory Animals*. 6-7 week old C57BL6/J male mice (Jackson Laboratories) or mice expressing channelrhodopin 2 (B6;129S-Gt(ROSA)26Sor$^{tm32(CAG-COP4*H134R/EYFP)Hze}$/J; ChR2) in parvalbumin (PV)-expressing inter-neurons (B6;129P2-Pvalb$^{tm1(cre)Arbr}$/J:PV) were used

for all studies in **Chapter III**. P45-P50 B6.129P2(C)-*Mecp2*$^{tm1.1\text{-}Bird}$/J on a C57BL6/J congenic background, Jackson Labs strain #003890 males (*Mecp2*$^{-/y}$), 18-20 week old *Mecp2*$^{+/-}$ females, or wild-type littermate controls (*Mecp2*$^{+/y}$ or Mecp2$^{+/+}$) were used for all studies in **Chapter IV**.

Brain Slice Electrophysiology: Chapter III

Slice Preparation

6 week old male C57BL6/J mice (Jackson Laboratories) were anesthetized with isofluorane, and the brains were removed and submerged in ice-cold cutting solution (in mM: 230 sucrose, 2.5 KCl, 8 $MgSO_4$, 0.5 $CaCl_2$, 1.25 NaH_2PO_4, 10 D-glucose, 26 $NaHCO_3$). Coronal slices containing the hippocampus were cut at 400 μm using a Compresstome (Precisionary Instruments). Slices were transferred to a holding chamber containing NMDG-HEPES recovery solution (in mM: 93 NMDG, 2.5 KCl, 1.2 NaH_2PO_4, 30 $NaHCO_3$, 20 HEPES, 25 D-glucose, 5 sodium ascorbate, 2 thiourea, 3 sodium pyruvate, 10 $MgSO_4$, 0.5 $CaCl_2$, pH 7.3, 305 mOsm) for 15 minutes at 32 ºC. Slices were then transferred to a room temperature holding chamber for at least 1 hour containing aCSF (in mM: 126 NaCl, 1.25 NaH_2PO_4, 2.5 KCl, 10 D-glucose, 26 $NaHCO_3$, 2 $CaCl_2$, 1 $MgSO_4$) supplemented with 600 μM sodium ascorbate for slice viability. All buffers were continuously bubbled with 95% O_2/5% CO_2. Subsequently, slices were transferred to a 32 ºC submersion recording chamber where they were perfused with aCSF at a rate of 2 mL/min. Borosilicate glass electrodes were pulled using a Flaming/Brown

micropipette puller (Sutter Instruments) and had a resistance of 3-5 MΩ when filled with aCSF.

Extracellular Field Potential Recordings

Paired-pulse field excitatory post synaptic potentials (fEPSPs) were recorded by from the stratum radiatum of CA1 and evoked by electrical stimulation (100 μs duration, every 20 sec) delivered through a concentric bi-polar stimulating electrode placed near the CA3-CA1 border. Input-output curves were generated for each slice and the stimulation intensity was adjusted to 50-60% of the maximum response. The effect of $mGlu_7$ compounds on basal synaptic transmission was monitored by applying paired-pulse stimulation with an inter-pulse interval of 20 ms at 0.05 Hz. After a 10 minute baseline recording, 30 μM LSP4-2022 was bath-applied for 10 minutes and then washed out for 15 minutes. Alternatively, after a 5 minute baseline, slices were pre-treated with 3 μM ADX71743 for 5 minutes prior to co-application of 3 μM ADX71743 and 30 μM LSP4-2022 for 10 minutes, followed by a 15 minute washout period. For frequency-dependent fEPSP experiments, two different stimulation paradigms were used. For both paradigms, slices were perfused with bicuculline for the entire experiment and a cut was made at the CA3-CA1 border to prevent recurrent burst firing. A train of 5 fEPSPs was evoked by stimulating 5 times at a frequency of 10 Hz with a 30 sec ITI. Baseline values were recorded for 10 minutes prior to the addition of ADX71743 for 10 minutes. Additionally, a second stimulation paradigm was also used in which a single pulse was delivered 550 ms prior to 10 pulses delivered at 100 Hz followed by a second test pulse 550 ms later. Baseline values were recorded for 10 minutes prior to addition of

ADX71743 for 10 minutes. The slopes from two sequential sweeps were averaged. All slopes calculated were normalized to the average slope calculated during the pre-drug period (percent of baseline).

Saturated LTP was induced by applying either two or three trains of 100 Hz stimulation (1 sec duration, 20 sec inter-train interval (ITI)) directly following a 10 minute baseline. Threshold LTP was induced by applying one train of 100 Hz stimulation (1 sec). LTP in the presence of bicuculline was performed in a modified aCSF (in mM: 126 NaCl, 1.25 NaH_2PO_4, 2.5 KCl, 10 D-glucose, 26 $NaHCO_3$, 4 $CaCl_2$, 4 $MgSO_4$, 20 µM bicuculline). A surgical cut was made between CA3 and CA1 regions to prevent epileptiform activity. Slices were perfused with 20 µM bicuculline and the fEPSP slope was allowed to stabilize before an input-output curve was generated and the stimulation intensity was adjusted to 50% of the maximum fEPSP slope generated in bicuculline. For a subset of LTP experiments performed in the presence of bicuculline, an input-output curve was first generated in normal aCSF. Slices were then perfused with 20 µM bicuculline, and the stimulation intensity was adjusted so that the fEPSP slope used at baseline in bicuculline was the same as the 50% slope value calculated from the input-output curve in normal aCSF. Sampled data was analyzed offline using Clampfit 10.2 (Molecular Devices). The slopes from three sequential sweeps were averaged. All slopes calculated were normalized to the average slope calculated during the pre-drug period (percent of baseline). Data were digitized using a Multiclamp 700B, Digidata 1322A, and pClamp 10 software (Molecular Devices). All drugs were diluted in aCSF and bath applied.

Whole-Cell Patch-Clamp Recordings

Whole-cell patch-clamp recordings were performed using coronal slices prepared from either 6 week old male C57BL6/J mice (Jackson Laboratories) or 6 week old male mice expressing channelrhodopin 2 (B6;129S-Gt(ROSA)26Sor$^{tm32(CAG-COP4*H134R/EYFP)Hze}$/J; ChR2) in parvalbumin (PV)-expressing inter-neurons (B6;129P2-Pvalb$^{tm1(cre)Arbr}$/J:PV). The PV-ChR2 mice were generated by crossing mice expressing cre recombinase under the control of a PV promoter with mice expressing conditional ChR2. All animals were anesthetized using a 0.2 mL intraperitoneal injection of ketamine/ xylazine (20 mg/ 2mg per ml) and then transcardially perfused with ice-cold cutting solution. Mice were then decapitated and the brains were removed and submerged in ice-cold cutting solution as described above. Coronal slices containing the hippocampus were cut at 300 μm using a Compresstome (Precisionary Instruments). Slices were then transferred to a holding chamber containing a modified NMDG-HEPES recovery solution (in mM: 93 NMDG, 2.5 KCl, 1.2 NaH_2PO_4, 30 $NaHCO_3$, 20 HEPES, 25 D-glucose, 5 sodium ascorbate, 2 thiourea, 3 sodium pyruvate, 10 $MgSO_4$, 0.5 $CaCl_2$, 12 *N*-acetyl-L-cysteine, pH 7.3, 305 mOsm) and recovered as described above. After the initial recovery period, slices were transferred to a holding chamber containing modified aCSF for at least 30 minutes (in mM: 126 NaCl, 1.25 NaH_2PO_4, 2.5 KCl, 10 D-glucose, 26 $NaHCO_3$, 2 $CaCl_2$, 1 $MgSO_4$) supplemented with 600 μM sodium ascorbate for slice viability. Slices were perfused with 2 ml/min aCSF at 32ºC in a submersion recording chamber. A cut was made at CA3 in all slices to prevent recurrent burst firing. Neurons were visualized with a 40X water-immersion lens with Hoffman modulation contrast optics coupled with an Olympus BX50WI upright microscope (Olympus). Borosilicate

glass pipette electrodes were pulled as described above and had a resistance of 5-7 MΩ when filled with an intracellular solution containing (in mM: 120 $CsMeSO_3$, 1 $CaCl_2$, 1 $MgSO_4$, 11 CsCl, 10 HEPES, 11 EGTA, 3 magnesium-ATP, 0.3 sodium-GTP, pH adjusted to 7.3 with CsOH; 290 mOsm).

Whole-cell recordings were made from visualized CA1 pyramidal neurons. Inhibitory post-synaptic currents (IPSCs) were evoked by placing a concentric bi-polar stimulating electrode near the CA3-CA1 border. After formation of a whole cell configuration, the membrane potential was voltage-clamped at 0 mV by injection of current. Evoked IPSCs (eIPSCs) were recorded by applying paired-pulse stimulations 200 ms apart with a 20 second inter-sweep interval for mono- and poly-synaptic experiments. Input-output curves were generated for each cell and the stimulation intensity was adjusted to 50-70% of the maximum response. For monosynaptic eIPSC experiments and frequency-dependent IPSC experiments, slices were continuously perfused with 20 μM CNQX and 50 μM D-AP5 to block glutamatergic transmission. For frequency-dependent IPSC experiments, two different stimulation paradigms were used that were similar to those used in the frequency-dependent fEPSP experiments. A train of 5 IPSCs was evoked by stimulating 5 times at a frequency of 5 Hz with a 30 sec ITI. Baseline values were recorded for 5 minutes prior to the addition of either LY341495 or ADX71743 for 10 minutes. Additionally, a second stimulation paradigm was also used in which a single pulse was delivered 550 ms prior to 10 pulses delivered at 100 Hz followed by a second test pulse 550 ms later. Baseline values were recorded for 5 minutes prior to addition of either LY341495 or ADX71743 for 10 minutes. The amplitudes from two sequential sweeps were averaged. All amplitudes calculated were

normalized to the average amplitude calculated during the pre-drug period (percent of baseline).

Optogenetically-induced IPSCs (oIPSCs) were generated using a CoolLED pE-100 illumination system (CoolLED) connected to an Olympus microscope (Olympus). A 473 nm blue light beam was applied to the slice through the 40X water immersion objective as described previously (Pancani et al., 2014). Paired oIPSCs were generated by applying paired light pulse stimulation (1 ms in duration each spaced 700 ms apart). This stimulation paradigm was repeated every 20 seconds for the duration of the experiment. Input-output curves were generated for each cell and the light intensity was adjusted to 50-70% of the maximum response. The amplitudes from three sequential sweeps were averaged into minute bins. All data were digitized using a Multiclamp 700B, Digidata 1322A, and pClamp 10 software (Molecular Devices). All drugs were diluted in aCSF and bath applied.

Statistical Analysis: Chapter III

All data shown represent mean ± SEM for at least three replicates. Statistical significance between groups was determined using unpaired or paired Student's t tests, one-way ANOVA (with Bonferroni's post test), or two-way ANOVA (with Bonferroni's posttest) as specified in each figure legend.

Sequence Alignment

The promoter region of human *GRM7* (Accession Number NC_000003.12) was manually analyzed for the presence of CG dinucleotides and stretches of A/T base pairs

upstream of the proposed transcription start site. The putative MECP2 binding site within *GRM7* was manually aligned with the promoter sequences from chimpanzee (Accession Number NC_006490.3), mouse (Accession Number NC_000072.6), bovine (Accession Number NC_007320.5), and rat (Accession Number NC_005103.4).

Chromatin Immunoprecipitation and ChIP-PCR

Chromatin immunoprecipitation (ChIP) and ChIP-PCR experiments were performed from 6 week old male C57BL6/J mice (Jackson Laboratories) using the published protocol from (Chao et al., 2010). The following primer sequences were used to amplify specific genes of interest. BLAST (blast.ncbi.nlm.nih.gov) analysis confirmed the specificity of the amplified genes of interest.

Grm7: Forward 5' –CTTACCTCAGCACGCAGCCCCT- 3'

Reverse 5' –ACCTGGCACTGTAGCTCCGC- 3'

Grm4: Forward 5'- CCCTCTCCCAGGCTCCCGATG- 3'

Reverse 5' –AAGGGAGCCGCGCTCCTATCC- 3'

Gad-2: Forward 5' –ACCTGCTGATGGCAAGAACT- 3'

Reverse 5' –AAATCCCAGGAAAAGGCACT- 3'

Reporter Gene Construction and Luciferase Assay

The *GRM7* promoter was cloned into the pGL4 expression vector (Promega) using SacI and HindIII. Human *MeCP2* was cloned into the pIRESpuro3 vector (Clontech) using NotI and BamHI. HEK293 cells were plated in 24-well plates at a density of 5 x 10^4 cells per well and transfected with the pGL4 vector with and without

MECP2 using Fugene 6 at a 3:1 ratio of transfection reagent to DNA (Promega) and were tested for luciferase activity after 48 hours. Luciferase was detected using the Dual-Glo Luciferase Assay System® (Promega). The growth media was aspirated and 100 µl of 5X passive lysis buffer (Promega) was added to the cells. The cells were freeze-thawed twice and then 10 µl of each sample was transferred to a 96-well plate. The luminescence was measured using a Synergy 2 luminescence plate reader (BioTek). After luciferase was measured, samples were treated with 10 µl of the Dual-Glo® Stop & Glo® reagent (Promega) to neutralize luciferase luminescence and allow for the detection of renilla luminescence. The ratio of luciferase luminescence to renilla luminescence was calculated for each well and normalized to the control condition with no MECP2 transfection (relative luciferase units, RLU).

Decoy DNA Transfection into H4 Glioma Cells

Decoy DNA was designed to mimic the *GRM7* promoter AT run, flanked by lock bases, with the goal of saturating MECP2's ability to bind AT hooks, but not its ability to bind to methylated DNA. Decoy chimeric DNA was synthesized for the following sequences [U]AAGAATTTAAATACA[U] and [A]TTCTTAAATTTATGT[A], where [bracketed] bases indicate a 2'O-Methyl modified backbone for improved stability. 100 µL of 100 µM single-stranded chimeric DNA stocks were combined in a single 1.5 mL microcentrifuge tube, heated to 95 °C for 5 minutes, and allowed to anneal at room temperature for 30 minutes to form double stranded (ds) DNA. 1, 2, and 4 nM of ds-decoy DNA or scramble control (Dharmacon, D-001810-01-05) were then transfected into the H4-human neuroglioma cell line, which endogenously expresses both MECP2

and *GRM7* transcripts. Cells were harvested 24 hours after transfection, and RNA was prepared using the RNeasy® kit with DNase digestion (Qiagen). RNA quality was determined by gel electrophoresis and complementary DNA (cDNA) was prepared using the Superscript® Variable Input Linear Output (VILO™) kit (Invitrogen). Quantitative Real Time PCR (RT-qPCR) was performed using cDNA at a concentration that equated to 50 ng of the original RNA template. The RT-qPCR reaction employed Life Technologies Taqman Fast® reaction buffer and the gene expression primer/probe sets for *MECP2* (Hs0012845_m1), *GRM7* (Hs00356067_m1), and *GAPDH* (Hs02758991_g1). Cycle threshold (Ct) values for each sample were normalize to *GAPDH* expression and analyzed using the delta-delta Ct method. Values exceeding two times the standard deviation were classified as outliers and results were compared relative to the scramble control at each concentration.

Quantitative Real-time PCR (RT-qPCR)

Cortex, hippocampus, striatum, and cerebellum were microdissected from P45-50 *Mecp2*$^{-/y}$ and wild-type mice. Samples were homogenized with a mortar and pestle and total RNA was prepared using TRIzol Reagent® (Invitrogen) in accordance with manufacturer's instructions. Total RNA from each brain region was DNase-treated with Roche Turbo™ DNase kit, and cDNA from 2 μg total RNA was synthesized using the VILO™ kit (Invitrogen). RT-qPCR on cDNA from 25 ng of initial RNA template was then run in triplicate using Taqman Fast® Reagent Mix (Life Technologies) and Life Technologies gene expression assays for *Grm4* (Mm01306128_m1), *Grm7* (Mm0118924_m1), and *Gad2* (Mm00484623_m1). Ct values for each sample were normalize to *Gapdh* (Mm03302249_g1) expression and analyzed using the delta-delta Ct

method. Values exceeding two times the standard deviation were classified as outliers. Each value was compared to the average delta-Ct value acquired for wild-type mice and calculated as percent-relative to the average control delta-Ct.

Total and Synaptosomal Protein Preparation

For mouse total protein preparation, the cortex, hippocampus, striatum, and cerebellum were microdissected from P49-50 day old *Mecp2*$^{-/y}$ and wild-type mice. For human motor cortex protein preparation, frozen sections were acquired from the Harvard Brain Tissue Resource Center (for Rett syndrome samples), or The University of Maryland Brain and Tissue Bank (for control samples) and first homogenized under liquid nitrogen using a hand-held mortar and pestle. Tissue samples were homogenized using a hand-held motorized mortar and pestle in radioimmunoprecipiation assay buffer (RIPA) containing 10 mM Tris-HCL, 150 mM NaCl, 1 mM ethylenediaminetetraacetic acid (EDTA), 0.1% sodium dodecyl sulfate (SDS), 1% Triton^{TM} X-100, and 1% Deoxycholate. After homogenization, samples were spun for 20 minutes at 15,000 x g at 4 ºC. The supernatant was then transferred to new tubes and the protein concentration was determined using a bicinchoninic acid (BCA) protein assay (Pierce^{TM}). For synaptosome preparations, the cortex and hippocampus were microdissected from P45-50 day old *Mecp2*$^{-/y}$ and wild-type mice. The tissue was homogenized in 9 ml of ice-cold sucrose/HEPES (0.32 M sucrose, 4.2 mM HEPES, pH 7.4) using a Teflon-glass homogenizer (Wheaton Science Products). The homogenate was centrifuged at 1,000 x g for 5 minutes at 4 °C and the resultant supernatant was centrifuged at 12,000 x g for 15 minutes at 4°C. The final pellets containing synaptosomes were re-suspended in Krebs-

Ringer-HEPES buffer (KRH, 120 mM NaCl, 4.7 mM KCl, 1.2 mM KH_2PO_4, 2.2 mM $CaCl_2$, 1 mM $MgSO_4$ and 10 mM HEPES pH 7.4). Protein concentrations were determined using a BCA protein assay (Pierce™).

SDS-PAGE and Western Blotting

Mouse and human proteins were electrophoretically separated using a 10% SDS Polyacrylamide gel and then transferred onto a nitrocellulose membrane (Bio-Rad). Membranes were blocked with 5% nonfat milk (Bio-rad) for one hour at room temperature. Membranes containing mouse protein were then probed with either a rabbit anti-$mGlu_7$ primary antibody (1:500, Upstate) or a mouse anti-tubulin primary antibody (1:2500, Abcam) overnight at 4 °C. Membranes were washed three times with Tris-buffered Saline and Tween 20 (TBS-T, 25 mM Tris, 150 mM NaCl, 0.05% Tween 20) and then incubated with either a goat anti-rabbit-horse radish peroxidase (HRP) secondary antibody (1:7500, Santa Cruz Biotechnology) or a goat anti-mouse-HRP secondary antibody (1:7500, Santa Cruz Biotechnology). Antibody visualization was performed using Pierce™ ECL Western Blotting Substrate reagents. Quantitation of band density was performed using Quantity One® software for 1-D electrophoresis gel analysis (Bio-rad, Version 4.6.8). Each value for $mGlu_7$, $mGlu_4$, or Gad-2 protein expression was first normalized to the value calculated for tubulin expression. For human protein, membranes were visualized using standard quantitative fluorescent western blotting techniques (Odyssey). 96 µg of total protein was loaded. Antibodies were diluted in Odyssey block (LiCor #927-40000) and used at the following

concentrations: primary: MECP2 (1:1000, Millipore), $mGlu_7$ (1:1000, Upstate), secondary: goat anti-rabbit 800 (1:5000, LiCor).

Brain Slice Electrophysiology: Chapter IV

Slice preparation

P45-P50 *Mecp2*$^{-/y}$ and wild-type male mice were anesthetized with isoflurane. Brains were rapidly removed and submerged in ice-cold sucrose cutting buffer containing: 230 mM sucrose, 2.5 mM KCl, 8 mM $MgSO_4$, 0.5 mM $CaCl_2$, 1.25 mM NaH_2PO_4, 10 mM glucose, and 26 mM $NaHCO_3$ saturated with 95%/5% O_2/CO_2. A block of tissue containing hippocampus was trimmed, embedded in agarose, and coronal slices 400 μm thick were cut using a Compresstome^{TM} VF-200 (Precisionary Instruments). Slices were transferred to a holding chamber containing N-methyl-D-glucamine (NMDG)-HEPES recovery solution (in mM, 93 NMDG, 2.5 KCl, 1.2 NaH_2PO_4, 30 $NaHCO_3$, 20 HEPES, 25 $_D$-glucose, 5 sodium ascorbate, 2 thiourea, 3 sodium pyruvate, 10 $MgSO_4$, 0.5 $CaCl_2$, pH 7.3, 305 mOsm) for 15 minutes at 32^{0}C. Slices were then transferred to a room temperature modified artificial cerebral spinal fluid (ACSF) containing (in mM) 126 NaCl, 1.25 NaH_2PO_4, 2.5 KCl, 10 $_D$-glucose, 26 $NaHCO_3$, 2 $CaCl_2$ and 1 $MgSO_4$, and 600 μM sodium ascorbate for at least 1 hour. Subsequently, slices were transferred to a submersion recording chamber and continuously perfused (2 mL/min) with ACSF containing (in mM) 126 NaCl, 1.25 NaH_2PO_4, 2.5 KCl, 10 $_D$-glucose, 26 $NaHCO_3$, 2 $CaCl_2$, 1 $MgSO_4$ heated to 32°C. All solutions were continuously bubbled with 95%/5% O_2/CO_2. Borosilicate glass electrodes

were pulled using a Flaming/Brown micropipette puller (Sutter Instruments, CA) and had a resistance of 3-5 MΩ when filled with ACSF.

Extracellular field potential recordings

A concentric bi-polar stimulating electrode was positioned near the CA3-CA1 border and paired-pulse field excitatory postsynaptic potentials (fEPSPs) were evoked (100 μs duration, every 20 sec spaced 20-500 ms apart) by placing a glass recording electrode in the stratum radiatum of CA1. Input-output curves were generated for each slice and the stimulation intensity was adjusted to 50% of the maximum response for subsequent experiments. Paired-pulse ratios (PPR) were calculated as the ratio between the slope of the second fEPSP divided by the slope of the first fEPSP. PPRs were calculated at several inter-stimulus intervals (ISI) ranging from 10-500 ms. For basal synaptic transmission experiments, paired-pulse fEPSPs were generated with a 20 ms ISI at 0.05 Hz. After 5-10 minutes of stable baseline recordings, DMSO vehicle, 1 μM VU0422288, or 30 μM VU0155094 were bath applied for 5 minutes prior to the addition of 30 μM LSP4-2022 for 10 minutes followed by a 15 minute washout period.

Long term potentiation (LTP) was induced by applying two trains of 100 Hz stimulation (HFS, 1 sec duration, 20 sec inter-train interval (ITI)) after a 10-15 minute baseline. 1 μM VU0422288 was applied for 10 minutes prior to application of HFS. For all electrophysiological experiments, the slopes of three consecutive sweeps were averaged and normalized to the average slope during the baseline period. Data were digitized using a Multiclamp 700B, Digidata 1322A, and pClamp 10 software (Molecular Devices).

Drug metabolism and pharmacokinetic analysis

In vivo pharmacokinetic analysis

VU0422288 was formulated in 10% tween 80 in sterile water (4 mg/mL) at a concentration of 10 milligrams/kilogram (mg/kg) and administered intraperitoneally (i.p.) to adult male Sprague-Dawley rats (Harlan Laboratories). 1 hr following VU0422288 administration, animals were euthanized and decapitated to obtain blood and brain samples. Plasma was isolated from the blood samples by centrifugation and stored at -80 ºC until analysis. Brain samples were quickly washed with ice-cold phosphate-buffered saline (PBS) and frozen on dry ice. Analysis of plasma and brain VU0422288 concentrations was performed as previously described(Felts et al., 2013; Bubser et al., 2014). Briefly, plasma and brain samples were protein-precipitated by employing three volumes of ice-cold acetonitrile containing internal standard, centrifuged (4000 g, 4 ^{o}C, 5 min), and the supernatants transferred and diluted 1:1 (v/v) for LC-MS/MS analysis. Samples were analyzed via electrospray ionization (ESI) LC-MS/MS on an AB Sciex API-4000 (Foster City, CA) triple-quadrupole instrument that was coupled with Shimadzu LC-10AD pumps (Columbia, MD) and a Leap Technologies CTC PAL auto-sampler (Carrboro, NC) and concentrations (ng/mL) of VU0422288 were determined using a matrix-matched 10-point standard curve.

Brain Homogenate Binding

The brain homogenate binding of VU0422288 was determined in rat brain homogenates using equilibrium dialysis using RED plates (Thermo Fisher Scientific). A

mixture of brain homogenate and VU0422288 at a final concentration of 5 µM was added to the *cis* side (red) of a RED plate while an equal volume of PBS (25 mM, pH 7.4) was added to the *trans* side. The plate was then sealed and incubated at 37ºC for 4 hours. At the completion of the incubation, an aliquot from each chamber was removed and diluted 1:1 with either plasma (*cis*) or PBS (*trans*) and transferred to a new 96-well plate. The proteins were precipitated using ice-cold acetonitrile and the samples were then centrifuged at 3000 rcf for 10 minutes to isolate the supernatant. After centrifugation, the supernatant was removed and the concentrations of VU0422288 from each sample were determined via liquid chromatography-tandem mass spectrometry as previously described (Wenthur et al., 2013).

Contextual Fear Conditioning Assay

18-20 week old symptomatic *Mecp2*$^{+/-}$ and wild-type females were used for these studies due to the presence of severe motor impairments in symptomatic *Mecp2*$^{-/y}$ males. Animals were fear conditioned on day 1 of the task and the percent of time spent freezing was assessed 24 hours later. On training day of the task, mice were injected 30 minutes prior to the task with either vehicle (10% tween 80), 30 mg/kg of VU0422288, a combination of 30 mg/kg of VU0422288 and 60 mg/kg of ADX71743, or 60 mg/kg of ADX71743 (intraperitoneal (i.p.) 10 mL/kg). Mice were then placed into an operant chamber with a shock grid (Medassociates Inc.) in the presence of a 10% vanilla odor cue. Following a 3 minute habituation period, mice were exposed to two 1 second, 0.7 mA foot shocks spaced 30 seconds apart. Mice remained in the context for an additional 15 seconds after the second foot shock. 24 hour later, mice were placed back into the

same shock chamber with a 10% vanilla odor cue and the percent of time spent freezing during a 3 minute testing period was assessed.

Statistical Analyses: Chapter IV

All data shown represent mean ± SEM for at least three replicates. Statistical significance between groups was determined using unpaired or paired Student's t tests, one- or two-way ANOVA (with Bonferroni's posttest or individual Student's t test), and one- or two-way repeated measures ANOVA (with Bonferroni's posttest) as specified in each figure legend.

CHAPTER III

ACTIVATION OF METABOTROPIC GLUTAMATE RECEPTOR 7 IS REQUIRED FOR INDUCTION OF LONG TERM POTENTIATION AT SC-CA1 SYNAPSES IN THE HIPPOCAMPUS

Introduction

Glutamate and GABA are the main excitatory and inhibitory neurotransmitters in the central nervous system. They act on two classes of receptors: fast-conduction ion channels and neuromodulatory 7 transmembrane receptors (7TMRs). For glutamate, these 7TMRs are termed metabotropic glutamate (mGlu) receptors, and consist of eight members divided into three groups. Group I ($mGlu_1$ and $mGlu_5$), primarily mediate post-synaptic excitation. Group II ($mGlu_2$ and $mGlu_3$) are expressed pre-synaptically, post-synaptically, and on glial cells. Group III mGlu receptors include $mGlu_4$, $mGlu_6$, $mGlu_7$, and $mGlu_8$, which, with the exception of retinal $mGlu_6$, are primarily expressed pre-synaptically and regulate neurotransmitter release (for review see Niswender and Conn, 2010). Among the group III mGlu receptors, $mGlu_7$ has the lowest affinity for glutamate and is expressed on glutamatergic and GABAergic terminals (Bradley et al., 1996; Dalezios et al., 2002; Summa et al., 2013). $mGlu_7$ is also widely expressed throughout the brain and is the most highly conserved of all the mGlu receptors, suggesting that its function is evolutionarily important (Bradley et al., 1996; Flor et al., 1997; Kinoshita et al., 1998).

$mGlu_7$ appears to be the only group III mGlu present at the SC-CA1 synapse in the hippocampus in adult animals (Baskys and Malenka, 1991; Kosinski et al., 1999; Ayala et al., 2008) where it is localized presynaptically in the cleft of glutamatergic SC terminals (Shigemoto et al., 1996) and perfectly poised to serve as an autoreceptor activated by synaptically released glutamate to inhibit neurotransmission. Consistent with this observation, agonists that activate $mGlu_7$ inhibit transmission at the SC-CA1 synapse (Baskys and Malenka, 1991; Gereau and Conn, 1995b; Ayala et al., 2008; Jalan-Sakrikar et al., 2014). While activation of $mGlu_7$ can reduce SC-CA1 transmission, previous studies have failed to provide clear evidence that $mGlu_7$ serves as an autoreceptor that can be activated by glutamate released from SC terminals (Losonczy et al., 2003). This has largely been due to a lack of selective $mGlu_7$ antagonists and reliance on the non-selective group III orthosteric agonist, L-AP4 (Rosemond et al., 2004). Recently, two novel compounds have been developed that now allow for more focused studies regarding $mGlu_7$. While also a highly potent $mGlu_4$ agonist, the compound LSP4-2022 is an agonist that is the most potent orthosteric activator of $mGlu_7$ reported to date (Goudet et al., 2012). Additionally, the novel negative allosteric modulator (NAM), ADX71743, is a highly selective $mGlu_7$ antagonist with both in vitro and in vivo efficacy (Kalinichev et al., 2013). Using these new tools, we provide evidence that stimulation of glutamatergic SC afferents does not activate $mGlu_7$ on presynaptic glutamatergic terminals but predominantly activates $mGlu_7$ heteroceptors to reduce GABA release from inhibitory synapses. Furthermore, $mGlu_7$-dependent disinhibition is required for induction of LTP by high frequency stimulation at this synapse. These findings challenge the prevailing view that $mGlu_7$ is an autoreceptor at SC terminals and suggest that

activation of $mGlu_7$ by glutamatergic afferents may increase overall excitatory drive by reducing synaptic inhibition and enhancing LTP. These data add to an emerging interest in $mGlu_7$ as a novel therapeutic target for enhancing cognition.

Results

Stimulation of SC afferents does not induce feedback inhibition of transmission by activation of $mGlu_7$.

If $mGlu_7$ functions as a classical autoreceptor to provide feedback inhibition of transmission at the SC-CA1 synapse, stimulation of SC afferents should induce an activity-dependent decrease in EPSP amplitude that can be reversed by $mGlu_7$ antagonists. This phenomenon has been observed for group II mGlu receptors in the dentate gyrus, where an $mGlu_{2/3}$ antagonist inhibits an activity-dependent reduction in EPSC amplitude that is seen with stimulation of glutamatergic afferents (Doherty et al., 2004). We found that the new highly selective $mGlu_7$ NAM, ADX71743 (3 μM) (Kalinichev et al., 2013), inhibits the ability of the recently described $mGlu_7$ agonist, LSP4-2022 (30 μM) (Goudet et al., 2012), to reduce transmission at the SC-CA1 synapse, confirming a role for $mGlu_7$ in reducing transmission with exogenous agonists (LSP4-2022 alone: 82.3 ± 1.7 % of baseline, ADX71743 + LSP4-2022: 102.6 ± 2.2 % of baseline, n = 4 slices) (**Figure 7A, B**). While LSP4-2022 activates $mGlu_4$, $mGlu_7$, and $mGlu_8$, this compound is the most potent $mGlu_7$ agonist to date and is the first $mGlu_7$ agonist that provides selectivity for $mGlu_7$ relative to $mGlu_8$ (Goudet et al., 2012). Since $mGlu_4$ is not present or active at SC-CA1 synapses (Ayala et al., 2008), LSP4-2022

provides an excellent tool to probe $mGlu_7$ function at SC-CA1 synapses in adult animals. The concentrations of ADX71743 and LSP4-2022 used in these studies were based on extensive studies evaluating the potencies of these compounds $mGlu_7$-expressing cell lines. These studies were consistent with published results and an established IC_{50} of 300 nM for ADX71743 and an EC_{50} of 10 μM for LSP4-2022 at $mGlu_7$, respectively (data not shown).

To test the hypothesis that $mGlu_7$ serves as an autoreceptor at the SC-CA1 synapse, we measured fEPSPs in 6 week old C57BL6/J male mice in response to repeated, low-frequency stimulation in the presence of bicuculline to isolate a pure glutamatergic component. We chose to study this phenomenon in adult animals due to the presence of a developmental switch that occurs between the expression of $mGlu_8$ and $mGlu_7$ at SC-CA1 synapses, where $mGlu_8$ is the only group III mGlu receptor expressed in neonatal animals and $mGlu_7$ is the only one present in adult animals (Ayala et al., 2008). Initially, we applied 10 Hz stimulation for 0.5 sec to induce a series of 5 fEPSPs. In contrast to previous studies of group II mGlu receptors at the mossy fiber-hilar interneuron synapse (Doherty et al., 2004), there was a slight increase, rather than decrease, in fEPSP slope relative to the initial fEPSP with each subsequent stimulation in the train (**Figure 7C, D**). To determine if fEPSP slope was influenced by activation of $mGlu_7$ during this train, 3 μM ADX71743 was bath applied after a 10 minute baseline recording. We have determined that this concentration of ADX71743 completely blocks effects of LSP4-2022 on fEPSP slope at this synapse (**Figure 7A, B**). Interestingly, ADX71743 had no significant effect on fEPSP slope for any of the five fEPSPs in the train (**Figure 7C, D**; black traces vs. red traces). These results indicate that $mGlu_7$ does

not function as a traditional autoreceptor to reduce presynaptic glutamate release using this low-frequency repeated stimulation paradigm.

The lack of effect of ADX71743 on fEPSP slope with low-frequency stimulation, coupled with $mGlu_7$'s extremely low affinity for glutamate, raises the possibility that $mGlu_7$ is only activated with stronger, higher frequency activity that may be necessary to release sufficient glutamate into the SC-CA1 synapse to activate $mGlu_7$. If so, rather than being activated under conditions of normal low-frequency activity, $mGlu_7$ could act as a brake to reduce glutamate release only under conditions of extremely high frequency firing. To investigate this possibility, we employed a stimulation paradigm that mimicked a classical high frequency stimulation (HFS) paradigm used to induce LTP at the SC-CA1 synapse. For this high-frequency protocol, an initial fEPSP was generated 550 ms prior to a train of 10 pulses delivered at 100 Hz. 550 ms after the last pulse of the train, a second fEPSP was generated as a test response. This paradigm was repeated every 30 seconds. We then measured the ratio between the slope of the initial fEPSP (stimulation 1) and the slope of the test response fEPSP (stimulation 2) (ratio calculated as fEPSP slope 2/ fEPSP slope 1). We found no significant change in the ratio between the two fEPSP slopes in response to ADX71743 treatment (black traces vs. red traces) (**Figure 7 E, F**). These results suggest that $mGlu_7$ does not act as an autoreceptor at SC-CA1 synapses to decrease glutamate release, even with this high frequency stimulation protocol.

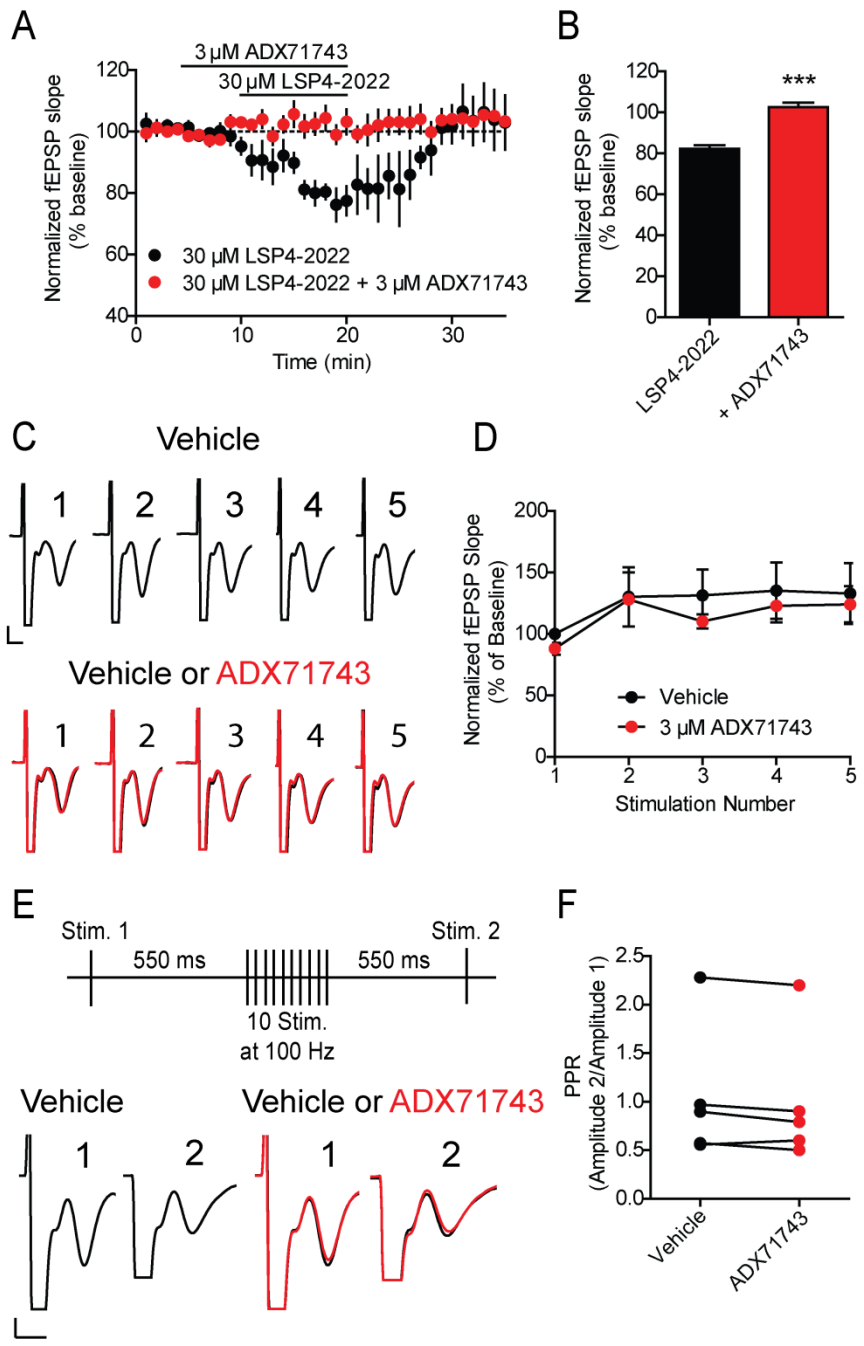

Figure 7. mGlu$_7$ does not act as an auto-receptor at SC-CA1 synapses. fEPSPs were recorded at SC-CA1 synapses after stimulation of axon fibers originating in CA3 with a bipolar electrode. ADX71743 or LSP4-2022 was bath applied. (A) Application of 30 µM LSP4-2022 results in a depression of the fEPSP slope. Pre-treatment with 3 µM ADX71743 for 5 minutes prior to co-application of 3 µM ADX71743 and 30 µM LSP4-2022 prevented the effects of LSP4-2022 alone. Data are normalized to the averaged baseline fEPSP slope. Drug addition is denoted by black lines. (B) Quantification of normalized fEPSP slopes during LSP4-2022 alone and co-application of both LSP4-2022 and ADX71743. Values represent mean ± SEM (*** p = 0.004, two-tailed Student's t

test, n = 4 slices, df = 6). (C) fEPSPs were recorded at SC-CA1 synapses in the presence of 20 µM bicuculline after stimulation of axon fibers from CA3 with a bipolar electrode. ADX71743 or DMSO vehicle was bath applied. Sample traces from an individual, representative experiment. Five fEPSPs were generated by applying 5 stimulations at 10 Hz. The black traces indicate the fEPSPs stimulated during DMSO vehicle conditions, while the red traces represent the fEPSPs stimulated during addition of 3 µM ADX71743. Scale bars represent 1 mV by 4 ms. (D) Application of 3 µM ADX71743 did not significantly alter the slope of any of the fEPSPs in the train. Values represent mean ± SEM (p = 0.318, two-way ANOVA, n = 5 slices, df = 1, 30). (E) Sample traces from an individual, representative experiment. A stimulation paradigm was utilized in which an initial stimulation was applied. 550 ms later, a burst of 10 stimulations delivered at 100 Hz was given, followed 550 ms later by a second single stimulation. The black traces indicate the fEPSPs resulting during DMSO vehicle conditions, and the red traces indicate the fEPSPs during addition of 3 µM ADX71743. Scale bars represent 1 mV by 4 ms. (F) Application of 3 µM ADX71743 did not significantly alter the calculated ratio between the two fEPSPs. Values represent mean ± SEM (p = 0.093, two-tailed Student's t test, n = 5 slices, df = 4).

mGlu$_7$ decreases monosynaptic GABAergic IPSCs

In addition to its localization on presynaptic terminals of excitatory synapses onto CA1 pyramidal cells, mGlu$_7$ is also localized on presynaptic terminals of excitatory synapses onto inhibitory interneurons and on inhibitory GABAergic synapses onto pyramidal cells. If stimulation of SC afferents activates mGlu$_7$ at either of these locations, this could reduce inhibitory transmission in CA1 pyramidal cells. Due to the lack of a clear role for mGlu$_7$ as a classical autoreceptor at SC-CA1 pyramidal cell synapses, we evaluated the potential role of mGlu$_7$ in regulating inhibitory transmission in area CA1. Whole cell patch-clamp techniques were used to record evoked IPSCs (eIPSCs) in visually identified CA1 pyramidal cells from acute brain slices from 6 week old C57BL6/J male mice. Studies of the effect of LSP4-2022 on paired-pulse IPSCs revealed that application of 30 µM LSP4-2022 caused a significant decrease in IPSC amplitude (80.2 ± 2.4% of baseline, n = 7 cells) (**Figure 8 A, B, D**) with a concomitant increase in the paired pulse ratio (PPR, 0.69 ± 0.04 in baseline vs. 0.87 ± 0.06 in LSP4-

2022) (**Figure 8 F**). The effect of LSP4-2022 on eIPSC amplitude washed out from most cells (5 out of 7 cells) after 15 minutes of perfusion with normal aCSF (**Figure 8 E**). Additionally, LSP4-2022 had no effect on IPSC kinetic parameters, including the rise time or decay time of IPSCs (rise time: 9.23 ± 0.7 ms at baseline vs. 9.32 ± 0.7 ms during LSP4-2022 addition, decay time: 129.4 ± 6.6 at baseline vs. 116.9 ± 7.9 ms during LSP4-2022 addition) (**Figure 8 C, G, H**). Consistent with the hypothesis that the effects of LSP4-2022 are mediated by $mGlu_7$, these effects were completely blocked by the $mGlu_7$ NAM, ADX71743 (data not shown).

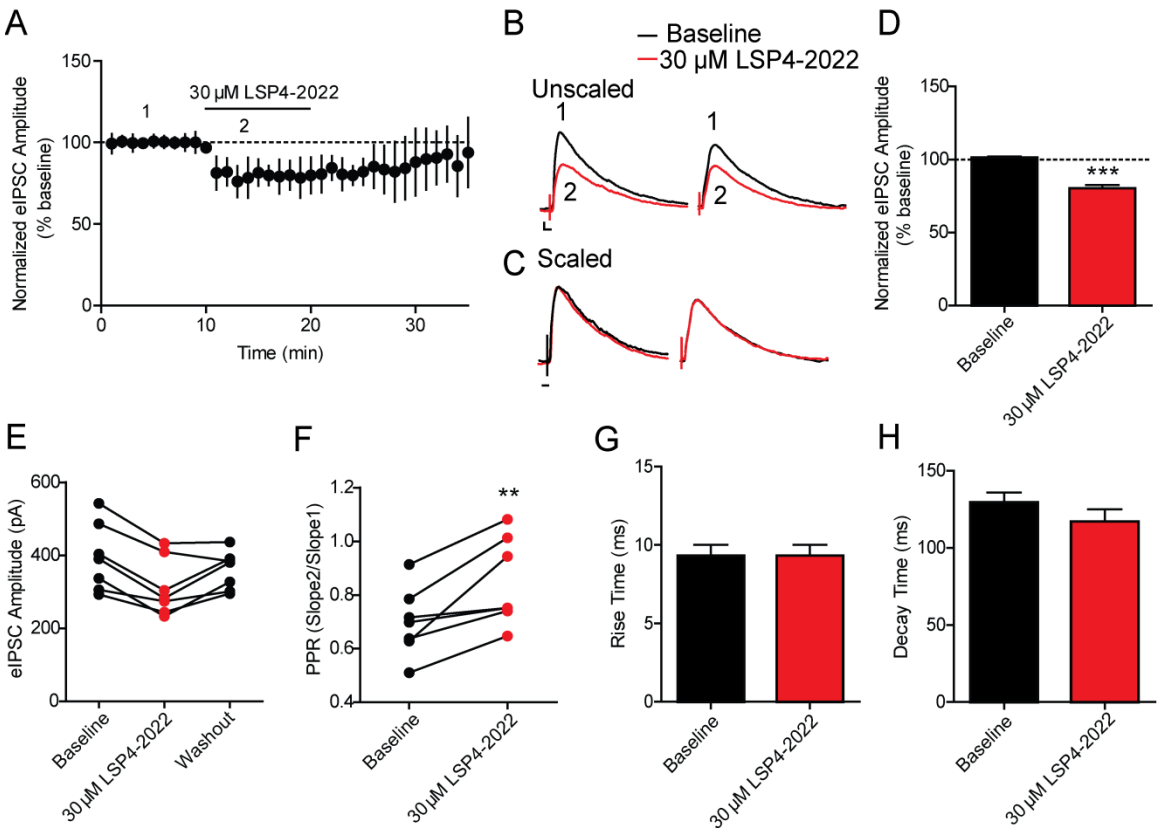

Figure 8. Application of the mGlu$_7$ agonist, LSP4-2022, decreases poly-synaptic eIPSC amplitudes. eIPSCs were recorded in hippocampal CA1 pyramidal neurons after stimulation of axon fibers from CA3 with a bipolar electrode. (A) Application of 30 µM LSP4-2022 caused a reduction in polysynaptic eIPSC amplitude over time. Data are normalized to the average baseline eIPSC amplitude. Drug application is denoted by the solid black line. (B) Sample traces from an individual, representative experiment. Paired pulses were applied 200 ms apart. (1, black trace) Baseline poly-synaptic eIPSC amplitudes were reduced by application of (2, red trace) 30 µM LSP4-2022. Scale bars represent 50 pA by 10 ms. (C) Scaling of LSP4-2022 traces (red trace from (B)) to baseline traces indicates no changes in eIPSC kinetics. Scale bar represents 10 ms. (D) Quantification of normalized poly-synaptic eIPSC amplitudes during baseline and LSP4-2022 addition. Values represent mean ± SEM. (***$p < 0.0001$, two-tailed Student's t test, $n = 7$ cells, df = 12). (E) The effects of LSP4-2022 addition washed out in most cells (5 of 7 cells) after 15 minutes of perfusion with normal aCSF. Values of eIPSC amplitudes for individual experiments during baseline, LSP4-2022 addition, and washout are represented by points connected by a line. (F) Application of 30 µM LSP4-2022 resulted in a significant increase in the PPR. PPR was calculated as the amplitude of the second IPSC divided by the amplitude of the first IPSC. Values for individual experiments are represented by points connected by a line. (** $p = 0.0074$, two-tailed Paired t test, $n = 7$ cells, df = 6). (G, H) Application of 30 µM LSP4-2022 had no effect on the rise time (G) or decay time (H) of polysynaptic eIPSCs (rise time: $p = 0.98$, two-

tailed Student's *t* test, $n = 7$ cells, df = 12, decay time: $p = 0.251$, two-tailed Student's *t* test, $n = 7$, df = 12).

These results suggest that activation of $mGlu_7$ decreases GABAergic synaptic transmission in CA1 pyramidal cells, and that this is likely mediated by a presynaptic mechanism. However, these studies do not provide insights as to whether $mGlu_7$ reduces inhibitory transmission by actions at excitatory synapses onto inhibitory interneurons or direct inhibition of GABA release at inhibitory synapses onto pyramidal cells. To determine if $mGlu_7$ functions presynaptically on GABAergic terminals, we isolated monosynaptic IPSCs by incubating slices with a combination of CNQX and D-AP5, antagonists of AMPA receptor and NMDA receptors, respectively, to block glutamatergic transmission. This experimental paradigm allowed us to remove the contribution of any $mGlu_7$ expressed presynaptically on glutamatergic terminals synapsing onto interneurons and allowed us to isolate monosynaptic IPSCs to evaluate effects of $mGlu_7$ expressed on GABAergic interneurons. Slices were pre-treated with a combination of 20 µM CNQX and 50 µM D-AP5 for several minutes until stable monosynaptic IPSCs were obtained. These IPSCs could be completely blocked by the application of 20 µM bicuculline (data not shown). 30 µM LSP4-2022 was then perfused for 10 minutes onto the slice, which resulted in a significant decrease in IPSC amplitude (78.4 ± 1.8% of baseline, $n = 7$ cells) (**Figure 9 A, B, D**) and also resulted in a significant increase in PPR (0.6 ± 0.02 during baseline vs. 0.7 ± 0.02 in LSP4-2022) (**Figure 9 F**). The effect of LSP4-2022 on eIPSC amplitude washed out from most cells (5 out of 7 cells) after 15 minutes of perfusion with normal aCSF (**Figure 9 E**). The kinetic parameters of the IPSCs did not significantly change with application of LSP4-2022 (rise time: 7.9 ± 1.2 ms at baseline vs. 7.8 ± 1.0

ms during LSP4-2022 addition, decay time: 111.6 ± 10.2 ms at baseline vs. 107.9 ± 13.1 ms during LSP4-2022 addition) (**Figure 9 C, G, H**). These results support previous anatomical studies suggesting that $mGlu_7$ is expressed presynaptically on GABAergic terminals (Kinoshita et al., 1998), and demonstrate that LSP4-2022 can activate $mGlu_7$ and decrease GABA release from these cells.

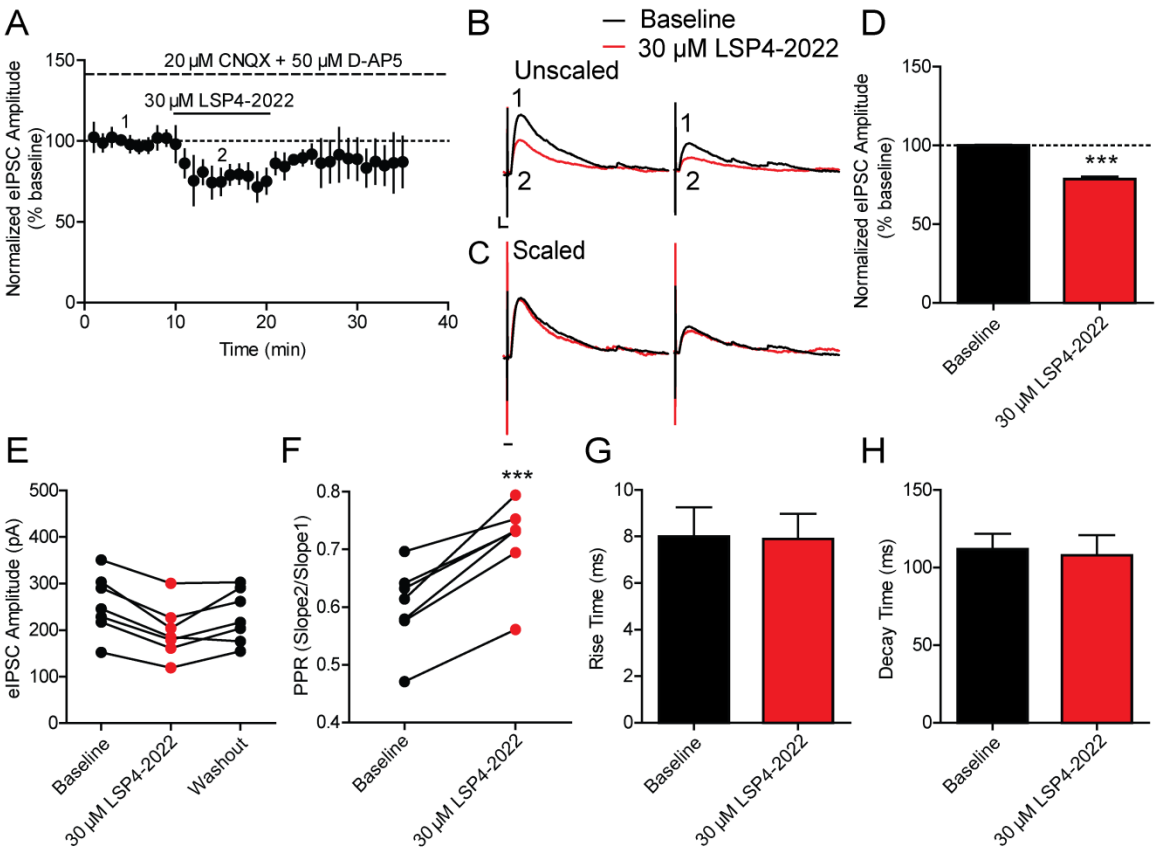

Figure 9. Application of 30 µM LSP4-2022 decreases monosynaptic eIPSCs. (A) 20 µM CNQX and 50 µM D-AP5 were bath applied (large dashed line) prior to application of 30 µM LSP4-2022 (black solid line) to isolate mono-synaptic eIPSCs. (B) Sample traces from individual, representative experiment. Paired pulses were applied 200 ms apart. (1, black trace) Baseline monosynaptic eIPSC amplitudes were reduced by application of (2, red trace) 30 µM LSP4-2022. Scale bars represent 50 pA by 10 ms. (C) Scaling of LSP4-2022 trace (red trace from (B)) to baseline traces indicates no change in eIPSC kinetics. Scale bar represent 10 ms. (D) Quantification of normalized mono-synaptic eIPSC amplitudes during baseline and LSP4-2022 addition. Values represent mean ± SEM. (***p = 0.001, two-tailed Student's t test, n = 7 cells, df = 12). (E) The effects of LSP4-2022 addition washed out in most cells (5 of 7 cells) after 15 minutes of perfusion with normal aCSF. Values of eIPSC amplitudes for individual experiments during baseline, LSP4-2022 addition, and washout are represented by points connected by a line. (F) Application of 30 µM LSP4-2022 resulted in a significant increase in the PPR. Values for individual experiments are represented by points connected by a line. (*** p = 0.0004, two-tailed Paired t test, n = 7 cells, df = 6). (G, H) Application of 30 µM LSP4-2022 had no effect on rise time (G) or decay time (H) of monosynaptic eIPSCs (rise time: p = 0.94, two-tailed Student's t test, n = 7, df = 12, decay time: p = 0.82, two-tailed Student's t test, n = 7, df = 10).

The ability of LSP4-2022 to reduce eIPSC amplitude even when glutamatergic transmission is blocked strongly suggests that the primary location of $mGlu_7$ is directly on GABAergic terminals. However, while the previous experimental set-up eliminates the contribution of $mGlu_7$ expressed in glutamatergic terminals, it does not prevent the effects of neuromodulators that may be released in response to electrical stimulation. To remove the contribution of neuromodulators, such as norepinephrine, acetylcholine, serotonin, brain derived neurotrophic factor (BDNF) and others, and to further isolate only $mGlu_7$ expressed on interneurons, we utilized mice that expressed channel rhodopsin 2 (ChR2) in parvalbumin (PV)-expressing interneurons, as PV interneurons represent the largest populations of interneurons in this area (Kawaguchi et al., 1987; Klausberger et al., 2005). This allowed us to directly activate only interneurons without the co-incident release of other neuromodulatory factors. Paired optically-activated IPSCs (oIPSCs) were recorded from CA1 pyramidal cells and evoked using 473 nm light. After a 10 minute baseline period, 30 μM LSP4-2022 was perfused for an additional 10 minutes, which resulted in a significant decrease in oIPSC amplitude (76 ± 65.1% of baseline, n = 6 cells) (**Figure 10 A, B, D**) and also resulted in a significant increase in PPR (0.6 ± 0.02 during baseline vs. 0.73 ± 0.03 in LSP4-2022) (**Figure 10 F**). The effect of LSP4-2022 on oIPSC amplitude washed out from most cells (4 out of 6 cells) after 15 minutes of perfusion with normal aCSF (**Figure 10 E**). The kinetic parameters of the IPSCs did not significantly change with application of LSP4-2022 (rise time: 3.2 ± 0.5 ms during baseline vs. 3.0 ± 0.6 ms in LSP4-2022, Decay Time: 205.4 ± 26.6 ms during baseline vs. 182.7 ± 18.2 ms in LSP4-2022) (**Figure 10 C, G, H**). These results further support the

hypothesis that $mGlu_7$ can decrease GABA release in a monosynaptic fashion, particularly without the contribution of other neuromodulators.

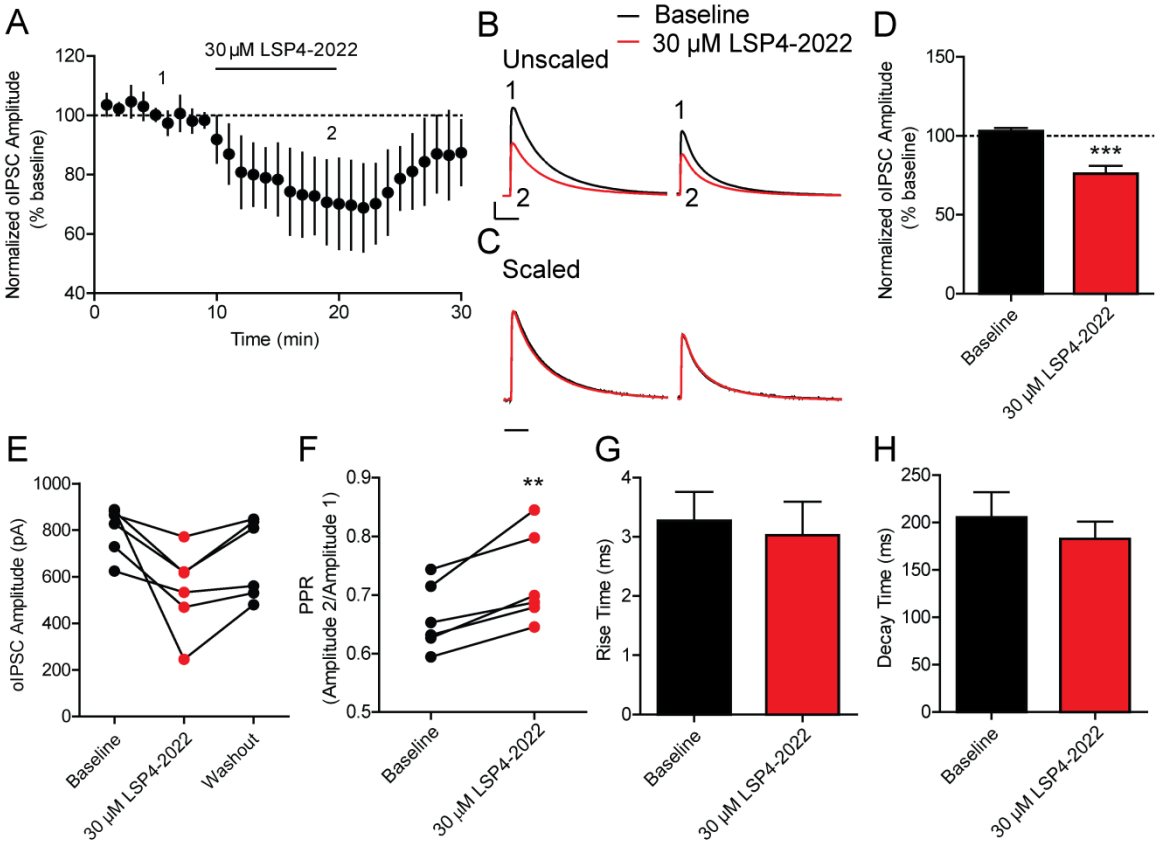

Figure 10. Application of 30 µM LSP4-2022 decreases GABAergic interneuron-specific optically-induced IPSCs. Paired oIPSCs were delivered by stimulating using 473 nm blue light. (A) Application of 30 µM LSP4-2022 (black line) resulted in a decrease of oIPSC amplitude over time. (B) Sample traces from an individual, representative experiment. Paired stimulations were applied 700 ms apart. (1, black trace) Baseline oIPSC amplitudes were reduced by (2, red trace) 30 µM LSP4-2022. Scale bars represent 400 pA by 60 ms. (C) Scaling of LSP4-2022 trace (red trace from (B)) to baseline traces indicated no change in oIPSC kinetics. Scale bar represents 60 ms. (D) Quantification of normalized oIPSC amplitudes during baseline and LSP4-2022 addition. Values represent mean ± SEM. (*** $p = 0.0006$, two-tailed Student's t test, $n = 6$ cells, df = 10). (E) The effects of LSP4-2022 addition washed out in most cells (4 of 6 cells) after 15 minutes of perfusion with normal aCSF. Values of oIPSC amplitudes for individual experiments during baseline, LSP4-2022 addition, and washout are represented by points connected by a line. (F) Application of 30 µM LSP4-2022 resulted in a significant increase in the PPR. Values for individual experiments are represented by points connected by a line (** $p = 0.005$, two-tailed Paired t test, $n = 6$ cells, df = 5). (G, H) Application of 30 µM LSP4-2022 had no effect on rise time (G) or

decay time (H) of oIPSCs (rise time: $p = 0.75$, two-tailed Student's t test, $n = 6$ cells, df = 10, decay time: $p = 0.49$, two-tailed Student's t test, $n = 6$ cells, df = 10).

High frequency stimulation of SC afferents induces an $mGlu_7$-dependent decrease in monosynaptic GABAergic IPSCs

Our results and previous studies (Losonczy et al., 2003), suggest that $mGlu_7$ may not act as a traditional autoreceptor to decrease glutamate release in response to synaptic activation at glutamatergic synapses in area CA1. It is possible that a more prominent role of $mGlu_7$ in responding to activation of SC afferents is as a heteroceptor, where it could decrease GABA release in response to activation of SC afferents. If so, this could lead to a net increase, rather than decrease, in excitatory drive through area CA1. To assess the role of $mGlu_7$ heteroceptors in modulating responses to activation of SC afferents, we measured the effects of low-frequency and high-frequency stimulation on monosynaptic IPSCs in CA1 pyramidal cells. Initially, we measured IPSCs evoked by low frequency stimulation (5 Hz stimulation for 1 sec). Using this stimulation paradigm, we observed a decrease in IPSC amplitude with each subsequent stimulus (Figure 5 A, B, black line). To determine whether activation of $mGlu_7$ contributes to this activity-dependent depression of IPSCs, we established a baseline response for 5 minutes and then applied ADX71743 (3 μM) for 10 minutes and measured the change in amplitude for each IPSC as a percent of the first IPSC amplitude during the baseline period. ADX71743 did not induce a significant change in any of the IPSCs in the train (**Figure 11 A, B** black line vs. red line), suggesting that $mGlu_7$ activation does not contribute to activity-dependent depression of IPSCs with low-frequency stimulation. We then utilized a high-frequency stimulation paradigm, similar to the one used to investigate the

effect of $mGlu_7$ antagonists on fEPSPs. As in studies of excitatory transmission, an initial IPSC was generated 550 ms prior to a train of 10 pulses delivered at 100 Hz, repeated every 30 seconds. 550 ms later, a second IPSC was generated as a test response (**Figure 11 C**). Under baseline conditions, the test response elicited 550 ms after the 100 Hz train was smaller in amplitude than the first IPSC induced prior to 100 Hz stimulation. Interestingly, application of ADX71743 (3 µM) reversed the ability of the stimulus train to reduce IPSC amplitude and increased the ratio between the amplitude of the second IPSC and the first IPSC (ratio calculated as IPSC amplitude 2/ IPSC amplitude 1) (ratio = 0.58 ± 0.03 at baseline vs. 0.65 ± 0.02 during ADX71743 addition) (**Figure 11 D, E**). To confirm the effects of ADX71743, we repeated these experiments using the nonselective but well characterized orthosteric mGlu receptor antagonist, LY341495, which has an IC_{50} at $mGlu_7$ of approximately 1 µM (Kingston et al., 1998). Consistent with the effects of ADX71743, 100 µM LY341495 had no effect on IPSCs using the low frequency (0.5 Hz) protocol (**Figure 11 F, G**). However, 100 µM LY341495 had an effect that was similar to that of ADX71743 on responses to 100 Hz (**Figure 11 H, I**; ratio = 0.59 ± 0.03 at baseline vs. 0.68 ± 0.03 during LY341495 addition). To confirm that the effect on the ratio was drug-induced and not due to current run-down, we performed several experiments in which the stimulation protocol was run for 15 minutes with no drug addition, and observed no significant change in the ratio (data not shown). Collectively, these results suggest that $mGlu_7$ decreases GABA release in a frequency-dependent manner, and that, under HFS conditions, $mGlu_7$ activation reduces GABA release.

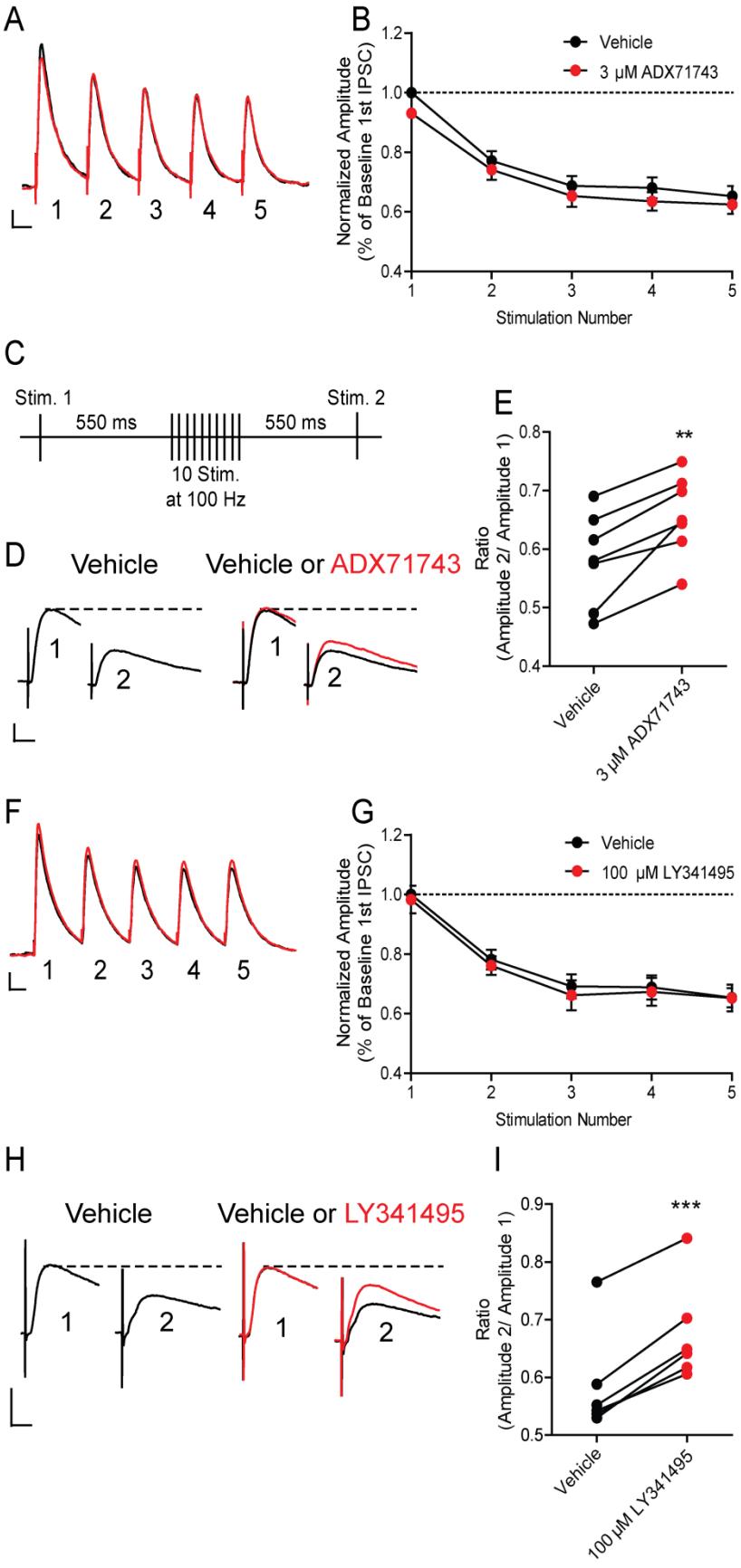
A
1 2 3 4 5
B
Vehicle
3 μM ADX71743
Normalized Amplitude
(% of Baseline 1st IPSC)
1.2
1.0
0.8
0.6
0.4
1 2 3 4 5
Stimulation Number
C
Stim. 1
Stim. 2
550 ms
550 ms
10 Stim.
at 100 Hz
D
Vehicle
Vehicle or ADX71743
1 2
1 2
E
Ratio
(Amplitude 2/ Amplitude 1)
0.8
0.7
0.6
0.5
0.4
**
Vehicle
3 μM ADX71743
F
1 2 3 4 5
G
Vehicle
100 μM LY341495
Normalized Amplitude
(% of Baseline 1st IPSC)
1.2
1.0
0.8
0.6
0.4
1 2 3 4 5
Stimulation Number
H
Vehicle
Vehicle or LY341495
1 2
1 2
I
Ratio
(Amplitude 2/ Amplitude 1)
0.9
0.8
0.7
0.6
0.5
***
Vehicle
100 μM LY341495

Figure 11. $mGlu_7$ reduces GABA release in a frequency-dependent manner. (A) Sample traces from an individual, representative experiment. Application of 3 µM ADX71743 (red line) has no effect on any of the IPSC amplitudes in the train. Scale bars represent 200 pA by 200 ms. (B) Normalized amplitude of each IPSC represented as percent of the baseline 1st IPSC amplitude with or without 3 µM ADX71743 ($p = 0.299$, two-way ANOVA, $n = 5$, df = 1, 32). (C) Schematic of stimulation paradigm. An initial stimulation was applied 550 ms prior to 10 stimulations at 100 Hz. 550 ms later, a second test stimulation was applied. (D) Sample traces from an individual, representative experiment with ADX71743. 1st IPSC represents stimulation 1 from schematic and 2nd IPSC represents stimulation 2. During vehicle conditions, there is a reduction in the 2nd IPSC amplitude. Application of 3 µM ADX71743 results in an increase in the second IPSC amplitude after the 100 Hz stimulation. Scale bars represent 100 pA by 20 ms. (E) Application of 3 µM ADX71743 results in a significant increase in the ratio of the two IPSCs (** $p = 0.0021$, two-tailed Paired *t* test, $n = 7$, df = 6). (F) A train of 5 IPSCs was evoked by stimulating CA3 axon fibers with a bipolar electrode at a frequency of 5 Hz. Sample traces from an individual, representative experiment. Application of 100 µM LY341495 (red line) had no effect on any of the IPSC amplitudes in the train. Scale bars represent 200 pA by 200 ms. (G) Normalized amplitude of each IPSC represented as percent of the baseline 1st IPSC amplitude with or without 100 µM LY341495 ($p = 0.504$, two-way ANOVA, $n = 3$ cells, df = 1, 20). (H) Sample traces from an individual, representative experiment with LY341495. Application of 100 µM LY341495 resulted in an increase in the second IPSC after the 100 Hz stimulation. Scale bars represent 100 pA by 10 ms. (G) Application of 100 µM LY341495 resulted in a significant increase in the ratio of the two IPSCs. The ratio was calculated as the amplitude of stimulation 2 IPSC divided by the amplitude of stimulation 1 IPSC (*** $p = 0.0001$, two-tailed Paired *t* test, $n = 6$, df = 5).

$mGlu_7$ activation is necessary for induction of LTP at SC-CA1 synapses in the hippocampus

High frequency stimulation (HFS) at the SC-CA1 synapse results in a long term potentiation (LTP) that has previously been shown to be mediated by NMDA receptors (Morris et al., 1986). Induction of NMDA receptor (NMDAR)-dependent LTP at the SC-CA1 pyramidal cell synapses requires coincident release of glutamate from presynaptic SC terminals and depolarization of CA1 pyramidal cells to allow release of voltage-dependent block of NMDARs by magnesium (Granger and Nicoll, 2014). Activation of inhibitory interneurons in area CA1 by SC activation can oppose pyramidal cell

depolarization required for induction of LTP, and $GABA_A$ receptor antagonists facilitate LTP induction (Debray et al., 1997). Because $mGlu_7$ decreases GABA release under HFS conditions, we sought to determine if this mechanism played a role in the induction of LTP. To probe this possibility, HFS was applied and fEPSPs were recorded in area CA1 of the hippocampus. A saturating form of LTP was induced by applying 2 trains of HFS (100 Hz, 1 sec in duration, 20 sec ITI). Consistent with previous studies (Harris and Teyler, 1984; Collingridge et al., 1988), this resulted in a robust LTP assessed one hour post-HFS (141.9 ± 7.1% of baseline). Pre-treatment of slices with the $mGlu_7$ NAM, ADX71743 (3 µM), for 20 minutes prior to HFS resulted in an almost complete blockade of LTP induction (100.6 ± 1.4% of baseline) (**Figure 12 A, B**). As ADX71743 is a newly described $mGlu_7$ NAM, we performed the same experiment in the presence of 300 nM ADX71743, which is a concentration that should no longer fully block $mGlu_7$ in slices (the IC_{50} in in-house cell lines is 300 ± 57 nM (data not shown)) . Pre-treatment with 300 nM ADX71743 for 20 minutes prior to HFS was no longer sufficient to block LTP (control: 143.2 ± 6.4% of baseline, 300 nM ADX71743: 147.1 ± 6.4% of baseline) (**Figure 12 A, B**). Furthermore, pretreatment with either 10 µM or 100 µM LY341495, two concentrations well above the IC_{50} at $mGlu_7$, for 20 minutes prior to HFS stimulation resulted in a similar blockade of LTP (100.2 ± 2.7% of baseline for 10 µM LY341495, 106.9 ± 5.8% of baseline for 100 µM LY341495) (**Figure 12 C, D**). Pretreatment with 100 nM LY341495, a concentration well below the IC_{50} at $mGlu_7$ but one that blocks the group II mGlu receptors, did not result in a significant blockade of LTP (134.6 ± 19.6 % of baseline) (**Figure 12 C, D**). To determine if there was an effect of either ADX71743 or LY341495 on any of the responses generated during the HFS, we measured the slopes

of the fEPSPs generated during the first train of 100 Hz stimulation. We observed no significant change in the slope of the fEPSP generated after the first stimulation in the train with addition of either 3 µM ADX71743 or 10 µM LY341495, indicating that $mGlu_7$ is not active prior to the HFS (Control: 100.0 ± 14.8%, ADX71743: 114.7 ± 29.6%, LY341495: 104.4 ± 20.5% of control 1^{st} fEPSP slope) (**Figure 12 E, F, G**). We chose to investigate the 10 µM LY341495 concentration because this was the lowest concentration sufficient to block LTP. Examining the fEPSP slopes at stimulus 20, 40, 60, 80, or 100 within the train, we observed a significant reduction in the fEPSP slopes at stimulus 20 and 40 when compared to the slope of the first fEPSP with ADX71743 or LY341495 treatment, indicating that the responses decayed faster when $mGlu_7$ was blocked (stimulus 20: control: 18.7 ± 2.3%, ADX71743: 9.7 ± 2.5%, LY341495: 7.0 ± 2.1% of first fEPSP slope, stimulus 40: control: 12.6 ± 1.9%, ADX71743: 4.6 ± 2.1%, LY341495: 1.8 ± 1.6% of first fEPSP slope) (**Figure 12 H**). These results are consistent with our finding described above (**Figure 11**) and indicate that $mGlu_7$ activation during the HFS, which leads to an increase in excitation of CA1 cells resulting from $mGlu_7$-mediated disinhibition, is required for induction of LTP at SC-CA1 synapses.

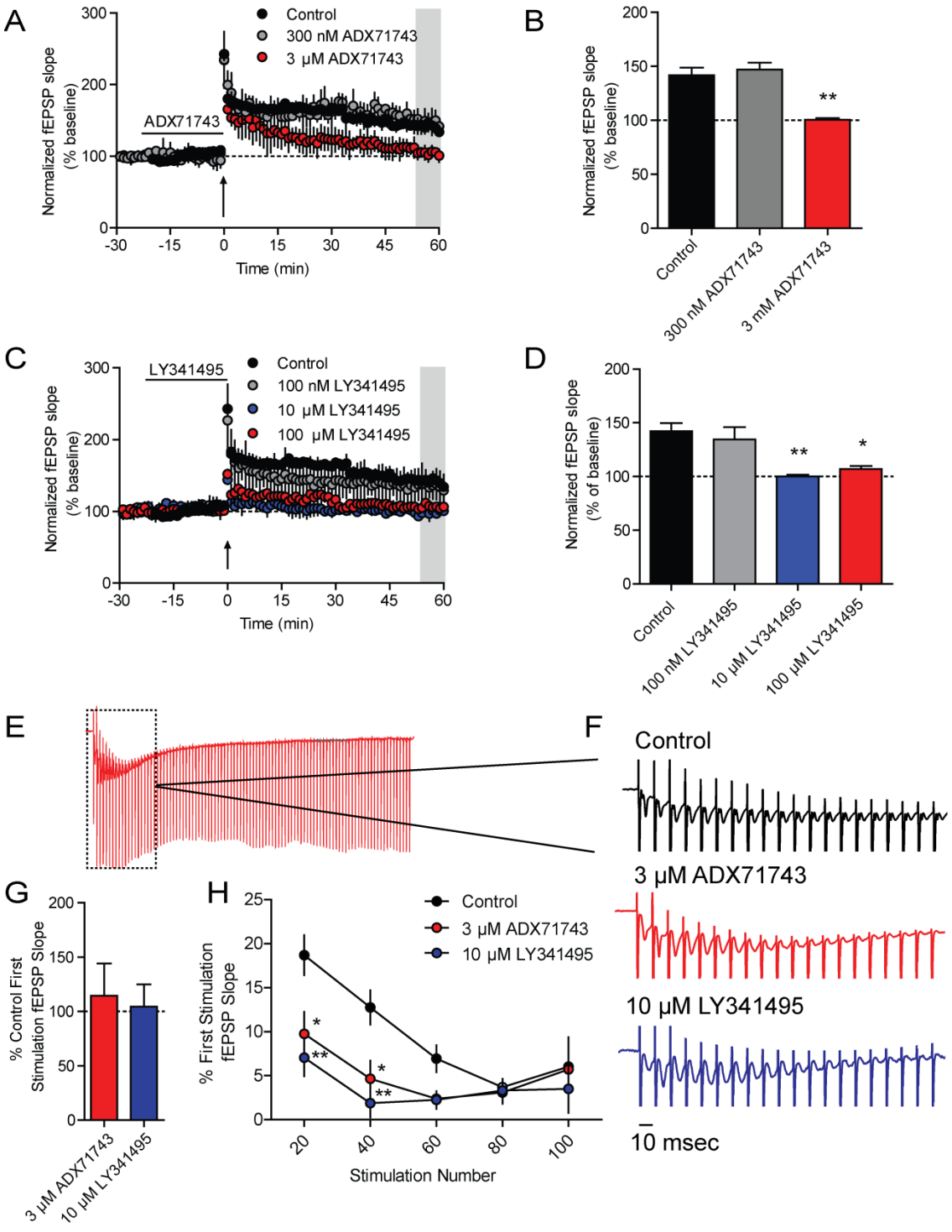

Figure 12. Antagonism of $mGlu_7$ impairs long term potentiation at SC-CA1 synapses. fEPSPs were recorded at SC-CA1 synapses after stimulation of the axon fibers coming from CA3 with a bipolar electrode. All compounds were bath applied. (A) Application of the $mGlu_7$ NAM, ADX71743 (3 μM), for 20 minutes prior to 100 Hz HFS (indicated by arrow) impairs long term potentiation. Application of a lower

concentration of ADX71743 (300 nM) is no longer sufficient to block LTP. (B) Quantification of long term potentiation was determined by averaging the values during the last 5 minutes of recording (shaded grey area in (A)). Values represent mean ± SEM (Overall $p = 0.0004$, one-way ANOVA with Bonferonni's posttest, Control vs. 3 µM ADX71743 $^{**}p < 0.01$, $n = 3\text{-}4$, df = 2, 10). (C) Application of high concentrations of LY341495 (10 µM and 100 µM) are sufficient to impair long term potentiation, whereas a low concentration, 100 nM, does not. (D) Quantification of long term potentiation was determined by averaging the values during the last 5 minutes of recording (shaded grey area in (C)). Values represent mean ± SEM (overall $p = 0.003$, one-way ANOVA with Bonferonni's posttest, Control vs. 10 µM LY341495 $^{**}p < 0.01$, Control vs. 100 µM LY341495 $^{*}p < 0.05$, $n = 3\text{-}4$, df = 3, 9). (E) Representative trace of the first train of 100 Hz stimulation in control conditions. The dashed box indicates the area that is magnified in (F). (F) Sample traces of the first 20 stimulations of the HFS. Application of either 3 µM ADX71743 or 10 µM LY341495 results in a faster decay in the fEPSP response throughout the train. Scale bar represents 10 ms. (G) Quantification of the fEPSP generated after the first stimulation within the train. There was no significant effect of either ADX71743 or LY341495 on the slope of the first response. Values represent mean ± SEM ($p = 0.8930$, one-way ANOVA with Bonferonni's posttest, $n = 3\text{-}4$, df = 2, 9). (H) Application of either ADX71743 or LY341495 resulted in a significant reduction in the fEPSP slope at both 20 and 40 stimulations within the HFS train. Values represent mean ± SEM (overall $p = 0.0147$, two-way ANOVA with Bonferonni's posttest, Control vs. ADX71743 at 20 and 40 stimulations $^{*}p < 0.05$, Control vs. LY341495 and 20 and 40 stimulations $^{**}p < 0.01$, $n = 3\text{-}4$, df = 2, 48)

To confirm that the mechanism by which $mGlu_7$ facilitates LTP is via disinhibition, we pre-treated slices with 20 µM bicuculline, a $GABA_A$ antagonist, to remove any contribution of GABAergic transmission to the fEPSPs. Application of 20 µM bicuculline resulted in a significant increase in the fEPSP slope (217.8 ± 10.9% compared to baseline fEPSP slope, data not shown), which stabilized after 10 minutes of continuous bicuculline perfusion. After a stable fEPSP slope was obtained in the presence of 20 µM bicuculline, LTP was induced either in the presence or absence of 20 minute pretreatment with 3 µM ADX71743. LTP was induced with the saturating LTP paradigm of two trains of HFS. Bicuculline alone produced a significantly greater level of LTP compared to normal ACSF conditions (159.2 ± 2.4% for bicuculline vs. 135.2 ± 0.3% for normal ACSF) (**Figure 13 A, B**). The addition of a 20 minute pretreatment with 3 µM

ADX71743 was no longer sufficient to block induction of LTP in the presence of bicuculline (153.1 ± 3.4% of baseline) (**Figure 13 A, B**). To ensure that the increased level of LTP in the presence of bicuculline did not result in changes in local circuitry that could confound the lack of ADX71743 blockade, we modified the stimulation paradigm to achieve a similar magnitude of LTP induction in normal aCSF and in the presence of bicuculline. An input-output curve was first generated in normal aCSF in order to determine the 50% slope value. Slices were then perfused with 20 μM bicuculline, and the stimulation intensity was reduced to generate fEPSPs with the same slope value calculated in normal aCSF. LTP was then generated using two trains of HFS. Under these conditions, we observed no significant difference in the level of LTP between normal aCSF and bicuculline (140.3 ± 2.3% in bicuculline) (**Figure 13 C, D**, small dashed line indicates level of LTP observed in normal aCSF). Additionally, pretreatment with ADX71743 was still not sufficient to block LTP (139.1 ± 2.5%). As a modified version of aCSF was used in these experiments, we next confirmed that the form of LTP induced in the presence of bicuculline was still NMDA receptor-dependent. 20 μM bicuculline was again bath applied until a stable fEPSP slope was obtained. Slices were then pretreated for 10 minutes with 50 μM D-AP5, an NMDA receptor antagonist, prior to HFS. This resulted in a complete blockade of LTP induction (98.2 ± 2.3% compared to LTP induced in the presence of bicuculline alone, data not shown). Taken together, these data indicate that the mechanism by which $mGlu_7$ activation contributes to LTP induction is through a frequency-dependent reduction of GABAergic tone at SC-CA1 synapses. Additionally, the finding that the ability of ADX71743 to block LTP is

completely abolished in the presence of bicuculline further suggests that disinhibition is the primary, if not only mechanism, by which $mGlu_7$ regulates LTP induction.

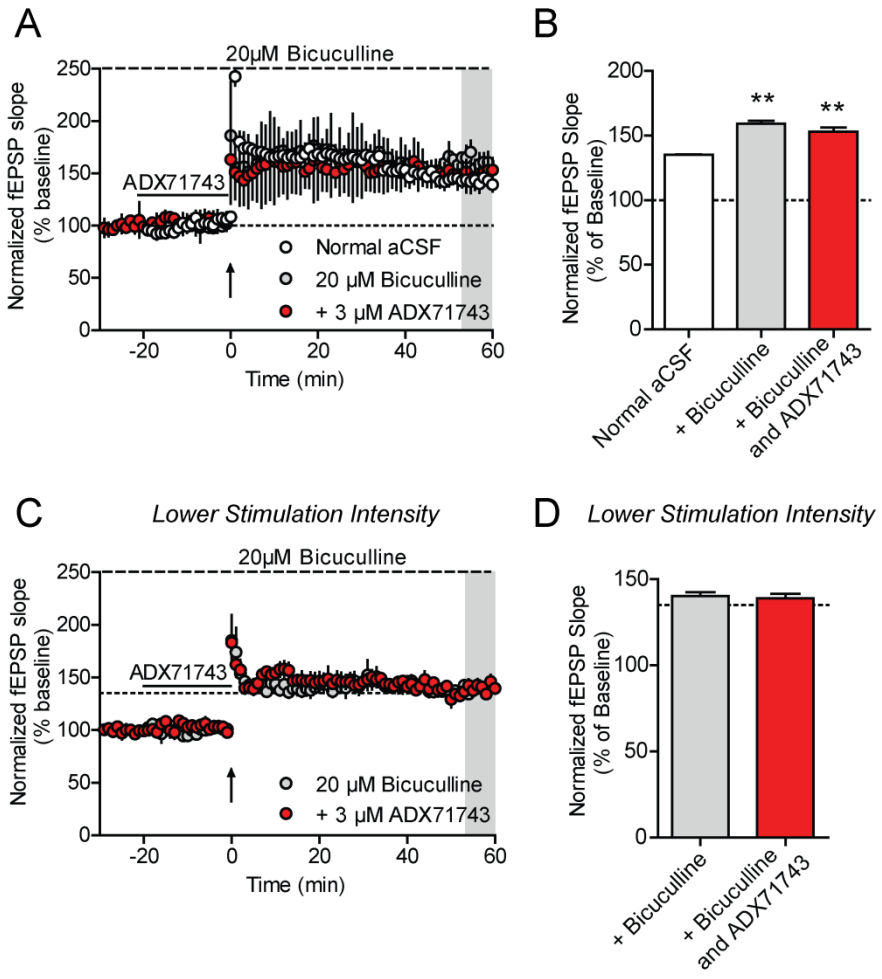

Figure 13. Pretreatment with bicuculline prevents blockade of LTP by ADX71743. (A) 20 μM bicuculline was bath applied to slices either alone or prior to addition of 3 μM ADX71743 (black line). LTP was induced with 2 trains of 100 Hz stimulation (upward-facing arrow). ADX71743 does not block LTP in the presence of bicuculline. (B) Quantification of LTP as determined by averaging the values during the last 5 minutes of recording (shaded grey area in (A)). Addition of bicuculline resulted in a significantly higher level of LTP compared to regular aCSF, which was not blocked by ADX71743. Values represent mean ± SEM (Overall $p = 0.0008$, one-way ANOVA with Bonferonni's posttest, Normal aCSF vs. bicuculline $p < 0.001$, Normal aCSF vs. bicuculline and ADX71743 $p < 0.01$, $n = 3$-4, df = 2, 8). (C) The stimulation intensity was reduced such that the slope value during baseline in the presence of bicuculline was equal to the 50% max slope achieved in normal aCSF. 20 μM bicuculline was bath applied to sliced alone

or prior to addition of 3 μM ADX71743 (black line). LTP was induced with 2 trains of 100 Hz stimulation (upward-facing arrow). The level of LTP induced in normal aCSF is represented by a small dashed line. ADX71743 does not block LTP in the presence of bicuculline at lower stimulation intensities. (D) Quantification of LTP as determined by averaging the values during the last 5 minutes of recording (shaded area in (C)). The level of LTP induced in normal aCSF is represented by a dashed line. There was no significant difference in the level of LTP between normal aCSF, 20 μM bicuculline, and 3 μM ADX71743. Values represent mean ± SEM. (Overall p = 0.3147, one-way ANOVA with Bonferonni's posttest, n = 3-4, df = 2, 8).

Agonism of $mGlu_7$ can potentiate LTP

To further investigate the role of $mGlu_7$ in induction of LTP at SC-CA1 synapses, we performed experiments using a submaximal HFS stimulation paradigm to induce a threshold level of LTP to determine if agonism of $mGlu_7$ could potentiate this threshold level of LTP. Three different HFS paradigms were first used to identify saturating and threshold levels of LTP in our system. One train of HFS (100 Hz, 1 sec) produced a moderate level of LTP (113.8 ± 4.9% of baseline), whereas 2 trains of HFS (20 sec ITI) produced a significantly greater level of LTP (142.4 ± 14.1% of baseline). Additionally, three trains of HFS (20 sec ITI) gave a level of LTP that was not significantly greater than two trains of HFS (151.4 ± 5.0% of baseline) (**Figure 14 A, B**). We next determined if activation of $mGlu_7$ using LSP4-2022 could potentiate induction of LTP in response to a threshold stimulus. Pre-treatment of slices with 30 μM LSP4-2022 for 10 minutes prior to the threshold HFS (1 train of 100 Hz) resulted in a significant potentiation of the level of LTP measured one hour post-HFS (131.6 ± 4.2% of baseline) (**Figure 14 C, D**). As additional validation of an $mGlu_7$-mediated effect, we performed the same experiment with a lower concentration of LSP4-2022 (3 μM), which should no longer activate $mGlu_7$ (Goudet et al., 2012). Pre-treatment of slices with 3 μM LSP4-2022 was no longer sufficient to potentiate LTP induced by one train of HFS (111.5 ±

1.3% of baseline) (**Figure 14 E, F**). Finally, to confirm that the mechanism by which LSP4-2022 potentiates LTP is via disinhibition, we again pre-treated slices with 20 µM bicuculline to remove any GABAergic contribution to the fEPSPs. We utilized the same experimental paradigm as used in **Figure 13 C, D** in order to achieve a similar magnitude of LTP in the presence of bicuculline to that of control conditions. One train of HFS applied in the presence of bicuculline induced a similar magnitude of LTP to that induced in control conditions (114.6 ± 1.5% of baseline) (**Figure 14 G, H**, small dashed line indicates level of LTP observed in normal aCSF). Additionally, in the presence of bicuculline, 30 µM LSP4-2022 was no longer sufficient to potentiate the level of LTP (114.7 ± 1.8% of baseline) (**Figure 14 G, H**). These results are consistent with the hypothesis that activation of $mGlu_7$ can potentiate LTP at SC-CA1 synapses via a disinhibition of CA1 pyramidal cells. Moreover, when considered with the results from the $mGlu_7$ NAM experiments, our results suggest that activation of $mGlu_7$ is necessary for induction of LTP at this synapse.

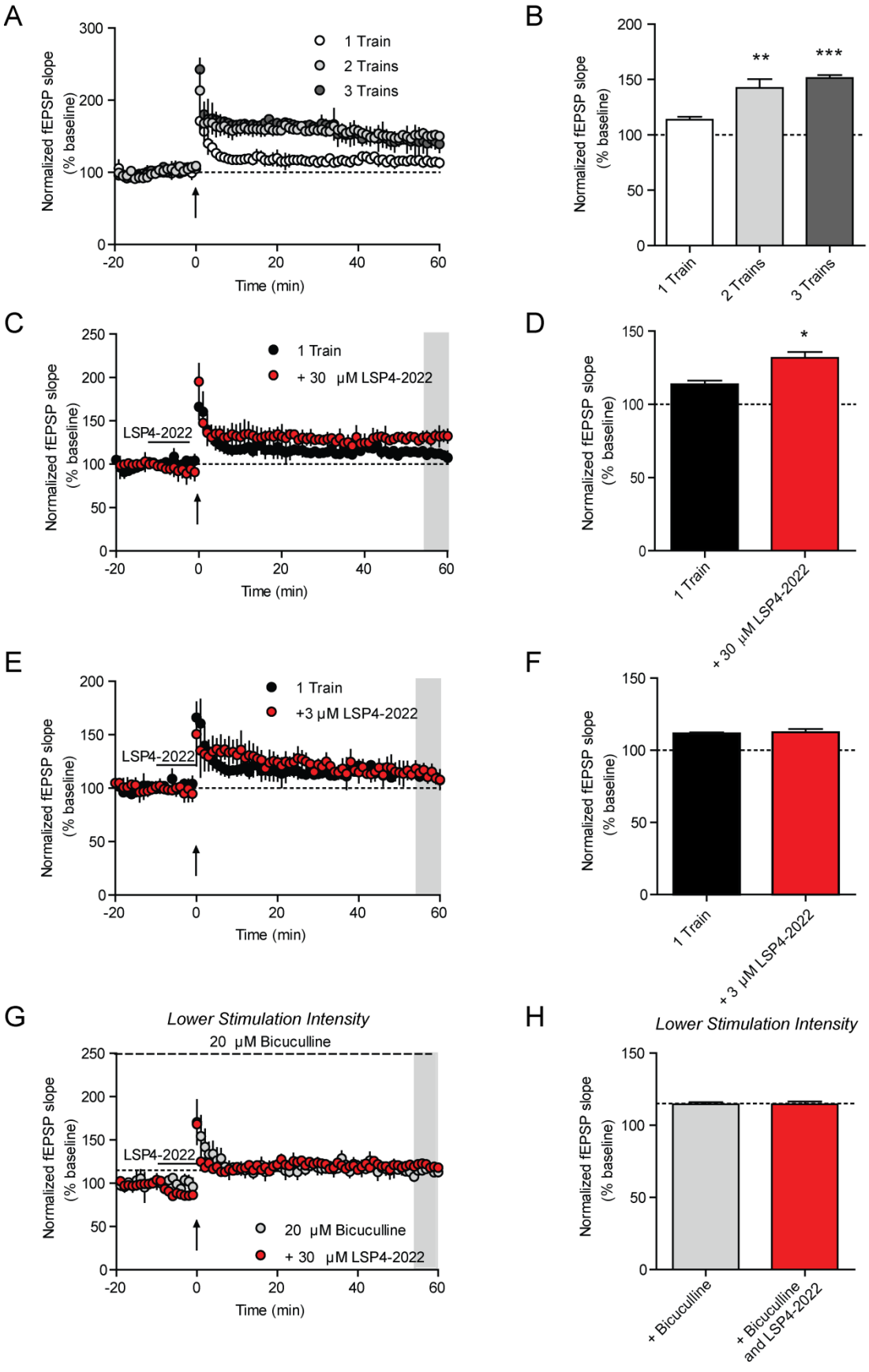
A
Normalized fEPSP slope (% baseline)
1 Train
2 Trains
3 Trains
Time (min)
B
Normalized fEPSP slope (% baseline)
**
***
1 Train
2 Trains
3 Trains
C
Normalized fEPSP slope (% baseline)
1 Train
+ 30 µM LSP4-2022
LSP4-2022
Time (min)
D
Normalized fEPSP slope (% baseline)
*
1 Train
+ 30 µM LSP4-2022
E
Normalized fEPSP slope (% baseline)
1 Train
+3 µM LSP4-2022
LSP4-2022
Time (min)
F
Normalized fEPSP slope (% baseline)
1 Train
+ 3 µM LSP4-2022
G
Lower Stimulation Intensity
20 µM Bicuculline
Normalized fEPSP slope (% baseline)
LSP4-2022
20 µM Bicuculline
+ 30 µM LSP4-2022
Time (min)
H
Lower Stimulation Intensity
Normalized fEPSP slope (% baseline)
+ Bicuculline
+ Bicuculline and LSP4-2022

Figure 14. Agonism of $mGlu_7$ potentiates sub-maximal long term potentiation. (A) Three different high frequency stimulation paradigms were used to induce varying levels of long term potentiation. One train of 100 Hz stimulation induced a sub-maximal level of LTP, whereas 2 or 3 trains of 100 Hz stimulation both induced saturated LTP. All HFS stimulations are represented by upward facing arrows on each graph. (B) Quantification of LTP as determined by averaging the values during the last 5 minutes of recording (shaded grey area in (A)). Values represent mean ± SEM (overall $p = 0.0005$, one-way ANOVA with Bonferonni's posttest, 1 train vs. 2 trains $p < 0.01$, 1 train vs. 3 trains $p < 0.001$, $n = 3$-4, df = 2, 8). (C) Pretreatment with 30 µM LSP4-2022 significantly potentiated LTP induced by application of 1 train of 100 Hz stimulation. (D) Quantification of LTP as determined by averaging the values during the last 5 minutes of recording (shaded grey area in (C)). Values represent mean ± SEM (*$p = 0.012$, two-tailed Student's t test, $n = 3$-4, df = 5). (E) Pretreatment with 3 µM LSP4-2022 did not significantly alter the level of LTP induced by application of 1 train of 100 Hz stimulation. (F) Quantification of LTP as determined by averaging the values during the last 5 minutes of recording (shaded area in (E)). Values represent mean ± SEM ($p > 0.05$, two-tailed Student's t test, $n = 3$-4, df = 5). (G) 20 µM bicuculline was bath applied to slices and the stimulation intensity was reduced such that the slope of the baseline fEPSPs were similar in magnitude to the 50% maximum fEPSP slope in normal aCSF determined via an intensity input-output curved. Pre-treatment with bicuculline alone or with a 10 minute treatment with 30 µM LSP4-2022 (black line) did not significantly enhance the level of LTP induced with 1 train of 100 Hz stimulation (upward facing arrow). The level of LTP induced in normal aCSF is represented by a small dashed line. (H) Quantification of LTP as determined by averaging the values during the last 5 minutes of recording (shaded area in (G)). The level of LTP induced in normal aCSF is represented by a dashed line. Values represent mean ± SEM (Overall $p = 0.3258$, one-way ANOVA with Bonferonni's posttest, $n = 3$-4, df = 2, 8).

Discussion

$mGlu_7$ is unique from other group III mGlu receptors in that it has an extremely low affinity for glutamate, is present on both glutamatergic and GABAergic terminals, and is the only functional group III receptor present at SC-CA1 synapses in the hippocampus (Bradley et al., 1996; Kosinski et al., 1999; Dalezios et al., 2002; Ayala et al., 2008; Summa et al., 2013). Its role in regulating transmission in hippocampal area CA1 has been thought to be primarily through reduction of glutamatergic transmission, as $mGlu_7$ agonists reduce fEPSP slopes (Baskys and Malenka, 1991; Gereau and Conn,

1995b; Ayala et al., 2008; Jalan-Sakrikar et al., 2014). We and others, however, have not found a clear role for $mGlu_7$ in regulating endogenous glutamate release. In contrast to what has been seen for $mGlu_{2/3}$ in the dentate gyrus, we saw no activation of $mGlu_7$ in response to repeated SC afferent stimulations either at 5 Hz or at 100 Hz. These results suggest that $mGlu_7$ may not act as a traditional autoreceptor and does not decrease glutamatergic transmission in response to repeated bursts of endogenous glutamate release at this synapse. This novel finding is intriguing, given the substantial evidence for the presynaptic localization of $mGlu_7$ on SC terminals directly within the synaptic cleft (Shigemoto et al., 1996). Despite this localization, the functional significance of this population of $mGlu_7$ in the regulation of glutamatergic transmission is unclear, and additional studies will be necessary to determine if there are specific conditions or firing patterns necessary for synaptic activation of $mGlu_7$.

Both electron microscopy and functional studies indicate that, in addition to its localization of glutamatergic terminals, $mGlu_7$ is located presynaptically on a variety of GABAergic interneuron terminals within the SC-CA1 region of the hippocampus where it can decrease GABAergic transmission onto CA1 pyramidal cells in response to agonist (Summa et al., 2013). We again sought to determine if we could observe $mGlu_7$ activation in response to endogenous glutamate release using the same stimulation paradigms used to study glutamatergic transmission. We observed no activation of $mGlu_7$ under low-frequency stimulation; however, a consistent and significant activation of $mGlu_7$ was observed only using a 100 Hz stimulation paradigm. Thus, under periods of repeated, high frequency firing of glutamatergic afferents, sufficient concentrations of glutamate are achieved at GABAergic synapses to activate $mGlu_7$ and decrease

GABAergic transmission onto CA1 cells. The direct actions of $mGlu_7$ at GABAergic synapses are confirmed by our finding that $mGlu_7$ ligands have effects on IPSCs induced by monosynaptic and optogenetic activation of GABAergic terminals, both of which eliminate potential effects of $mGlu_7$ on excitatory synapses onto inhibitory interneurons. The optogenetic activation of GABAergic interneurons also eliminates the contribution that other neuromodulators may have on GABA release, as electrical stimulation could cause the release of other neurotransmitters or factors that would not be eliminated in our monosynaptic experimental paradigm.

LTP is one of the two forms of synaptic plasticity present in vertebrate animals. LTP and its counterpart, long term depression (LTD), have been postulated to be a molecular basis for learning and memory (for review see Barnes, 1995). Both of these forms of long-term synaptic plasticity have been most heavily characterized at the SC-CA1 synapse and proper function of these processes has been linked to several learning and memory animal behavioral tasks (Whitlock et al., 2006). Many of the molecular requirements for LTP at SC-CA1 synapses have been elucidated, including the requirement for NMDAR activation and post-synaptic depolarization (Malinow and Miller, 1986; Morris et al., 1986). Due to lack of subtype-selective compounds that do not exhibit complex pharmacology, the role that $mGlu_7$ plays in LTP has not been characterized, despite evidence indicating the loss of the receptor is detrimental to behavioral tasks reliant on proper hippocampal LTP (Bushell et al., 2002; Holscher et al., 2005; Goddyn et al., 2008). The current findings suggest that selective depression of GABAergic, but not glutamatergic, transmission induced by synaptic activation of $mGlu_7$ with high frequency afferent firing could be critical for induction of LTP. A central role

for $mGlu_7$-mediated disinhibition in induction of LTP is likely to be especially important under conditions in which pyramidal cells are not depolarized by other factors, such as other neuromodulatory influences or coincident activity at excitatory inputs from the perforant path or other glutamatergic projections (**Figure 15**).

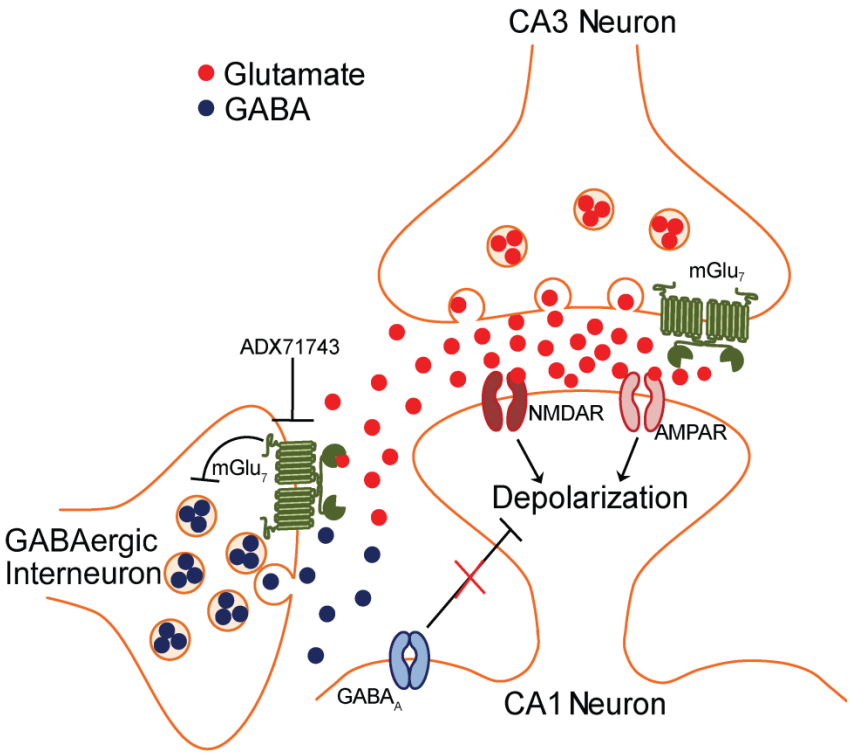

Figure 15. Working model of the mechanism by which $mGlu_7$ mediates induction of LTP at SC-CA1 synapses. $mGlu_7$ is a low-affinity mGlu receptor that is expressed presynaptically on both glutamatergic projections from CA3 and on interneurons in area CA1. Despite its localization directly within the synaptic cleft, it is only activated on GABAergic interneurons under strong synaptic activity when concentrations of glutamate are high. HFS induces robust glutamate release which is sufficient to activate $mGlu_7$ located presynaptically on GABAergic interneurons. This activation induces an inhibition of GABA release and a disinhibition of the circuit, thus facilitating LTP induction. Further investigation will be necessary to determine how and when $mGlu_7$ becomes active on glutamatergic terminals and what the consequences of this activation are on transmission.

The results of our whole-cell HFS experiments show that activation of $mGlu_7$ reduces inhibitory synaptic transmission in CA1 pyramidal cells. Antagonism of $mGlu_7$ reversed this disinhibition; however, we did not observe a full reversal of the disinhibition. This indicates that there may be a threshold level of disinhibition necessary for LTP induction to occur, which can be achieved by synaptic activation of $mGlu_7$. The remainder of the inhibition observed after HFS may be the result of other mechanisms, such as the production of endocannabinoids or release of other neuromodulators. There is evidence that group I mGlu receptor-mediated release of endocannabinoids and activation of CB1 receptors can reduce GABA release in area CA1 (termed depolarization-induced suppression of inhibition, DSI) (Varma et al., 2001; Ohno-Shosaku et al., 2002; Chevaleyre and Castillo, 2003, 2004). Despite strong literature evidence that group I mGlu receptor activation reduces IPSC amplitudes, we did not observe this using our whole-cell HFS protocol (data not shown). However, the difference in stimulation paradigm used in our study versus in previous studies (10 pulses at 100 Hz vs. TBS induction) could account for the differences observed between endocannabinoid-mediated disinhibition and our study. As such, it will be important to determine if $mGlu_7$-mediated disinhibition also occurs using TBS protocols to better understand how the two mechanisms functionally relate. The reduction in GABA release observed with the activation of CB1 receptors causes GABAergic interneurons to undergo LTD (termed I-LTD), which has been shown to act as a priming mechanism that can facilitate LTP induction at glutamatergic terminals (Chevaleyre and Castillo, 2003, 2004). The relative contributions of endocannabinoid-mediated and $mGlu_7$-mediated disinhibition have yet to be determined; however, the fact that blockade of $mGlu_7$ is

sufficient to prevent the induction of LTP alone coupled with the observation that LTP can still be induced in CB1 KO mice perhaps indicates that the roles that $mGlu_7$ and endocannabinoids play in disinhibition may be mechanistically distinct (Chevaleyre and Castillo, 2004). Indeed, endocannabinoid-mediated I-LTD serves to modulate the precise level of LTP (Chevaleyre and Castillo, 2004), whereas $mGlu_7$ activation during HFS appears to be necessary for LTP induction. Taken together, these findings could indicate that both mechanisms serve to fine-tune both the timing and strength of LTP at specific glutamatergic synapses. Additionally, DSI, and, consequently, I-LTD only occur in 20% of inhibitory connections found in CA1 cell dendrites (Chevaleyre and Castillo, 2004). This could indicate that perhaps there is a spatial difference in the expression of CB1- versus $mGlu_7$-mediated disinhibition, with $mGlu_7$-mediated disinhibition perhaps occurring at synapses that are I-LTD insensitive. These findings are particularly intriguing given that we observe $mGlu_7$ activation on PV-expressing interneurons, which are known to be CB1 receptor negative in the hippocampus, whereas the majority of CB1 receptors are found on cholecystokinin-expressing interneurons (Katona et al., 1999; Tsou et al., 1999). There have also been reports that $mGlu_7$ plays a role in mediating bidirectional plasticity of feed-forward inhibition at mossy fiber inputs onto CA3 stratum lucidum interneurons, where activation of $mGlu_7$ initially induces a robust LTD at this synapse, followed by LTP after agonist-induced $mGlu_7$ internalization (Pelkey et al., 2005; Pelkey et al., 2007; Pelkey et al., 2008). Though this phenomenon has only been studied at this synapse, it supports the idea that $mGlu_7$ is well positioned to be a controller of synaptic plasticity.

To date there have been few studies directly investigating the role of $mGlu_7$ in regulation of plasticity at the SC-CA1 synapse. There has been one report in $mGlu_7$ knockout mice in which the authors found a deficit in post tetanic potentiation (PTP); however, no change in the level of LTP was observed (Bushell et al., 2002). However, interpreting results from genetically modified animals can be complicated by developmental and compensatory changes. We have reported that $mGlu_8$ is the predominant group III mGlu receptor present in neonatal animals and that $mGlu_7$ becomes the predominant group III mGlu receptor present in adult animals (Baskys and Malenka, 1991; Ayala et al., 2008). It is feasible that, in an $mGlu_7$ knockout mouse, this switch between $mGlu_7$ and $mGlu_8$ cannot occur, leading to prolonged $mGlu_8$ expression. Due to the high conservation of the LTP phenomenon among vertebrate species and its speculated crucial role in learning and memory, it is possible that expression of $mGlu_8$ remains to compensate for the loss of $mGlu_7$, which could explain the lack of LTP deficits in $mGlu_7$ KO animals.

Polymorphisms in the $mGlu_7$ gene have been associated with the pathophysiology of affective disorders, such as major depression and anxiety, autism spectrum disorders, and schizophrenia (Ganda et al., 2009; Pergadia et al., 2011; Yang and Pan, 2013). Additionally, genetic deletion of $mGlu_7$ results in a variety of behavioral deficits that mimic human phenotypes seen in several of the aforementioned disease states and point to its role in learning and memory. Loss of $mGlu_7$ has been attributed to deficits in working memory (Holscher et al., 2004, 2005) and fear learning (Callaerts-Vegh et al., 2006; Goddyn et al., 2008). Specifically, there are impairments in contextual fear conditioning in these animals and systemic administration of a different, structurally

distinct $mGlu_7$ NAM, MMPIP, to wild-type mice results in deficits in object recognition and object localization tasks, which are models of non-spatial and spatial memory, respectively (Hikichi et al., 2010). All of these data point towards a role for $mGlu_7$ in modulating learning in memory associated with the hippocampus.

Taken together, our results indicate that $mGlu_7$ does not act as a traditional autoreceptor in hippocampal area CA1 but instead functions under intense synaptic firing as a heteroceptor to decrease GABAergic transmission. We also provide the first evidence for a direct role of $mGlu_7$ in mediating induction of LTP at SC-CA1 synapses using a common induction paradigm. Additionally, we have shown that $mGlu_7$'s role as a frequency-dependent presynaptic heteroeceptor located on GABAergic interneurons is critical for this mechanism. It will be important in future studies to determine the precise role of $mGlu_7$ in hippocampal-based learning and memory tasks as well as to investigate if $mGlu_7$ also plays a role in induction of LTP using theta-burst stimulation paradigms. It will also be important to determine if $mGlu_7$'s role in synaptic plasticity is restricted to SC-CA1 synapses, or whether it functions more broadly as a global regulator of plasticity in other circuits throughout the brain. One recent study found deficits in lateral amygdala LTP when $mGlu_7$ was blocked using a newly described orthosteric antagonist, XAP044 (Gee et al., 2014), suggesting that this role for $mGlu_7$ could be observed in other brain regions. Finally, these data also indicate that compounds that agonize or potentiate $mGlu_7$ function could be efficacious in disease states where hippocampal LTP is deficient.

CHAPTER IV

IDENTIFICATION OF METABOTROPIC GLUTAMATE RECEPTOR 7 AS A THERAPEUTIC TARGET FOR RETT SYNDROME: RESCUE OF DEFICITS IN HIPPOCAMPAL LONG TERM POTENTIATION AND COGNITION THROUGH ALLOSTERIC MODULATION

Introduction

Rett syndrome is an X-linked neurodevelopmental disorder that is caused by loss of function mutations in the *Methyl CpG Binding Protein 2* (*MECP2*) gene (Amir et al., 1999). Patients with Rett syndrome develop relatively normally for the first 6-18 months of life, after which they undergo severe developmental regression coinciding with the presentation of mental retardation, seizures, and cognitive impairments and the loss of language and motor skills (Weng et al., 2011a). While MECP2 is ubiquitously expressed, almost all of the symptoms of Rett syndrome can be recapitulated when the protein is removed exclusively from the central nervous system (CNS) in mice (Chen et al., 2001). MECP2 preferentially binds to DNA containing a sequence at least 4 base pairs (bp) long of A and T nucleotides (termed an A/T run) flanked by methylated CG dinucleotides (Klose et al., 2005; Baude et al., 2007). Among other proposed functions, MECP2 can act functionally to either repress or activate transcription of genes in the brain (Chahrour et al., 2008), and, as such, several large-scale microarray studies have been performed to identify genes specifically regulated by MECP2 (Traynor et al., 2002; Tudor et al., 2002; Ben-Shachar et al., 2009). These studies, however, have failed to find

gross changes in gene expression and, particularly, have failed to identify targets regulated by MECP2 that are amenable to drug development.

Metabotropic glutamate receptor 7 ($mGlu_7$) is a G-protein-coupled receptor (GPCR) that is highly expressed in regions of the brain known to be affected in Rett syndrome, such as the cortex, hippocampus, cerebellum, and striatum (Bradley et al., 1998). It is expressed presynaptically on both GABAergic and glutamatergic synapses and acts to decrease neurotransmitter release when stimulated (Bradley et al., 1996; Dalezios et al., 2002; Somogyi et al., 2003; Summa et al., 2013). Mouse models of Rett syndrome display attenuated long term potentiation (LTP) at the Schaffer collateral (SC)-CA1 synapse (SC-CA1) in the hippocampus, as well as deficits in hippocampal-based learning and memory tasks consistent with the cognitive impairments present in Rett syndrome patients (Asaka et al., 2006; Moretti et al., 2006; Pelka et al., 2006; Weng et al., 2011b; Ma et al., 2014). As $mGlu_7$ is the only presynaptic metabotropic glutamate receptor (mGlu receptor) present at the SC-CA1 synapse in the hippocampus and is necessary for induction of LTP (Baskys and Malenka, 1991; Kosinski et al., 1999; Ayala et al., 2008; Jalan-Sakrikar et al., 2014; Klar et al., 2015), we predicted that the electrophysiological changes and behavioral deficits observed in Rett syndrome could be due to $mGlu_7$ dysfunction. This is further supported by the fact that $mGlu_7$ knockout mice are similar to Rett syndrome mice in that they also display deficits in plasticity at the SC-CA1 synapse and in performance in hippocampal-based tasks of learning and memory (Bushell et al., 2002; Holscher et al., 2004, 2005; Callaerts-Vegh et al., 2006; Goddyn et al., 2008). Additionally, the promoter of the gene encoding $mGlu_7$ (*GRM7)* has been shown to be epigenetically regulated by methylation status (Rush et al., 2004),

perhaps indicating that $mGlu_7$ is an unexplored MECP2-regulated gene linked to cognitive impairments in Rett syndrome.

Here we demonstrate that the expression of *GRM7*, a GPCR highly amenable to drug development, is directly regulated by MECP2. In *in vitro* systems, MECP2 activates *GRM7* transcription, which translates into a loss of $mGlu_7$ mRNA and protein expression in *Mecp2* homozygous male (*Mecp2*$^{-/y}$) mice. Additionally, this loss of $mGlu_7$ is observed in the primary motor cortex of patients diagnosed with Rett syndrome, indicating that our findings have translational value in therapeutic development. We also show that reduced $mGlu_7$ expression in mouse hippocampus leads to a functional deficit in $mGlu_7$-modulated control of transmission at the SC-CA1 synapse. Excitingly, $mGlu_7$ function and LTP induction can be restored by application of two structurally-distinct small molecule positive allosteric modulators (PAMs), VU0422288 and VU0155094, that target $mGlu_7$. Finally, VU0422288 pretreatment can reverse deficits in contextual fear memory in *Mecp2* heterozygous females (*Mecp2*$^{-/+}$). Taken together, these results suggest that potentiation of $mGlu_7$ could serve as a novel therapeutic approach for treat the cognitive impairments in Rett syndrome.

Results

The promoter region of GRM7 and its homologs contains an MECP2 binding site

MECP2 preferentially binds to CpG islands within the promoter region of genes in the DNA, where it has been shown to lead to both activation and repression of gene transcription (Chahrour et al., 2008). In addition to its affinity for CG dinucleotides,

MECP2 binding has been shown to be enriched on DNA sequences containing A/T runs of 4 bp or longer (Klose et al., 2005). This A/T run has been shown to be necessary for interaction with the AT hook domains present in MECP2 and patient mutations that disrupt both CG dinucleotide and AT hook binding often correlate with a more severe phenotype (Baker et al., 2013). We identified a large CpG island 800 bp upstream of the predicted transcriptional start site within the human *GRM7* promoter (**Figure 16A**). Within the promoter, we further identified a potential MECP2 binding site containing an A/T run of 7 bp that was flanked on either side by CG dinucleotides. Using sequence alignment, we observed an almost complete conservation of both the CG dinucleotides and the A/T run between the human *GRM7* promoter and the *Grm7* promoter regions from chimpanzee, mouse, bovine, and rat (**Figure 16B**). We next performed chromatin immunoprecipitation (ChIP) experiments from 6 week-old wild-type C57BL6/J mouse cortex to determine if mouse Mecp2 occupied the potential binding site in the *Grm7* promoter *in vivo*. We found that Mecp2 occupies a 300 bp region containing our previously identified binding site, and that binding is absent in IgG controls and within a control region of the *Grm4* promoter that contains no CpG islands or AT runs. Additionally, we confirmed that our immunoprecipitation was specific as we were also able to detect the presence of *Gad2* DNA, a known Mecp2-regulated target (Chao et al., 2010), in the Mecp2-specific pull-down, but not in the IgG control (**Figure 16C**). Taken together, these results indicate that the mouse homologue of MECP2 specifically binds to the *Grm7* promoter in wild-type mouse brain tissue.

A

agaaagtg*cg*ctctg*cg*gagttctcagttgttccctctctgcaa*cg*aagtaaaaagaagggatg*cg*tc*cg*agg
ttttt*g*acacagacatgctggggaaa*cgcg*tcagttcaaggagctctgactctagtgactactgaagaccagt
gatgcactcccatgcctagcatctcctcttgacttctgtttccctgcagccaagctcagctcctggccctgga
aacccctttggg*taaag**cg*tctttaagtcaagaatcaggctcctgtgtgca*cg*tgtggctttcttagcaaaaa
actagcacagg*cg*gctcaggagtagagtctagctagggtcttcc*cgcg*cccctccctcactggtttctctgcc
cctgcct*cg*ctttctcccagagctaagagcctaggctc*cg*gacctagggtttgggagcagtcagca*cg*a*cg*tc
ct*cg*ccccatcc*cgcg*gctgatgacacc*cg*tgcccagaa*cg*tgggtgtgggtagggaggcttccacagtgagt
tagggt*cg*agagctaggctct*cg*cttgctccc*cg*caatccctagattccctggggacca*cg*aaactcccattc
*cg*aggaaacctcccccattccccagc*cg*cccacc*cg*tttcccccccttacctcagca*cg*cagccctcccctg
*cg*tgatgatgcaaaccagtggggagggctgg*cg*ctgggaagggtggggagagaaggagagccag*cg*agggagg
gagggagt[gggaggaggaggagagggagc*cg*aa*cg*accatttaaag*cg*atagcagtccctgccctctcccc]
agtgctgggctgttggagagag*cg*agcagcaagc*cg*gtgag*cgcg*ag*cgcg*g*cgcg*c*cg*gc*cg*gctaacc*cg*a
gag*cgcg*agg*cg*ccccaggctggcagg*cg*c*cgcg*ggacccctcaccctctctggt*cg*cccctccc*cg*gattcc
cccaccctc*cg*tgcctgcaggagcccctgggctttcc*cg*gaggagct*cg*ccctgaagggcc*cg*gacct*cg*g*cg*
agcccaccac*cg*ttccctccag*cg*c*cg*c*cg*c*cg*ccac*cg*cagcagc*cg*gagcagcatg

B

Human: gggaggaggagagggagc*cg*aa*cg*accatttaaag*cg*atagcagtccctgccctctcccc
Chimp: gggaggaggagagggagc*cg*aa*cg*accatttaaag*cg*atagcaatccctgccctctcccc
Mouse: gggaggaggagagggagcccaa*cg*accatttaaag*cg*atagcaatccctgccctctcccc
Bovine: gggaggaggagagggagc*cg*aa*cg*accatttaaag*cg*atagcaatc*cg*tgccctctccct
Rat: gggaggaggagagggagcccaa*cg*accatttaaag*cg*atagcaatccctgccctctcccc

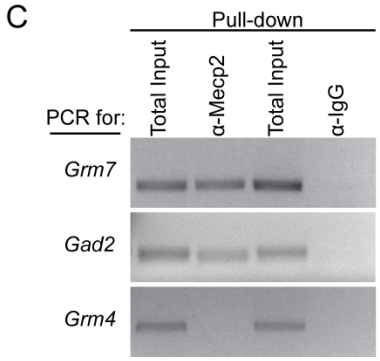

Figure 16. The promoter of *GRM7* contains an MECP2 binding site. (A) The promoter region of the human *GRM7* gene contains a large CpG island. CG dinucleotides are denoted by red and italic text and A/T runs of 4 bp or longer are colored in blue text. A putative MECP2 binding site is denoted by [brackets] and underlined in red as containing an A/T run of 7 bp, which is flanked by three CG dinucleotides. (B) The predicted MECP2 binding site (A) is conserved among several different species, including chimpanzee, mouse, bovine, and rat. (C) Chromatin immunoprecipitation of a 300 bp region of the mouse *Grm7* promoter containing the region denoted in (B) was performed from wild-type mouse cortex. The presence of all three genes of interest, *Grm7*, *Gad-2*, and *Grm4*, was observed in both the input lane for the α-Mecp2 pull-down and the α-IgG pull-down. Specific amplification of *Grm7* was observed after immunoprecipitation using the α-Mecp2 antibody, but not using the α-IgG antibody. Specific amplification of *Gad-2* was also observed using the α-Mecp2 antibody but not using the α-IgG antibody and was used as a positive control (Chao et al., 2010). No amplification of *Grm4* was observed from either the α-Mecp2 or the α-IgG antibodies, serving as a negative control (n = 3 immunoprecipitations from separate wild-type mice).

MECP2 activates GRM7 transcription

MECP2 plays a variety of roles in the regulation of chromatin homeostasis and gene expression (Guy et al., 2011). While MECP2 was initially identified as a transcriptional repressor, it can also activate gene transcription when interacting with specific cellular proteins (Kosinski et al., 1999). Because of these two opposing functions, we next sought to determine whether MECP2 was acting as a transcriptional activator or repressor of *GRM7* expression. We generated a reporter construct, using a pGL4 luciferase expression vector, containing 1000 bp of the human *GRM7* promoter upstream of a luciferase gene (**Figure 17A**). Both the *GRM7*-containing and empty vector constructs were then transfected independently with and without human MECP2 into HEK293 cells and the expression of luciferase was measured by calculating the relative luciferase units (RLU) compared to transfection of a renilla control vector. We observed no significant change in luciferase expression when the empty vector was transfected with or without MECP2 (**Figure 17B**). Conversely, a significant increase in RLU was observed when the pGL4/*GRM7* construct was transfected with increasing amounts of MECP2 (**Figure 17B**).

It has previously been reported that the function of the AT hook domains in MECP2 is predictive of disease severity in Rett syndrome patients (Baker et al., 2013). Indeed, mouse models harboring point mutations that disrupt AT hook function display a more severe disease progression than those with mutations elsewhere in *Mecp2* that retain AT hook function (Baker et al., 2013). As MECP2 preferentially binds to CpG islands adjacent to runs of A/T's that are 4 bp or greater (Klose et al., 2005), coupled with the fact that we observe mouse Mecp2 binding within a 300 bp region containing a 7 bp run

of A/Ts, we assessed if the binding of MECP2 to the A/T run was critical for regulation of *GRM7* expression. We generated a short, double-stranded decoy DNA with a 2'O-Methyl modified backbone that mimicked the A/T run in *GRM7*, with the goal of saturating MECP2's AT binding capabilities. Increasing concentrations of either decoy DNA or scramble control were transfected into human H4 neuroglioma cells, which we have identified endogenously express both *GRM7* and *MECP2*. We observed a significant decrease in the expression of *GRM7* when 4 ng of the decoy DNA was transfected (**Figure 17C**); however, we observed no significant change in *MECP2* expression (**Figure 17D**). Taken together, these data indicate that MECP2 acts as an activator of *GRM7* expression via a mechanism that requires binding to a run of A/T's in the *GRM7* promoter. Additionally, the requirement for AT hook binding to *GRM7* indicates that $mGlu_7$ expression may also correlate with disease severity.

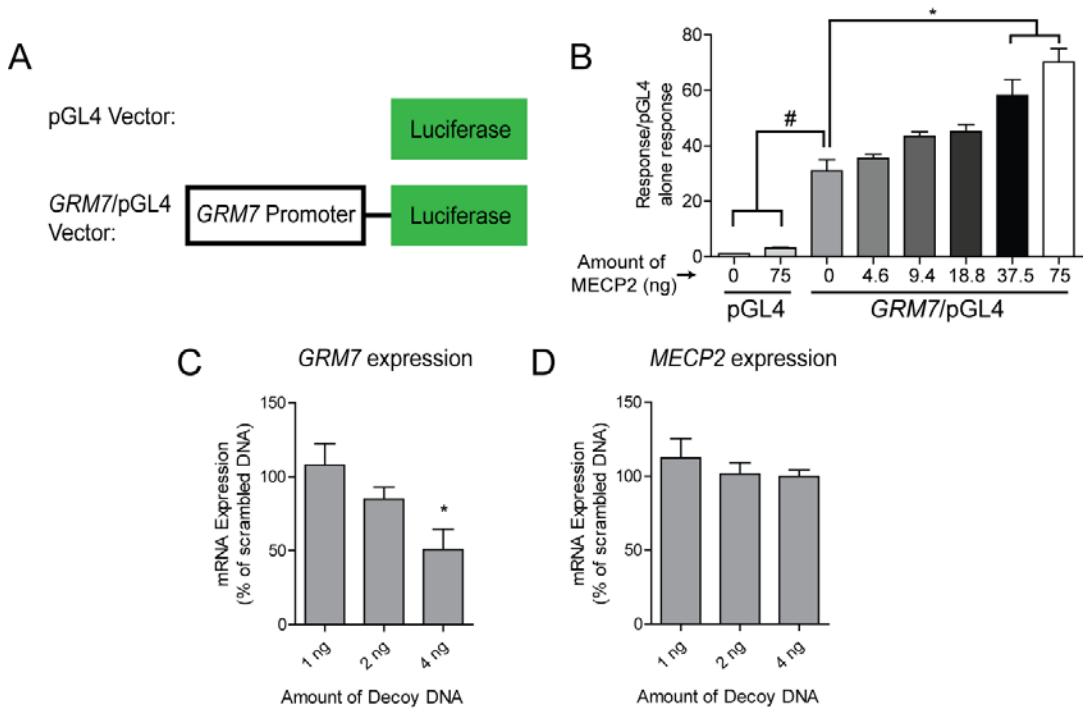

Figure 17. MECP2 activates *GRM7* expression. (A) Diagram of luciferase reporter constructs. Approximately 1000 bp of the human *MECP2* promoter was cloned upstream of a sequence encoding luciferase within the pGL4 vector. (B) Transfection of increasing amounts of human MECP2 (denoted in ng) into HEK293 cells leads to a concentration-dependent, significant increase in luciferase expression only when the vector containing the *GRM7* promoter is employed (Empty vector: in RLU, 1.0 for 0 ng MECP2 vs. 3.06 ± 0.7 for 75 ng, pGL4/*GRM7* vector: 0 ng MECP2: 30.8 ± 4.2, 4.6 ng: 35.5 ± 1.4, 9.4 ng: 43.4 ± 1.6, 18.8 ng: 45.0 ± 2.8, 37.5 ng: 58.2 ± 5.7, and 75 ng: 70.3 ± 4.7, overall $p < 0.0001$, One-way ANOVA with Bonferroni's *post hoc* using 0 ng MECP2 + *GRM7*/pGL4 as a control, n = 3, df = 7, 16). No significant difference was observed between transfection of 0 ng and 75 ng MECP2 into cells co-expressing the empty pGL4 vector ($p > 0.05$). A significant difference in luciferase expression, however, was observed between both of the empty pGL4 vector conditions and the vector containing the *GRM7* promoter (# $p < 0.0001$). A significant increase in luciferase expression was observed for the *GRM7*/pGL4 construct when 37.5 ng and 75 ng of MECP2 was transfected compared to 0 ng of MECP2 + *GRM7*/pGL4 (* $p < 0.0001$). (C) A double-stranded decoy DNA mimicking the A/T run present in *GRM7* was transfected into H4 neuroglioma cells. There was a significant reduction in *GMR7* expression when 4 ng of the decoy DNA was transfected into H4 neuroglioma cells (*GRM7* expression: 1 ng decoy DNA: 107.8 ± 14.7% of scramble DNA, 2 ng: 84.7 ± 8.1%, 4 ng: 50.6 ± 14.1%, *p = 0.0385, One-way ANOVA with Bonferroni's *post hoc*, n = 3-5 independent experiments, df = 2, 9). (D) No significant change in *MECP2* expression was observed with any concentration of decoy DNA (*MECP2* expression: 1 ng: 112.3 ± 13.2%, 2 ng: 101.5 ± 7.7%, 4 ng: 99.8 ± 4.2%, p = 0.5352, One-way ANOVA with Bonferroni's *post hoc*, n = 3-5 independent experiments, df = 2, 11). These data were collected by Rocio Zamorano and Rocco Gogliotti.

$mGlu_7$ mRNA and protein expression is reduced in *Mecp2*$^{-/y}$ mice

We next performed studies to determine whether the regulation of human *GRM7* expression we observed *in vitro* correlated with changes in *Grm7* expression in a mouse model of Rett syndrome. Using a mouse model in which the *Mecp2* gene is globally deleted (B6.129P2(C)-*Mecp2*$^{tm1.1\text{-}Bird}$/J) (Guy et al., 2001), we performed quantitative real-time PCR (RT-qPCR) and Western blotting to probe for $mGlu_7$ mRNA and protein expression. This mouse model develops characteristic Rett syndrome symptoms at ~6 weeks of age (age in days, P39-55). These phenotypes include hind limb clasping, body tremors, apneas, and changes in gait dynamics (Guy et al., 2001). When animals developed all of these symptoms, they were characterized as "symptomatic" and phenotypically selected for inclusion in our studies. We observed significant reductions in *Grm7* expression at the mRNA level in the cortex and striatum from symptomatic *Mecp2*-null male mice (*Mecp2*$^{-/y}$) (**Figure 18A**).

To determine if the decreases in *Grm7* expression translated into decreased $mGlu_7$ protein expression, we used western blotting from total protein preparations from several brain areas. These studies revealed significant reductions in total $mGlu_7$ expression in the cortex, hippocampus, cerebellum, and striatum (**Figure 18B, C**). As $mGlu_7$ is expressed presynaptically directly within the synaptic cleft (Gereau and Conn, 1995b; Bradley et al., 1996; Bradley et al., 1998; Kosinski et al., 1999; Dalezios et al., 2002; Somogyi et al., 2003), we also prepared synaptosomes from cortex and hippocampus to isolate synaptic $mGlu_7$ to determine if there were also reductions in expression at the synapse. We observed significant reductions in both cortical and hippocampal synaptosomes (**Figure 18D, E**). To confirm that reductions in *Grm7* and $mGlu_7$ were consistent with the loss of

Mecp2, we also profiled the mRNA and protein expression of the *Gad2* (encoding Gad65) and *Grm4* (encoding $mGlu_4$) genes in the cortex. We observed a significant decrease in *Gad2* mRNA with no change in the levels of *Grm4* mRNA (**Figure 19A**). We observed the same profile in Gad65 and $mGlu_4$ protein expression as well (**Figure 19B**). Taken together, these results indicate that the loss of Mecp2 leads to significant reductions in $mGlu_7$ expression throughout the brain and, in particular, in synaptic structures in the cortex and hippocampus.

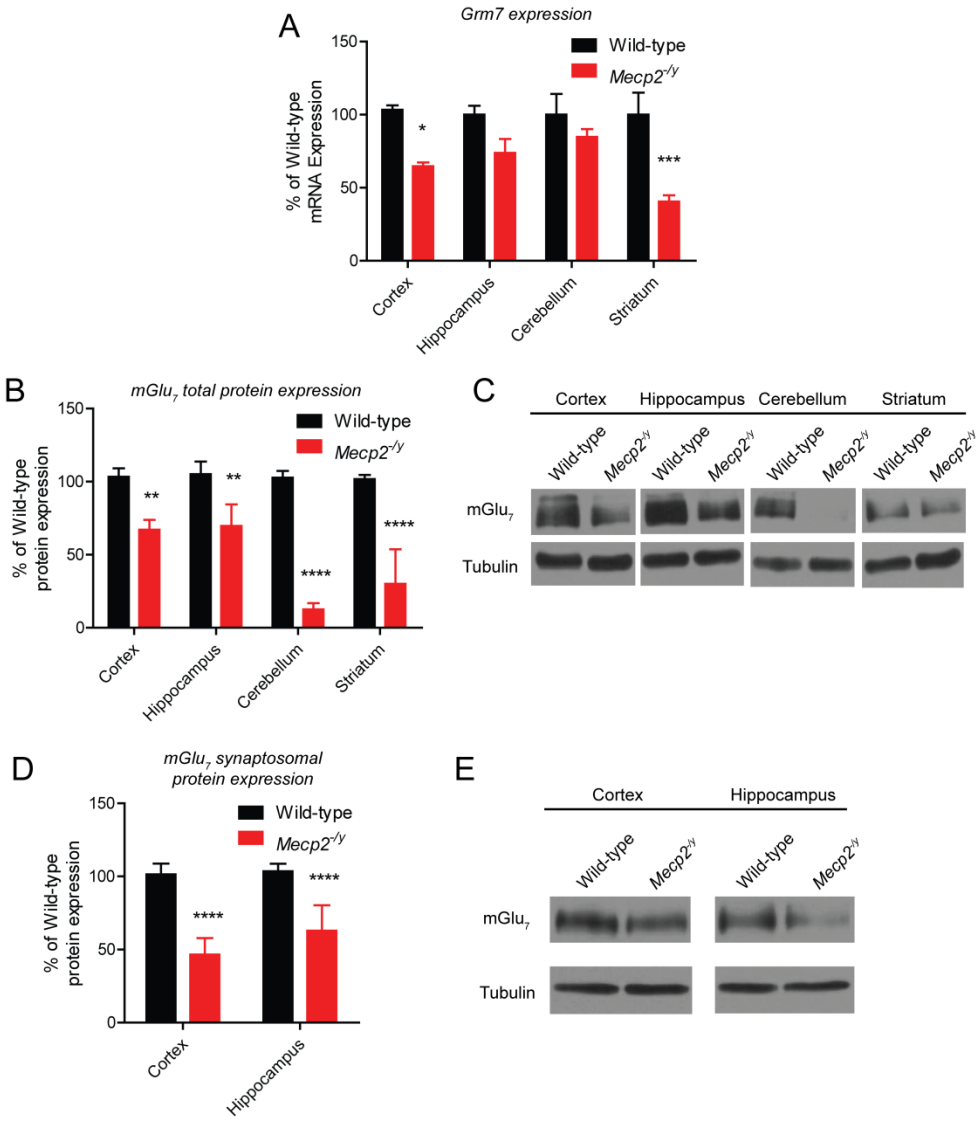

Figure 18. mGlu$_7$ expression is reduced in *Mecp2*$^{-/y}$ mice. (A) *Grm7* mRNA expression was profiled in the cortex, hippocampus, cerebellum, and striatum from wild-type and symptomatic *Mecp2*$^{-/y}$ mice. A significant decrease in *Grm7* mRNA expression was observed in the cortex (*$p < 0.05$) and striatum (***$p < 0.001$) from *Mecp2*$^{-/y}$ mice (% of wild-type, cortex: 64.7 ± 2.6, hippocampus: 73.8 ± 9.6, cerebellum: 84.8 ± 4.3, striatum: 40.5 ± 4.3, overall $p < 0.0001$, Two-way ANOVA, genotype x brain region with Bonferroni's *post hoc*, n = 3-5 samples from individual mice, df = 3, 21). Changes in *Grm7* expression observed in the hippocampus and cerebellum were not statistically different. (B) A significant decrease in mGlu$_7$ total protein expression was observed in the cortex (*$p < 0.01$), hippocampus (**$p < 0.01$), cerebellum (****$p < 0.0001$), and striatum (****$p < 0.0001$) from *Mecp2*$^{-/y}$ mice (% of wild-type, cortex: 67.0 ± 3.9, hippocampus: 69.7 ± 8.5, cerebellum: 12.6 ± 2.4, striatum: 30.1 ± 13.6, overall $p < 0.0001$, Two-way ANOVA, genotype x brain region with Bonferroni's *post hoc*, n = 3 samples from individual mice, df = 3, 16). (C) Representative western blots for mGlu$_7$

total expression from cortex, hippocampus, cerebellum, and striatum in wild-type and *Mecp2*$^{-/y}$ mice. $mGlu_7$ expression was normalized to the expression of tubulin and then calculated as a percent of wild-type expression. (D) A significant decrease in $mGlu_7$ expression was observed in synaptosomes prepared from cortical and hippocampal (****p < 0.0001) tissue samples from *Mecp2*$^{-/y}$ mice (% of wild-type, cortex: 46.5 ± 5.1, hippocampus: 62.9 ± 7.7, overall p < 0.0001, Two-way ANOVA, genotype x brain region with Bonferroni's *post hoc*, n = 5 samples from individual mice, df = 1, 16). (**e**) Representative western blots for synaptosomal $mGlu_7$ expression. Data were normalized to tubulin expression and calculated as percent of wild-type expression. Panel A was collected by Rocco Gogliotti.

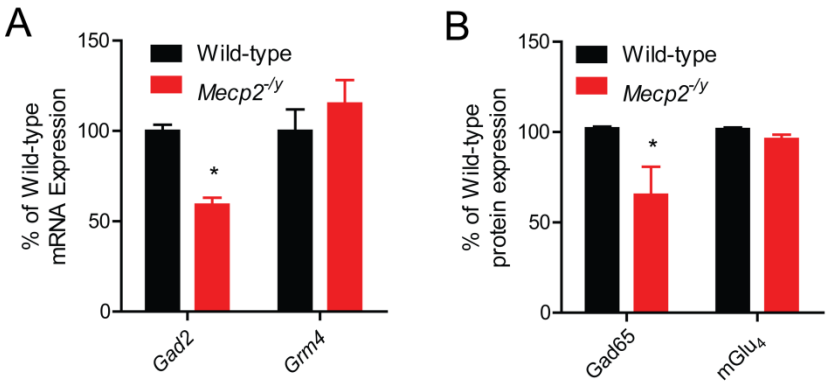

Figure 19. Gad65, but not $mGlu_4$, expression is reduced in *Mecp2*$^{-/y}$ mice. (A) *Gad2* mRNA expression was significantly reduced in the cortex from *Mecp2*$^{-/y}$ mice (*p < 0.05); in contrast, no reduction in *Grm4* mRNA expression was observed (% of wild-type, *Gad2*: 59.2 ± 3.9, *Grm4*: 115.2 ± 13.0, overall p = 0.0173, Two-way ANOVA, genotype x gene with Bonferonni's *post hoc*, n = 3-5 samples from individual mice, df = 1, 12). (B) Gad-2 total protein expression was significantly reduced in the cortex from *Mecp2*$^{-/y}$ mice (*p < 0.05); however, no reduction in $mGlu_4$ expression was observed (% of wild-type, Gad65: 65.3 ± 15.4, $mGlu_4$: 96.2 ± 2.4, overall p = 0.0452, Two-way ANOVA, genotype x gene with Bonferonni's *post hoc*, n = 3-4 samples from individual mice, df = 1, 10).

MECP2 and $mGlu_7$ expression are reduced in human motor cortical tissue

In order to determine if our findings from *Mecp2*$^{-/y}$ mice will translate into the human patient population, we acquired primary motor cortex samples (Brodmann area 4) from 7 female patients with diagnosed Rett syndrome and 8 female control samples (**Table 1-3**), and used western blotting to probe for MECP2 and $mGlu_7$ expression. Excitingly, we observed a significant reduction in both MECP2 and $mGlu_7$ expression in

the Rett syndrome patient samples compared to the control samples (**Figure 20A-C**). These data validate our findings from *Mecp2*$^{-/y}$ mice and demonstrate translation of the rodent findings to the relevant patient population. Additionally, these data indicate that the *Mecp2*$^{-/y}$ mouse is a valuable model to test novel $mGlu_7$-mediated therapies in Rett syndrome.

Table 1. Rett syndrome Patient Information. 7 motor cortical samples from patients diagnosed with Rett syndrome were obtained from the Harvard Brain Tissue Resource Center. *Postmortem* intervals (PMI) ranged from 2.9-23.5 hours. The specific mutation in MECP2 denoted for each patient and, where provided, the % of X chromosome inactivation (%XCI) are noted in the table. All samples were obtained from the subregion (sub-reg) BA4 in the cortex, which contains the motor cortex region.

Sample Number	AN Number	Age	Sex	PMI (hr)	Mutation	%XCI	Region	Sub-reg
1	AN05852	24	F	14	R168X		Cortex	BA4
2	AN19242	10	F	N/A	R255X	63.9	Cortex	BA4
3	AN15579	11	F	9.6	R255X	38.9	Cortex	BA4
4	AN08016	8	F	2.9	R255X		Cortex	BA4
5	AN02091	24	F	15.78	R255X		Cortex	BA4
6	AN04573	12	F	5	R270X	49.1	Cortex	BA4
7	AN04121	10	F	23.5	R270X		Cortex	BA4

Table 2. Control Patient Information. 8 age and sex-matched control motor cortical samples were obtained from the University of Maryland Brain and Tissue Bank (Maryland BB), which is a Brain and Tissue Repository of the NIH NeuroBioBank.

Sample Number	Maryland BB	Age	Sex	PMI (hr)	Mutation	Region	Sub-reg
1	#1038	24	F	7	None (WT)	Cortex	BA4
2	#1708	8	F	20	None (WT)	Cortex	BA4
3	#5161	10	F	22	None (WT)	Cortex	BA4
4	#5554	13	F	15	None (WT)	Cortex	BA4
5	#5669	24	F	29	None (WT)	Cortex	BA4
6	#5844	42	F	12	None (WT)	Cortex	BA4
7	#5566	15	F	23	None (WT)	Cortex	BA4
8	#5309	14	F	8	None (WT)	Cortex	BA4

Table 3. Average age and postmortem interval for all Rett syndrome and Control samples.

	Rett Syndrome		Control	
	Age	PMI	Age	PMI
Average	14.14	11.80	18.75	17.00
SEM	2.59	3.10	3.91	2.75

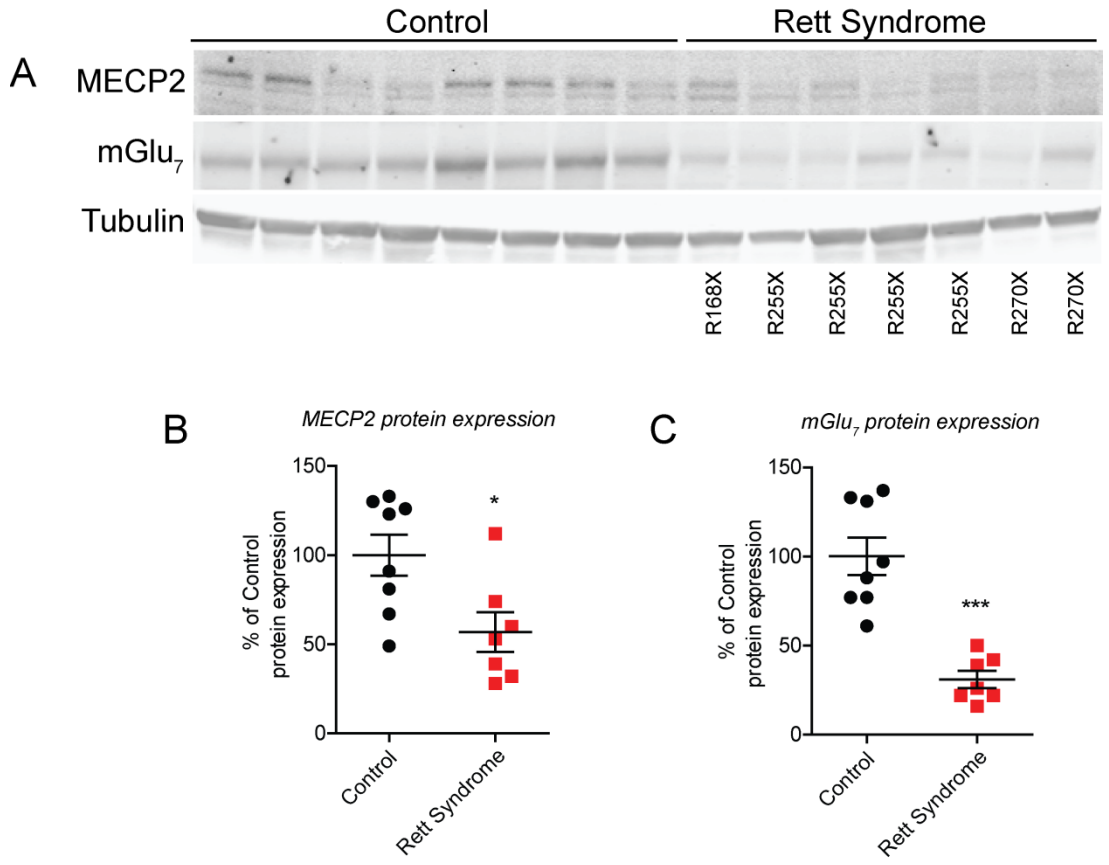

Figure 20. MECP2 and $mGlu_7$ protein expression is reduced in the motor cortex of Rett syndrome patients. (A) Representative western blots for MECP2 and $mGlu_7$ expression in control and Rett syndrome motor cortex samples. MECP2 and $mGlu_7$ expression was normalized to the expression of tubulin and then calculated as a percent of control expression. Individual genotypes of each Rett syndrome patient are listed below the representative images. (B) MECP2 expression was significantly reduced in Rett syndrome patient samples (% of control, MECP2: 56.8 ± 11.0, *p = 0.0184, two-tailed Student's *t* test, n = 7-8 individual patients, df = 13). (C) $mGlu_7$ expression was significantly reduced in Rett syndrome patient samples (% of control: $mGlu_7$: 31 ± 4.8 ***p < 0.0001, two-tailed Student's *t* test, n = 7-8 individual patients, df = 13). These data were collected by Rocco Gogliotti.

Loss of Mecp2 results in reduced $mGlu_7$ function at SC-CA1 in the hippocampus

Several previous studies have shown that $mGlu_7$ is the only presynaptic mGlu receptor expressed in adult rodents at the SC-CA1 synapse and that application of agonists that activate $mGlu_7$ results in a decrease glutamatergic transmission (Baskys and

Malenka, 1991; Gereau and Conn, 1995b; Kosinski et al., 1999; Ayala et al., 2008; Kalinichev et al., 2013; Jalan-Sakrikar et al., 2014; Klar et al., 2015). To determine if our observed decrease in $mGlu_7$ expression correlated with disrupted $mGlu_7$-mediated neurotransmission, we examined the effects of the newly described $mGlu_7$ agonist, LSP4-2022 at the SC-CA1 synapse. LSP4-2022 activates $mGlu_4$, $mGlu_7$, and $mGlu_8$; however, we previously confirmed that the effects observed with LSP4-2022 as SC-CA1 synapses are due to solely to the activation of $mGlu_7$ as 1) $mGlu_7$ is the only presynaptic mGlu receptor at the SC-CA1 synapse in adult mice (Baskys and Malenka, 1991; Kosinski et al., 1999; Ayala et al., 2008; Jalan-Sakrikar et al., 2014), and 2) the effects of LSP4-2022 can be completely blocked with a selective negative allosteric modulator (NAM) of $mGlu_7$, ADX71743 (Kalinichev et al., 2013; Klar et al., 2015). We recorded field excitatory postsynaptic potentials (fEPSPs) in the stratum radiatum of area CA1 in response to stimulation of SC axon fibers induced by paired-pulse stimulation. Similar to previous reports from other Rett syndrome mouse models (Asaka et al., 2006; Moretti et al., 2006), we observed altered basal synaptic properties in symptomatic *Mecp2*$^{-/y}$ mice, including an enhanced input-output curve and a reduction in the paired-pulse ratio (PPR) across a range of stimulation intensities (**Figure 21A, B**). To determine if there were differences in $mGlu_7$ function in symptomatic *Mecp2*$^{-/y}$ mice, we recorded baseline fEPSPs for 10 minutes and then bath applied 30 μM LSP4-2022 for 10 minutes, followed by a 15 minute washout period. In wild-type slices, LSP4-2022 induced a significant decrease in the slope of the first fEPSP, consistent with previous findings (Jalan-Sakrikar et al., 2014). In contrast, when we applied the same concentration of LSP4-2022 to *Mecp2*$^{-/y}$ slices, we observed no decrease in fEPSP slope (**Figure 22A, B, C**).

Furthermore, the decrease in fEPSP slope observed in wild-type slices was associated with a significant increase in PPR, but no change in PPR was observed in slices prepared from *Mecp2*$^{-/y}$ mice (**Figure 22D**).

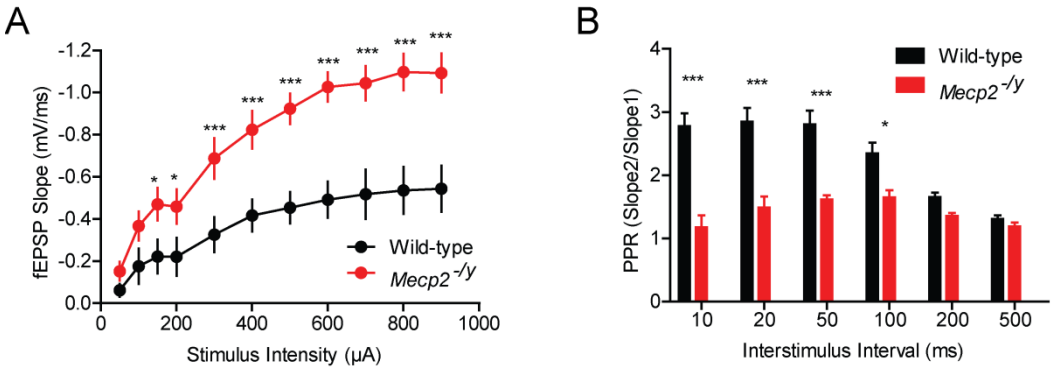

Figure 21. *Mecp2*$^{-/y}$ hippocampal slices display enhanced excitatory transmission at the SC-CA1 synapse. fEPSPs were generated by stimulating axon fibers from CA3 with a bipolar electrode. (A) fEPSPs were stimulated at increasing stimulation intensities from 50 μA-900 μA. *Mecp2*$^{-/y}$ slices display a significant enhancement in fEPSP slope from 150 μA – 900 μA (overall p = 0.0002, Two-way ANOVA with repeated measures, genotype x stimulation intensity with Bonferonni's *post hoc*, n = 7 slices from individual animals, df = 1, 120, *p < 0.05, ***p < 0.001). (B) *Mecp2*$^{-/y}$ slices display a significant reduction in PPR at inter-stimulus intervals (ISIs) between 10 - 100 ms (overall p = 0.0071, Two-way ANOVA, genotype x ISI with Bonferonni's *post hoc*, n = 3-4 slices from individual animals, df = 1, 25, *p < 0.05, ***p < 0.001).

The loss of LSP4-2022 efficacy in *Mecp2*$^{-/y}$ mice is consistent with the loss of synaptic $mGlu_7$ expression in the hippocampus. To determine if we could potentiate $mGlu_7$ function, we utilized two structurally distinct positive allosteric modulators (PAMs) targeting $mGlu_7$, VU0422288 and VU0155094 (Jalan-Sakrikar et al., 2014). We have previously shown that both VU0422288 and VU0155094 can potentiate the response of 30 μM LSP4-2022 in wild-type slices (Jalan-Sakrikar et al., 2014). We pre-treated *Mecp2*$^{-/y}$ slices for 5 minutes with either 1 μM VU0422288 or 30 μM VU0155094 and then co-applied 1 μM VU0422288 or 30 μM VU0155094 with 30 μM LSP4-2022 for

10 minutes. Both VU0422288 and VU0155094 did not significantly alter the fEPSP slopes alone, indicating that $mGlu_7$ is not tonically active under our stimulation conditions (**Figure 22E, F**, **Figure 23A, B**). We observed a significant reduction in fEPSP slope, however, when either PAM was co-applied with LSP4-2022 (**Figure 22E, F, G**, **Figure 23A, B, C**). Additionally, application of either PAM with LSP4-2022 resulted in a significant increase in PPR (**Figure 22H**, **Figure 23D**). Taken together, these data indicate that $mGlu_7$ function is reduced in *Mecp2*$^{-/y}$ slices, consistent with the decrease in receptor expression. However, $mGlu_7$ function can be restored with a PAM.

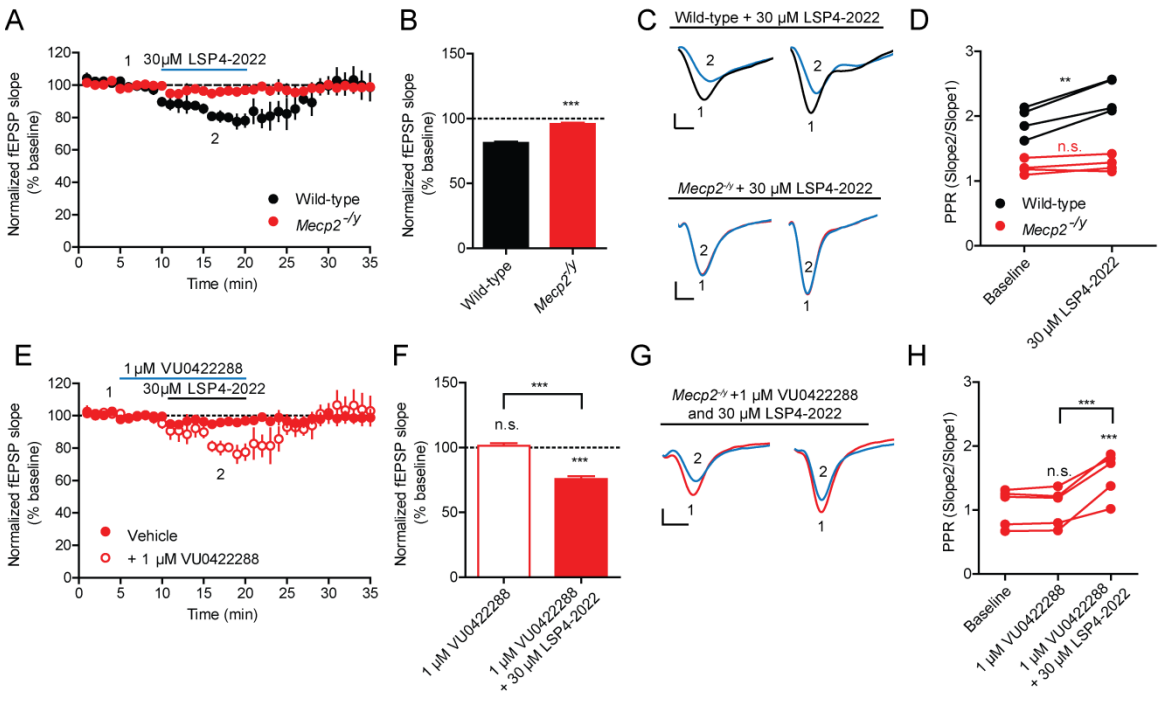

Figure 22. mGlu$_7$ function is impaired in *Mecp2*$^{-/y}$ slices and can be restored by application of VU0422288. fEPSPs were generated by paired-pulse stimulation (20 ms interstimulus interval) of the axon fibers from CA3 with a bipolar electrode. (A) Bath application of 30 μM LSP4-2022 results in a decrease in the first fEPSP slope; however, this effect is lost in *Mecp2*$^{-/y}$ slices. Data are normalized to the average baseline fEPSP slope for each genotype. Drug application is denoted by the solid blue line. (B) Quantification of normalized fEPSP slopes during 30 μM LSP4-2022 addition between wild-type and *Mecp2*$^{-/y}$ slices (% of baseline, wild-type: 81.1 ± 1.2, *Mecp2*$^{-/y}$: 95.5 ± 0.9, ***p < 0.0001, two-tailed Student's *t* test, n = 4 slices from individual animals, df = 6). (C) Sample traces from individual, representative experiments. Paired pulses were applied 20 ms apart. Baseline fEPSPs (1, black trace for wild-type, red trace for *Mecp2*$^{-/y}$) were reduced by 30 μM LSP4-2022 (2, blue line) in wild-type slices but not in *Mecp2*$^{-/y}$ slices. Scale bars represent 0.2 mV by 2 ms. (D) Application of 30 μM LSP4-2022 resulted in a significant increase in the PPR in wild-type, but not *Mecp2*$^{-/y}$, slices. PPR was calculated as the slope of the second fEPSP divided by the slope of the first fEPSP. Values for individual experiments are represented as points connected by a line. n.s. indicates no significant difference between baseline and LSP4-2022 (wild-type: 1.9 ± 0.06 at baseline vs. 2.4 ± 0.07 during LSP4-2022, *Mecp2*$^{-/y}$: 1.2 ± 0.05 at baseline vs. 1.3 ± 0.05 during LSP4-2022, **p = 0.0033, two-tailed Paired *t* test, n = 4 slices from individual animals, df = 3). (E) Pre-treatment with 1 μM VU0422288 for 5 minutes alone and for 10 minutes in combination with 30 μM LSP4-2022 results in a decrease in fEPSP slope in *Mecp2*$^{-/y}$ slices. Data are normalized to the average baseline fEPSP slope for each drug condition. VU0422288 addition is denoted by a solid blue line and LSP4-2022 addition is denoted by a solid black line. (F) Quantification of normalized fEPSP slopes during VU0422288 alone or in combination with LSP4-2022 in *Mecp2*$^{-/y}$ slices. VU0422288 alone does not significantly reduce fEPSP slope; however, in combination with LSP4-2022, there is a significant reduction in fEPSP slope from baseline and from

VU0422288 alone. n.s. indicates not significantly different from baseline (% of baseline, VU0422288 alone: 101.3 ± 1.8, VU0422288 + LSP4-2022: 75.7 ± 2.1, overall $p < 0.0001$, One-way repeated measures ANOVA with Bonferonni's *post hoc*, n = 4 slices from individual animals, df = 4, 8, ***$p< 0.0001$). (G) Sample traces from an individual, representative experiment. Baseline fEPSPs (1, red trace) were reduced by application of 1 μM VU0422288 and 30 μM LSP4-2022 (2, blue trace). Scale bars represent 0.2 mV by 2 ms. (H) Application of 1 μM VU0422288 and 30 μM LSP4-2022 significantly increases the PPR. No significant change in PPR was observed when 1 μM VU0422288 was applied alone. Values for individual experiments are represented as points connected by a line. n.s. indicates not significantly different from baseline (1.0 ± 0.1 at baseline vs. 1.1 ± 0.1 during VU0422288 alone vs. 1.6 ± 0.2 during VU0422288 + LSP4-2022, overall $p < 0.0001$, One-way repeated measures ANOVA with Bonferonni's *post hoc*, n = 5 slices from individual animals, df = 4, 8, ***$p < 0.001$).

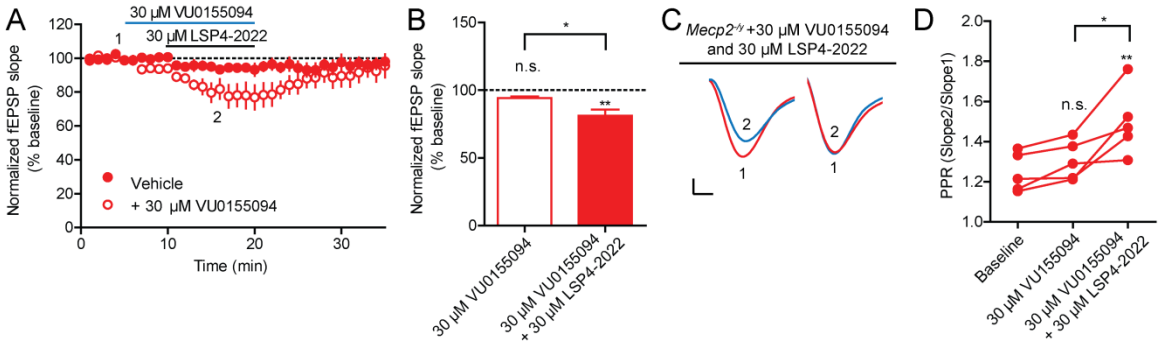

Figure 23. A structurally distinct mGlu$_7$ PAM, VU0155094, also rescues the efficacy of LSP4-2022 on fEPSPs at SC-CA1 in *Mecp2*$^{-/y}$ slices. Paired fEPSPs were generated by stimulating the axon fibers from CA3 with a bipolar electrode. (A) Bath application of 30 µM VU0155094 for 5 minutes alone and then for 10 minutes in combination with 30 µM LSP4-2022 results in a decrease in fEPSP slope which does not occur when 30 µM LSP4-2022 is applied alone. Data are normalized to the average baseline fEPSP slope. VU0155094 application is denoted by a solid blue line and LSP4-2022 addition is denoted by a solid black line. (B) Quantification of normalized fEPSP slopes during VU0155094 addition alone or in combination with LSP4-2022. VU0155094 alone does not significantly decrease fEPSP slopes; however, a significant decrease is observed when VU0155094 and LSP4-2022 are applied in combination. n.s. indicates not significantly different from baseline (% of baseline, VU0155094 alone: 94.2 ± 1.3, VU0155094 + LSP4-2022: 81.3 ± 4.6, overall $p = 0.0064$, One-way repeated measures ANOVA with Bonferonni's *post hoc*, n = 5 slices from individual mice, df = 4, 8, *$p < 0.05$). (C) Sample traces from an individual, representative experiment. Baseline fEPSPs (1, red trace) were reduced by application of 30 µM VU0155094 and 30 µM LSP4-2022 (2, blue trace). Scale bars represent 0.2 mV by 2 ms. (D) Application of 30 µM VU0155094 and 30 µM LSP4-2022 significantly increases the PPR. No significant change in PPR was observed when 30 µM VU0155094 was applied alone. Values for individual experiments are represented as points connected by a line. n.s. indicates not significantly different from baseline (1.2 ± 0.04 at baseline vs. 1.3 ± 0.04 during VU0155094 alone vs. 1.5 ±0.07 during VU0155094 + LSP4-2022, overall $p = 0.0021$, One-way repeated measures ANOVA with Bonferonni's *post hoc*, n = 5, df = 4, 8, *$p < 0.05$, **$p < 0.001$).

Potentiation of $mGlu_7$ rescues long term potentiation deficits and improves hippocampal learning and memory

Deficits in LTP at SC-CA1 synapses have been observed in several mouse models of Rett syndrome (Asaka et al., 2006; Moretti et al., 2006; Weng et al., 2011b; Ma et al., 2014). In wild-type slices, we found that an induction paradigm consisting of 2 trains of 100 Hz stimulation (high frequency stimulation, HFS) induces a robust LTP. This same stimulation produced a significant deficit in LTP in symptomatic *Mecp2*$^{-/y}$ slices (**Figure 24A, B**). The decrease in $mGlu_7$ expression, coupled with our previous report that this receptor is required for induction of LTP at SC-CA1 synapses (Klar et al., 2015), raised the possibility that the LTP deficits we observed could be caused by the loss of $mGlu_7$. Therefore, we next determined if potentiation of $mGlu_7$ could rescue LTP. Excitingly, we found that pre-treatment of *Mecp2*$^{-/y}$ slices with 1 μM VU0422288 for 10 minutes prior to and during HFS resulted in a complete rescue of LTP (**Figure 24A, B**). These data indicate that potentiation of $mGlu_7$ is sufficient to rescue LTP at the SC-CA1 synapse in *Mecp2*$^{-/y}$ mice. Additionally, the finding that application of VU0422288 alone can rescue LTP indicates that there is sufficient glutamatergic tone at the synapse during HFS for a PAM to potentiate $mGlu_7$ function without the need for application of an exogenous agonist.

Since application of VU0422288 was sufficient to rescue LTP at SC-CA1 synapses, we next determined if this rescue translated into improvements in learning and memory. The contextual fear conditioning assay is a behavioral task of learning and memory that relies on proper hippocampal function (Phillips and LeDoux, 1992). Additionally, deficits in contextual fear memory have been reported in *Mecp2* mutant

mice (Moretti et al., 2006; Pelka et al., 2006). 18-20 week old female *Mecp2*$^{+/-}$ mice were given an intraperitoneal (i.p.) injection of either vehicle, 30 mg/kg of the PAM VU0422288, 60 mg/kg of the $mGlu_7$ NAM ADX71743, or a combination of 30 mg/kg VU0422288 and 60 mg/kg ADX71743, and were then placed into an operant chamber where they received two foot shocks on day one of the task (training day). Twenty-four hours later, mice were placed back into the same chamber and the amount of time spent freezing was recorded to measure contextual fear memory (**Figure 24C**). The doses chosen for this study were based on in-house analysis of plasma and brain concentrations of VU0422288 and the published pharmacokinetic profile of ADX71743(Kalinichev et al., 2013). Using a 10 mg/kg i.p. dose of VU0422288, we achieved a total brain concentration of 10.5 μM at 1 hour post-dose. The fraction unbound in brain (F_u) for VU0422288 as determined by brain homogenate binding assays is 0.004 (or 0.4% unbound). Therefore, we determined that the unbound brain concentration achieved with a 10 mg/kg dose is 42 nM. As the EC_{50} for VU0422288 is 100 nM (Jalan-Sakrikar et al., 2014), we chose to increase the dose to 30 mg/kg to achieve a sufficient brain exposure of the compound. As VU0422288 is a group III mGlu receptor PAM, we confirmed that any effects of VU0422288 were due to activation of $mGlu_7$ by co-dosing animals with 30 mg/kg VU0422288 and 60 mg/kg of the $mGlu_7$ NAM, ADX71743.

We observed a significantly less freezing in vehicle-treated *Mecp2*$^{-/+}$ mice compared to wild-type mice (**Figure 24D**), confirming previous reports of impairments in hippocampally-dependent behaviors (Moretti et al., 2006; Pelka et al., 2006). Pre-treatment with 30 mg/kg VU0422288 had no significant effect on freezing behavior in wild-type animals; however, we observed significantly normalized freezing in *Mecp2*$^{-/+}$

mice (**Figure 24D**). Pre-treatment with ADX71743 and VU0422288 did not significantly alter freezing behavior in wild-type mice; however, ADX71743 treatment significantly blocked the improvement in freezing behavior observed with VU0422288 alone in *Mecp2*$^{-/+}$ mice (**Figure 24D**). Finally, we treated mice with 60 mg/kg ADX71743 alone and observed no change in freezing behavior in *Mecp2*$^{-/+}$ mice, most likely due to the already low level of freezing in these animals. In contrast, a significant impairment was observed in wild-type mice (**Figure 24D**), indicating that blockade of normal $mGlu_7$ function impairs fear memory, which supports the link between decreased $mGlu_7$ signaling and learning and memory defects in Rett syndrome. These data demonstrate that potentiation of $mGlu_7$ is sufficient to improve impairments in hippocampal-mediated cognitive function in a mouse model of Rett syndrome and, additionally, suggest that performance on this task is reliant on normal $mGlu_7$ function.

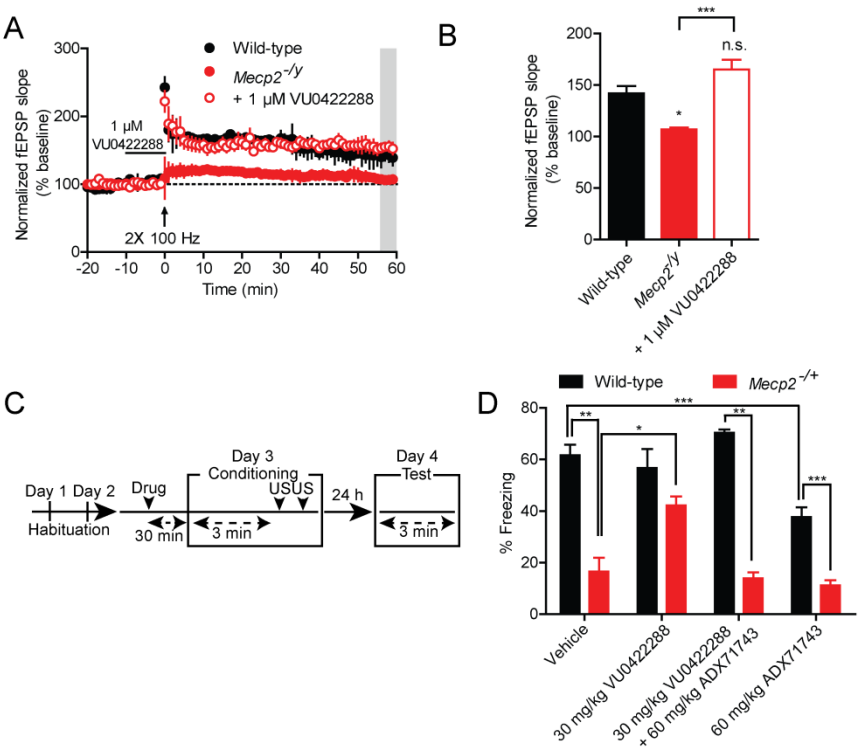

Figure 24. VU0422288 rescues LTP at SC-CA1 and improves performance in the contextual fear conditioning assay. (A) LTP was induced by applying two trains at a frequency of 100 Hz lasting 1 second with a 20 second inter-trial interval (indicated by upward-facing arrow). *Mecp2*$^{-/y}$ slices display a significant impairment in LTP, which can be reversed by pre-treatment for 10 minutes prior to and during the HFS with 1 μM VU0422288. (B) Quantification of LTP was determined by averaging the values during the last 5 minutes of recording (shaded grey area in (A)). n.s. indicates not significantly different from wild-type (% of baseline, wild-type: 141.9 ± 7.1, *Mecp2*$^{-/y}$: 106.9 ± 1.9, overall p = 0.0008, *Mecp2*$^{-/y}$ + VU0422288: 165.0 ± 9.6% of baseline, One-way ANOVA with Bonferonni's *post hoc*, n = 3-4 slices from individual animals, *p < 0.05, ***p < 0.0001). (C) Schematic of fear conditioning in *Mecp2*$^{-/+}$ female mice. Compounds were dosed at the following concentrations: vehicle (10% tween 80), 30 mg/kg VU0422288, a combination of 30 mg/kg VU0422288 and 60 mg/kg ADX71743, or 60 mg/kg ADX71743 (denoted by "drug") US indicates unconditioned stimulus. (D) Vehicle-treated *Mecp2*$^{-/+}$ mice (red) spent significantly less time freezing than vehicle-treated wild-type mice (wild-type: 61.7 ± 4.1%, *Mecp2*$^{-/+}$: 16.5 ± 5.4%, black, **p < 0.001). 30 mg/kg VU0422288 treatment resulted in a significant increase in freezing behavior in *Mecp2*$^{-/+}$ mice (wild-type: 56.7 ± 7.4%, *Mecp2*$^{-/+}$: 42.2 ± 3.5%, *p < 0.0017, *Mecp2*$^{-/+}$ + VU0422288 is not significantly different from wild-type + vehicle). Co-treatment with a combination of VU0422288 and ADX71743 resulted in a significant blockade of the effects of VU0422288 alone (wild-type: 70.4 ± 1.3%, *Mecp2*$^{-/+}$: 13.9 ± 2.3%, ** p < 0.001 between wild-type and *Mecp2*$^{-/+}$ treated with VU0422288 + ADX71743, *Mecp2*$^{-/+}$ treated with VU0422288 + ADX71743 is not significantly different from *Mecp2*$^{-/+}$ + vehicle alone). Additionally, 60 mg/kg ADX71743 caused a significant impairment in wild-type (37.6 ± 3.8%, ***p = 0.0009), but not *Mecp2*$^{-/+}$ mice; however, *Mecp2*$^{-/+}$ mice treated with ADX71743 still froze significantly less than wild-type (11.1 ± 2.0%, *** p <

0.0001) (overall $p < 0.0001$ for drug and genotype, Two-way ANOVA, genotype x drug, n = 7-8 mice, df = 3, 50 with two-tailed Student's *t* tests used for *post hoc* analysis).

Discussion

Since the identification of *MECP2* as the causative gene for Rett syndrome, there has been considerable effort to identify novel targets regulated by MECP2 that are amenable to drug development (Amir et al., 1999). Unfortunately, several large-scale microarray studies have failed to find substantial changes in gene expression with MECP2 loss and have identified very few genes regulated by MECP2 that are potential druggable targets (Traynor et al., 2002; Tudor et al., 2002; Ben-Shachar et al., 2009). Here we have shown that the expression of *GRM7* is directly regulated by MECP2. We found significant reductions in $mGlu_7$ expression throughout the brain and, in particular, at the synaptic level in the cortex and hippocampus in *Mecp2*$^{-/y}$ mice. Importantly, this reduction is also observed in motor cortical tissue from Rett syndrome patients. The reduction in receptor expression in the hippocampus of *Mecp2*$^{-/y}$ mice translates into a loss of $mGlu_7$ function at SC-CA1 synapses. Excitingly, we found that treatment with two structurally distinct $mGlu_7$ PAMs can restore $mGlu_7$ function and rescue learning and memory phenotypes in a mouse model of Rett syndrome. In addition, this decrease in *Grm7* mRNA has been also been observed in the cortex of *Mecp2*$^{-/y}$ mice beginning as early as postnatal day 8 (Bedogni et al., 2015).

The presence of deficits in LTP at the SC-CA1 synapse and in behavioral tasks reliant on proper hippocampal function in mouse models of Rett syndrome has been well-characterized in the literature (Asaka et al., 2006; Moretti et al., 2006; Weng et al., 2011b). We previously identified $mGlu_7$ as a necessary component of LTP induction at

SC-CA1 synapses via a mechanism that involves disinhibition of GABAergic tone onto CA1 pyramidal cells (Klar et al., 2015). This mechanism occurs through activation of $mGlu_7$ expressed pre-synaptically on GABAergic interneurons that synapse directly onto CA1 cells. Indeed, it has previously been reported that loss of Mecp2 from GABAergic interneurons in mice is sufficient to recapitulate many Rett syndrome endophenotypes, including deficits in LTP induction at SC-CA1 synapses (Chao et al., 2010). These studies show that the origin of the LTP deficit at this synapse is likely GABAergic in nature, which is consistent with the important role $mGlu_7$ serves in the induction of LTP. Taken together, these findings indicate that the loss of $mGlu_7$ could be the underlying cause of the deficits we and others have observed in the induction of LTP in mouse models of Rett syndrome (Asaka et al., 2006; Moretti et al., 2006; Weng et al., 2011b). Excitingly, we found that potentiation of $mGlu_7$ is able to rescue LTP and, in addition, improve deficits in hippocampally-dependent contextual fear memory, indicating that $mGlu_7$ PAMs can be efficacious *in vivo*. All of these studies lead to the exciting idea that modulation of $mGlu_7$ may be a novel therapeutic target for the treatment of Rett syndrome.

While loss of MECP2 leads to Rett syndrome, the doubling of MECP2 leads to a similar neurodevelopmental disorder called *MECP2* Duplication syndrome, which is an X-linked disorder with 100% penetrance in males that results in mental retardation, motor impairments, autistic-like features, and the recurrence of severe respiratory infections (Na et al., 2013). Interestingly, the gain of excessive Mecp2 in mouse models results in enhanced LTP (Collins et al., 2004). These data are extremely interesting in light of our findings that $mGlu_7$ expression is bi-directionally regulated by MECP2 and that $mGlu_7$ is

necessary for the induction of LTP and could point to a role for $mGlu_7$ in mediating this phenotype in opposite directions in both disorders.

In addition to $mGlu_7$'s role in the regulation of LTP induction in area CA1, $mGlu_7$ is also expressed in a variety of other brain regions that overlap with the major symptom domains of Rett syndrome. For example, the receptor is widely expressed throughout the cortex, which coincides with several areas where deficits in LTP have been observed in *Mecp2* mutant mice, including the primary sensory and motor cortex (Moretti et al., 2006). Additionally, antagonism of $mGlu_7$ blocks LTP induction in the lateral amygdala, which also results in decreases in anxiety-like behavior (Gee et al., 2014). This finding is particularly interesting because *Mecp2* mutant mice also display an anxiolytic phenotype, whereas *Mecp2* Duplication mice show enhanced anxiety (Na et al., 2013; Wegener et al., 2014). Finally, motor impairments are extremely prevalent in *Mecp2* mutant animal models, which could also partially be explained by the expression of $mGlu_7$ in the striatum and the severe decrease we observe in *Mecp2*-deficient mice in this brain region. The expression of $mGlu_7$ in all of these areas potentially indicates that the efficacy of $mGlu_7$ PAMs could expand beyond improvements in cognitive impairments and should be the focus of future studies.

GPCRs like $mGlu_7$ are considered to be highly druggable targets because their endogenous function is to integrate external signals in to intracellular responses upon ligand binding. This is evident by the fact that molecules targeting GPCRs represent 27% of all FDA approved drugs (Bartos et al., 2002). Here, we describe how the loss of MECP2 results in decreased $mGlu_7$ signaling, attenuated synaptic plasticity, and impaired learning and memory. Additionally, we have shown that potentiation of $mGlu_7$ function

using small molecule PAMs is sufficient to restore LTP at SC-CA1 synapses in the hippocampus and improve performance in a behavioral measure of learning and memory. These exciting data corroborate other studies suggesting that the plasticity defects and cognitive impairments in Rett syndrome mouse models are reversible and indicate that small molecule PAMs targeting $mGlu_7$ can be efficacious in affecting these phenotypes. Finally, as the molecular underpinnings for both Rett syndrome and *MECP2* duplication syndrome share a common protein in MECP2, the identification of a direct target in $mGlu_7$ may represent a key mediator of both disease states that can be targeted pharmacologically to provide symptom improvement in both disorders.

CHAPTER V

DISCUSSION AND FUTURE DIRECTIONS

Over the past several decades, there has been a growing interest in the development of novel pharmacological compounds that target the mGlu receptors as new treatments for a variety of neurological, psychiatric, and neurodevelopmental disorders (Conn et al., 2014). Many initial programs focused on the development of compounds that bind to the orthosteric binding site; however, most researchers in the field have shifted instead to the development of compounds that bind to allosteric sites (Nickols and Conn, 2014). These sites, which are less highly conserved among the mGlu receptor family members, have allowed for the more rapid and effective development of selective compounds targeting one specific receptor over the other family members. For many of the mGlu receptors, we now have selective tool compounds with low nanomolar-micromolar potencies for a particular receptor, thus providing the unique ability to probe specific receptor function without the confounding activation of other family members. In particular, for $mGlu_{1,\ 2,\ 3,\ and\ 5}$, selective PAMs and NAMs exist, which allows for studies of both the potentiation and antagonism of those receptors (Conn et al., 2014).

Unfortunately, though major advances have occurred in the development of selective tool compounds for many of the mGlu receptors, the identification of selective compounds targeting $mGlu_7$ has lagged behind. There are several compounds that have been developed for $mGlu_7$ that initially seemed promising. AMN082 was identified as the first selective allosteric agonist of $mGlu_7$. The use of this compound was encouraging

due to its ability to selectively activate $mGlu_7$ without the need for binding of orthosteric agonists. However, it is now appreciated that AMN082 functions as a biased agonist towards the activation of $G_{i/o}$ protein activation, with little to no activity observed for the activation of β Arrestin and ERK signaling (Mitsukawa et al., 2005; Iacovelli et al., 2014). In addition, AMN082 causes rapid internalization of $mGlu_7$ from the cell surface, indicating that perhaps it is also biased towards pathways mediating internalization (Pelkey et al., 2007). Finally, the use of AMN082 *in vivo* is limited by the fact that it is metabolized to a compound that modulates serotonergic activity, which could explain many of the reports classifying the activation of $mGlu_7$ as a novel antidepressant mechanism (Palucha et al., 2007; Sukoff Rizzo et al., 2011). As such, the use of AMN082, particularly for *in vivo* studies of $mGlu_7$ function, is limited by the production of active metabolites. In addition to the discovery of AMN082, MMPIP was the first selective NAM of $mGlu_7$ discovered. Like AMN082, this discovery was exciting because it was the first instance where $mGlu_7$ could be selectively antagonized. However, MMPIP exhibits context-dependent pharmacology similar to what is observed with AMN082, limiting its utility. Indeed, we have observed that, while MMPIP antagonizes the actions of L-AP4 *in vitro*, it does not block the effects of L-AP4 at the SC-CA1 synapse in the hippocampus (Niswender et al., 2010). While interesting from a pharmacological perspective, this discrepancy complicates MMPIP's use in *in vivo* settings.

Due to these set-backs in the development of selective tool compounds targeting $mGlu_7$, very little is known about the function of this receptor *in vivo.* Indeed, much of what is known about the receptor has been elucidated using a combination of non-

selective agonists and antagonists coupled with expression studies. It is clear from these studies that $mGlu_7$ is widely expressed throughout the CNS and most likely plays a critical role in the regulation of excitation: inhibition balance due to its high evolutionary conservation. Interestingly, despite its high evolutionary conservation, $mGlu_7$ has the lowest affinity for the orthosteric agonist, glutamate, among all of the mGlu receptors (Bradley et al., 1996; Flor et al., 1997; Kinoshita et al., 1998). This finding is particularly interesting because at several synapses throughout the brain, $mGlu_7$ is expressed directly within the synaptic cleft (Bradley et al., 1996; Flor et al., 1997; Dalezios et al., 2002). At this location, it would seem that the receptor would be subjected to extremely high concentrations of glutamate which, coupled with its low agonist affinity, suggests that $mGlu_7$ may become active under intense synaptic firing events to act as a "brake" on glutamatergic transmission. Indeed, this viewpoint was fairly well-accepted in the field, despite a lack of selective compounds to directly test this idea.

Recently, several compounds have been developed that now allow for the direct testing of $mGlu_7$ function in native systems. The most exciting compound is a novel, selective NAM termed ADX71743 (Kalinichev et al., 2013). This compound is potent and functions both *in vitro* and *ex vivo* in brain slice electrophysiology, making it an extremely useful tool compound. Additionally, it has a favorable pharmacokinetic profile suitable for *in vivo* use and has been shown to have behavioral efficacy in the marble burying assay, elevated plus maze, amphetamine-induced hyperlocomotion assay, and contextual fear conditioning assay, **Chapter IV** (Kalinichev et al., 2013; Klar et al., 2015).

The focus of this thesis is on the function of $mGlu_7$ at the SC-CA1 synapse in the hippocampus. This synapse is a particularly good location to study $mGlu_7$ function because it is the only group III mGlu receptor expressed at this synapse in adult animals (Baskys and Malenka, 1991; Bradley et al., 1998; Huber et al., 2002; Ayala et al., 2008). Indeed, our lab has extensively characterized a developmental switch that occurs between $mGlu_8$ and $mGlu_7$ expression at this synapse. In neonatal animals, $mGlu_8$ is the only group III mGlu receptor expressed at SC-CA1 terminals, whereas, in adults, only $mGlu_7$ is expressed. As such, this allows us to make use of non-selective compounds that have activity at $mGlu_7$ for the study of this synapse. We have extensively utilized LSP4-2022, an orthosteric agonist with activity at $mGlu_{4,\ 7,\ and\ 8}$, and two distinct group III PAMs that are equipotent at all of the group III receptors, VU0155094 and VU0422288 (Goudet et al., 2012; Jalan-Sakrikar et al., 2014). These compounds, together with ADX71743, have allowed us to directly investigate the role of $mGlu_7$ in synaptic transmission at the SC-CA1 synapse.

The extremely low affinity of $mGlu_7$ for glutamate, coupled with its localization directly within the synaptic cleft on CA3 terminals, has led to the hypothesis that $mGlu_7$ served as a brake on glutamatergic signaling. It is clear from many reports that $mGlu_7$ is active in this location, as application of agonists results in a decrease in glutamatergic transmission coinciding with an increase in paired-pulse ratios (Baskys and Malenka, 1991; Gereau and Conn, 1995b; Ayala et al., 2008; Jalan-Sakrikar et al., 2014; Klar et al., 2015). Together, these data indicate that $mGlu_7$ can decrease glutamate release via a presynaptic mechanism. Despite this evidence for functional $mGlu_7$ on glutamatergic terminals, we have not been able to observe activation of these receptors in response to

synaptic glutamate release, **Chapter III** (Klar et al., 2015). Indeed, neither low frequency nor high frequency SC afferent firing seems to result in the activation of $mGlu_7$ expressed presynaptically on glutamatergic terminals. In contrast, we instead identified a population of $mGlu_7$ expressed presynaptically on GABAergic terminals which becomes active only under intense SC firing to decrease GABAergic tone on CA1 pyramidal cells, **Chapter III** (Klar et al., 2015). These data are in agreement with several reports showing that $mGlu_7$ is expressed presynaptically on GABAergic interneurons in the CA1 region of the hippocampus and that, in *in vitro* systems, activation of $mGlu_7$ can decrease GABA release (Somogyi et al., 2003; Summa et al., 2013). Collectively, however, this indicates that, in area CA1, intense synaptic firing results in the activation of $mGlu_7$ heteroreceptors on GABAergic interneurons, leading to a net increase, rather than decrease, in excitatory drive through area CA1. Importantly, we have also found that this HFS-induced disinhibition is critically necessary for the induction of LTP at this synapse, **Chapter III** (Klar et al., 2015). Indeed, blockade of $mGlu_7$ using ADX71743 or the non-selective orthosteric antagonist LY341495 impairs the induction of LTP, indicating that the mechanism of LTP induction at this synapse requires not only NMDA receptor activation but also activation of $mGlu_7$. In this way, $mGlu_7$ acts as a co-incident detector of glutamate levels in the synapse in order to facilitate the required excitation of CA1 pyramidal cells necessary for LTP to occur. This finding is particularly intriguing because it perhaps indicates that the disinhibition caused by $mGlu_7$ activation directly contributes to the depolarization of CA1 cells and the subsequent necessary relief of the Mg^{2+} block of NMDA receptors. In this way, $mGlu_7$ may act upstream of NMDA

receptors in concert with AMPA receptors to first depolarize pyramidal cells sufficiently to allow for appropriate NMDA receptor activation to occur.

Our findings indicate that $mGlu_7$ activation is necessary for the induction of LTP at SC-CA1 synapses. Interestingly, there are many reports indicating that synaptic plasticity at this synapse is necessary for rodent performance on a variety of spatial and social learning and memory tasks. These tasks include the contextual fear conditioning assay, Morris water maze, novel object recognition task, and the inhibitory avoidance task (Davis et al., 1992; Phillips and LeDoux, 1992; Maren et al., 1994; Diana et al., 1995; Chen et al., 1996; Mumby, 2001; Cohen et al., 2013; Laeremans et al., 2014). Loss of $mGlu_7$ function, due to either antagonism or genetic deletion of the receptor, results in impairments in performance on many of these tasks, thus providing additional evidence that $mGlu_7$ activation at SC-CA1 synapses is fundamentally important for learning and memory *in vivo*. Indeed, $mGlu_7$ KO mice display deficits in contextual fear conditioning, novel object recognition, and several spatial maze tasks (Holscher et al., 2004, 2005; Callaerts-Vegh et al., 2006; Goddyn et al., 2008). Additionally, we observed a significant deficit in performance on the contextual fear conditioning assay in animals treated systemically with ADX71743, **Chapter IV**.

Taken together, the high degree of evolutionary conservation of the $mGlu_7$ amino acid sequence, coupled with our findings of a necessary role in the induction of LTP at SC-CA1 synapses, leads to the possibility that $mGlu_7$ may play a similar role at other synapses in the brain as well. $mGlu_7$ is widely expressed throughout the CNS, with strong expression in the cortex, cerebellum, striatum, and amygdala (Bradley et al., 1996; Bradley et al., 1998; Kinoshita et al., 1998). Many synapses in these brain regions can

also undergo synaptic plasticity, perhaps indicating that $mGlu_7$ may function via a similar mechanism at those synapses as well. Indeed, one recent study found that application of a novel $mGlu_7$ orthosteric antagonist, XAP044, was sufficient to block LTP induced at the thalamo-lateral amygdala synapse (Gee et al., 2014). It will be interesting to determine if $mGlu_7$ facilitates LTP at this synapse via the same or a similar mechanism as we observed at SC-CA1 synapses. This is feasible due to the fact that LTP at the thalamo-lateral amygdala synapse is also NMDA receptor-dependent, perhaps indicating that $mGlu_7$ activation is necessary for sufficient disinhibition of the glutamatergic principle cells in the lateral amygdala (Lee et al., 2002). In addition to the amygdala, $mGlu_7$ is also expressed in layers II/III of the cortex and at the cortico-striatal synapse and it will be important to determine if $mGlu_7$ plays a role in plasticity induction at these synapses as well (Bradley et al., 1998; Dalezios et al., 2002).

In addition to the possibility that $mGlu_7$ mediates the induction of LTP at other synapses in the brain, it is also possible that it is involved in the induction of other forms of synaptic plasticity as well. One particularly important question to be answered is whether the necessity for $mGlu_7$ activation for LTP induction with a 100 Hz HFS induction paradigm also occurs using a more physiological induction paradigm such as theta burst stimulation (TBS). Indeed, hippocampal pyramidal neurons have been shown to oscillate at the theta frequency *in vivo*, making the TBS induction paradigm more relevant to the natural processes *in vivo* that potentially allow for learning and memory to occur (Miles and Wong, 1983). In addition to confirming that $mGlu_7$ plays a role in the induction of other forms of LTP, it will also be important to determine if $mGlu_7$ can mediate the induction of other forms of synaptic plasticity. At the Mossy Fiber-stratum

lucidum interneuron (SLIN) synapse, a presynaptic form of NMDA receptor-independent LTD exists that has been shown to require the activation of group III mGlu receptors (Lei and McBain, 2002, 2004). This LTD can be blocked by the application of the group III mGlu receptor antagonist, MSOP, and is thought to be primarily mediated by $mGlu_7$ activation (Shigemoto et al., 1997; Pelkey et al., 2005; Pelkey and McBain, 2008). Moreover, application of L-AP4 at a concentration high enough to activate $mGlu_7$ in combination with basal synaptic stimulation induces a chemical form of LTD at the MF-SLIN synapses that shares the presynaptic expression profile observed for tetanus-induced LTD (Maccaferri et al., 1998; Pelkey et al., 2005). Interestingly, this form of chemical LTD is absent when presynaptic stimulation is interrupted during L-AP4 treatment (Pelkey et al., 2005) or when postsynaptic Ca^{2+} influx is blocked (Lei and McBain, 2002; Pelkey et al., 2005), indicating that this group III mGlu receptor-mediated LTD is hebbian in nature. In further studies, it has also been shown that MF-SLIN LTD relies on $mGlu_7$-mediated PKC signaling and subsequent reduction in the activity of P/Q-type voltage gated Ca^{2+} channels (Pelkey et al., 2005; Pelkey et al., 2006). The MF-SLIN synapses also show bidirectional metaplasticity, where the polarity of tetanus-induced-plasticity depends upon the recent history of the synapse. Therefore, if MF-SLIN synapses first undergo L-AP4-induced LTD, a subsequent tetanic stimulation reverses this depression by persistently enhancing neurotransmitter release and inducing LTP (Pelkey et al., 2005). It is hypothesized that $mGlu_7$ plays an important role in this bidirectional plasticity and acts as a 'metaplastic switch' (Pelkey and McBain, 2008). Indeed, exogenous agonist treatment can lead to $mGlu_7$ internalization from MF-SLIN

synapses (Pelkey et al., 2005; Pelkey et al., 2007) and the precise level of $mGlu_7$ in the presynaptic terminal can be the deciding factor between LTD and LTP at this synapse.

While the function of $mGlu_7$ as a metaplastic switch has been well-characterized at MF-SLIN synapses, very little is known about the function of $mGlu_7$ expressed presynaptically at glutamatergic SC-CA1 synapses. As we have reported, $mGlu_7$ expressed on GABAergic interneurons in this region is involved in the induction of LTP via disinhibition of CA1 cells; however, the function of $mGlu_7$ on glutamatergic terminals is unknown (Klar et al., 2015). One interesting finding is that a form of LTD, termed paired-pulse low frequency stimulation induced LTD (PP-LFS LTD) is thought to occur via a presynaptic mechanism and is does not require the activation of NMDA receptors (Kemp and Bashir, 1999; Kemp et al., 2000). Additionally, this form of LTD can be completely blocked by application of LY341495 at concentrations that are sufficient to block $mGlu_7$, but not group I mGlu receptors (Huber et al., 2000). It is possible that $mGlu_7$ expressed presynaptically on glutamatergic terminals in area CA1 becomes activated under the PP-LFS induction protocol to cause LTD via a similar mechanism to that seen at MF-SLIN synapses. Indeed, PP-LFS LTD requires the activation of PKC similar to LTD at MF-SLIN synapses, perhaps indicating that the mechanism of induction for PP-LFS LTD similarly requires presynaptic activation of $mGlu_7$ and a PKC-mediated decrease in neurotransmitter release probability (Oliet et al., 1997). This possibility leads to the idea that $mGlu_7$ may require very specific levels of glutamate to become active. The PP-LFS stimulation protocol consists of 900-1200 paired pulses delivered at low frequency over the course of 15 minutes. This time frame, in contrast to the HFS protocol used to induce LTP, should cause a slow rise in the

concentration of glutamate at the synapse that is perhaps ideal to activate $mGlu_7$ expressed in the synaptic cleft. As $mGlu_7$ has previously been shown to undergo agonist-induced internalization at MF-SLIN synapses, perhaps the same phenomenon occurs at SC-CA1 synapses as well such that HFS causes a rapid rise in glutamate concentration sufficient to cause internalization of $mGlu_7$ expressed on glutamatergic terminals (Pelkey et al., 2005). This internalization could shift the balance between LTD and LTP induction and allow for $mGlu_7$ expressed on GABAergic interneurons to become active and induce LTP (Klar et al., 2015).

Regardless of whether $mGlu_7$ functions to mediate other forms of synaptic plasticity at SC-CA1 synapses, its role in the induction of LTP and its ability to modulate fear memory indicate that disorders associated with deficits in both LTP and learning and memory may either be due to alterations in $mGlu_7$ function or could be improved by compounds that activate $mGlu_7$. Indeed, there is one recent report of a child with a *de novo* 303 kb deletion at location 3p26.1, which encompasses 5 coding exons of the *GRM7* gene (Liu et al., 2015). This child presented with autism spectrum disorder and hyperactivity, indicating that loss of $mGlu_7$ in humans is sufficient to cause the manifestation of autism-like symptoms. Indeed, this child displayed severe deficits in communication and cognition, which is consistent with rodent models where $mGlu_7$ has been genetically deleted (Bushell et al., 2002; Holscher et al., 2004, 2005; Callaerts-Vegh et al., 2006). These findings indicate that $mGlu_7$ may underlie some of the symptoms observed in patients with autism spectrum disorders. One such disorder, Rett syndrome, is a genetic form of autism caused by *de novo* mutations in the methyl CpG binding protein 2 (*MECP2*) gene in humans. The disorder manifests with a variety of symptom

domains, one of which is the presence of cognitive impairments and the inability to communicate, not unlike the phenotype observed in the child with a genetic deletion of *GRM7*. We have now reported that *GRM7* is a direct target of MECP2 and that loss of *Mecp2* in rodent models leads to reductions in $mGlu_7$ expression and function, **Chapter IV**. Importantly, we have also found that these same reductions in $mGlu_7$ expression observed in mouse models of the disorder are also present in human brain tissue as well. We were able to acquire *post mortem* motor cortical tissue samples from several female patients diagnosed with Rett syndrome and with known mutations in *MECP2*. Excitingly, we observed significant reductions in $mGlu_7$ expression in the patients harboring known *MECP2* mutations, indicating that our findings from animal models of Rett syndrome are likely to translate into the clinic.

These findings from *post mortem* human Rett syndrome tissue are exciting because they could indicate that $mGlu_7$ expression correlates with disease progression and could in fact be used as a biomarker for Rett syndrome. In addition, there are several reports indicating that the ability of Mecp2 to interact with runs of A/T's in DNA is correlated with disease progression (Klose et al., 2005; Baker et al., 2013). Indeed, Baker *et al.* found that mouse models harboring mutations that disrupted AT hook function in Mecp2 displayed more severe disease progression than mice harboring point mutations that retained AT hook function (Baker et al., 2013). Additionally, we have shown that the expression of $mGlu_7$ in native systems is directly regulated by the ability of Mecp2 to bind to runs of A/T's in the promoter of *GRM7*, **Chapter IV**. Taken together, these findings indicate that, for *GRM7* expression, Mecp2 regulation requires proper interaction with the A/T run we identified in the Mecp2 binding site of the *GRM7* promoter.

We have shown in **Chapter IV** of this thesis that potentiation of $mGlu_7$ function is sufficient to rescue LTP deficits and improve performance in the contextual fear conditioning assay. These findings, coupled with the fact that $mGlu_7$ is also reduced in the brains of human patients with Rett syndrome, provide strong evidence that selective PAMs of $mGlu_7$ could be a novel therapeutic mechanism to improve some of the cognitive impairments seen in patients. Because $mGlu_7$ is a direct target of MECP2 and there is a large clinical variability in the Rett syndrome population due both to mutation location and X chromosome inactivation, the precise level of $mGlu_7$ expression may vary greatly between patients. Indeed, we observe just such a phenomenon in our data from human Rett syndrome $mGlu_7$ protein expression studies. In our patient cohort, we received 4 samples from patients with the same mutation in MECP2, R255X. Even though these four patients have the same mutation, they express varying levels of $mGlu_7$. Since this variability potentially exists for other patients as well, it may be useful to image $mGlu_7$ levels in the hippocampus or in other brain regions in patients prior to beginning treatment with any $mGlu_7$ potentiators to help ensure that an inappropriate potentiation of $mGlu_7$ does not occur. In order to achieve this, it will be important to develop a selective radioligand for $mGlu_7$ that would allow physicians to determine the expression of $mGlu_7$ in specific patients. This personalized approach would allow for the discrimination between patients who have substantial reductions in $mGlu_7$ and those who do not. Indeed, there has been one study to date on the development of a novel radioligand for imaging $mGlu_7$ expression *in vivo* based on the NAM, MMPIP (Yamasaki et al., 2013). Yamasaki *et al.* synthesized [^{11}C]MMPIP with a reported binding constant (K_B) of 30 nM. While they observed specific binding in rat brain slices, they failed to see

any specific binding of the radioligand when it was dosed *in vivo* and imaged using positron emission tomography (PET), indicating that [^{11}C]MMPIP is not a good candidate for use in human imaging, most likely due to its low binding affinity for the receptor (Yamasaki et al., 2013). Despite a lack of utility *in vivo*, these studies demonstrate that novel $mGlu_7$ NAMs, such as ADX71743 or future compounds with high affinities for the receptor, may indeed make good candidates as PET tracers for use in Rett syndrome patients.

In order for imaging the levels of $mGlu_7$ in Rett syndrome patients to have utility, several basic science questions still remain to be answered. First, to date we have only investigated the effect of global loss of Mecp2 on $mGlu_7$ expression. It will be extremely important to determine if some of the newly developed point mutant mouse models also display the same deficits in $mGlu_7$ expression (Shahbazian et al., 2002; Moretti et al., 2006; Lawson-Yuen et al., 2007; Jentarra et al., 2010; Baker et al., 2013). Not only will this corroborate our findings from the global Mecp2 KO mice, but it will also provide a greater understanding of how particular mutations in Mecp2 effect $mGlu_7$ expression. Indeed, we have hypothesized that the function of the AT hook domains in Mecp2 are important for $mGlu_7$ expression and it will be interesting to see if there are differences in the expression of $mGlu_7$ between the Arg270X and Gly273X mouse models, which provide a direct comparison between functional and non-functional AT hook domains in Mecp2 (Baker et al., 2013). If we do observe differences in $mGlu_7$ expression between the varying point mutant mouse models, it will next be important to determine if the expression of $mGlu_7$ correlates with the presence of deficits in both LTP induction at SC-CA1 synapses and performance on the contextual fear conditioning assay. Indeed, based

on our findings that $mGlu_7$ expression is necessary for the induction of LTP at the SC-CA1 synapse, we would predict that mutant Mecp2 models that do not have concomitant decreases in $mGlu_7$ expression would not have deficits in LTP induction or contextual fear conditioning (Klar et al., 2015), **Chapter III**. In these cases, we would also predict that an $mGlu_7$ PAM would not have efficacy in improving cognitive impairments. In this way, we could build a greater understanding not only of the precise functional domains of Mecp2 that regulate $mGlu_7$ expression but also whether decreases in $mGlu_7$ expression are directly correlated with the presence of synaptic plasticity deficits and cognitive impairments which would provide strong rationale for the use of an $mGlu_7$ PET tracer in Rett syndrome patients.

In addition to determining whether $mGlu_7$ expression correlates with specific mutations in Mecp2, another important question that remains to be answered is when $mGlu_7$ levels decrease in relation to the course of disease. Rett syndrome is a unique disorder because it is characterized by a rapid regression phase (Chahrour and Zoghbi, 2007; Weng et al., 2011a). Girls born with mutations in *MECP2* develop normally for the first 6-18 months of life where they achieve developmental milestones, such as learning to walk and talk. After the first 6-18 months of life, however, girls undergo a regression phase in which they lose many of the skills they had learned and develop very characteristic symptoms of Rett syndrome, such as loss of purposeful hand movement, stereotyped behaviors, cognitive impairments, autism-like features, seizures, and breathing abnormalities (Chahrour and Zoghbi, 2007; Weng et al., 2011a). Despite the commonality of the regression phase among all children who develop Rett syndrome, the exact causes mediating this phase remain unknown. One finding that is particularly

interesting in light of the observed regression phase in Rett syndrome is the developmental switch described earlier that occurs at the SC-CA1 synapse between $mGlu_8$ and $mGlu_7$ (Ayala et al., 2008). It is possible that perhaps one of the reasons for children with mutations in *MECP2* to regress from normal cognitive development into a state of impairment is a loss of this developmental switch in the hippocampus. Indeed, Mecp2 KO mice display no significant impairment in the induction of LTP prior to the onset of symptoms (Asaka et al., 2006; Weng et al., 2011b). This finding could perhaps indicate that there is a time-lock between the developmental switch from the expression of $mGlu_8$ to $mGlu_7$ and the onset of deficits in LTP and cognitive impairments. It will be extremely important in the future to profile the expression of $mGlu_7$ over the entire lifespan of Mecp2 KO animals, particularly in neonatal and pre-weaning ages to determine if there is a correlation between $mGlu_7$ expression and symptom development. Indeed, in wild-type animals, it has been shown that $mGlu_7$ expression is low early in life and progressively increases with age (Bradley et al., 1996; Bradley et al., 1998; Ayala et al., 2008). This could indicate that, prior to the developmental switch at SC-CA1, $mGlu_8$ plays a predominant role in the induction of LTP, and that, in cases of Rett syndrome, a loss in the ability to up-regulate $mGlu_7$ expression results in the deficits in synaptic plasticity and cognition observed in animal models. Excitingly, a recent study has observed a significant reduction in *Grm7* mRNA in the cortex of *Mecp2*$^{-/y}$ mice beginning as early as postnatal day 8, indicating that the deficits in $mGlu_7$ expression may indeed precede the developmental regression (Bedogni et al., 2015).

The precise level of MECP2 in the brain is critical for normal neurological function (Na et al., 2013). This is best exemplified by two autism-like disorders resulting

from opposite levels of MECP2 function. As described in detail above, the loss of MECP2 function results in the autism spectrum disorder, Rett syndrome. For several years, it was thought that simply re-introducing a new, non-mutated, copy of MECP2 to mouse models of Rett syndrome would fix many of the symptoms (Luikenhuis et al., 2004; Guy et al., 2007). However, it is now appreciated that there is a precise level of MECP2 function which is necessary for proper neuronal function (Na et al., 2013). This finding primarily stemmed from the discovery of a second autism spectrum disorder, called MECP2 Duplication syndrome, which is a gain-of-function disorder that results from duplication or triplication of the MECP2 gene (Ramocki et al., 2010). Interestingly, MECP2 Duplication syndrome primarily affects boys and results in some opposite phenotypes to those observed in Rett syndrome. Of particular importance for this discussion, loss of Mecp2 function results in *reduced* paired-pulse ratios, impairments in the induction of LTP at the SC-CA1 synapse, and reduced performance in the contextual fear conditioning assay (Asaka et al., 2006; Moretti et al., 2006; Stearns et al., 2007; McGraw et al., 2011; Weng et al., 2011b). Interestingly, the duplication of Mecp2 results in *increased* paired-pulse ratios, an enhancement in the level of LTP, and enhanced fear conditioning (Collins et al., 2004). These opposite electrophysiological and behavioral phenotypes in mouse models harboring opposite levels of Mecp2 function indicate that perhaps genes that are directly regulated by Mecp2 are mediating these phenomenon. Importantly, as we have identified $mGlu_7$ as a direct target of Mecp2-mediated transcription and have found that, in Mecp2 KO mice, loss of $mGlu_7$ may result in the impairments in LTP induction, it will be particularly important to determine if there are also alterations in $mGlu_7$ in Mecp2 Duplication mouse models as well. We hypothesize

that duplication of Mecp2 may result in an over-expression of $mGlu_7$ at the SC-CA1 synapse in the hippocampus. If this is the case, then we would predict that the enhanced LTP at this synapse is mediated by increased $mGlu_7$ activation during HFS and a resulting enhancement in the disinhibition of CA1 pyramidal cells. This idea is in-line with our findings in wild-type animals that agonism of $mGlu_7$ can facilitate LTP induction, **Chapter III** (Klar et al., 2015). Additionally, these findings may also indicate that antagonism of $mGlu_7$, particularly using the $mGlu_7$ NAM, ADX71743, may be beneficial in normalizing the level of LTP induction in duplication animals and may also be efficacious in reversing the enhanced fear memory as well.

For several years, there has been a large effort in the Rett syndrome field to identify the role of Mecp2 in specific types of neurons. As such, several different mouse models have been generated where Mecp2 is deleted from only one type of neuron, including GABAergic, serotonergic, dopaminergic and noradrenergic, and from neurons of the hypothalamus (Chen et al., 2001; Gemelli et al., 2006; Fyffe et al., 2008; Samaco et al., 2009; Chao et al., 2010). Interestingly, for many of these mouse models, loss of Mecp2 only results in the recapitulation of very specific symptom clusters, indicating that Mecp2 plays a distinct role in each of those neuronal populations (Fyffe et al., 2008; Samaco et al., 2009). When Mecp2 is removed from GABAergic neurons, however, this recapitulates almost all of the symptoms observed when Mecp2 function is lost globally (Chao et al., 2010). These results indicate that perhaps Mecp2 plays a particularly important function in GABAergic neurons. Indeed, this is further evidenced by the finding that GABAergic interneurons express approximately two times as much Mecp2 as other neuronal populations (Chao et al., 2010). Of particular interest to our findings in

Chapter III and **Chapter IV**, deficits in the induction of LTP at the SC-CA1 synapse are observed when Mecp2 is removed selectively from forebrain GABAergic interneurons (Chao et al., 2010). This indicates that the LTP deficit is GABAergic in origin, which is precisely in-line with our findings that activation of $mGlu_7$ expressed on interneurons in this area is critical for the induction of LTP, **Chapter III** (Klar et al., 2015).

We have found strong evidence that positive allosteric modulators of $mGlu_7$ could be efficacious treatments for the cognitive impairments observed in Rett syndrome, **Chapter IV**. While it is appreciated that there most likely will not be one pharmacological agent that improves all of the symptoms associated with this disease, because $mGlu_7$ is widely expressed in other important brain structures and its expression is directly regulated by Mecp2, it is possible that PAMs of $mGlu_7$ may also improve other symptom clusters as well. Indeed, we have also observed significant reductions in protein expression of $mGlu_7$ in the cortex, striatum, and cerebellum of Mecp2 KO animals and it will be important to determine if these reductions are responsible for some of the symptoms associated with those brain regions as well, **Chapter IV**. One important question to answer will be to determine if $mGlu_7$ plays a role in the induction of LTP in the motor cortex. Focus on this brain region is important for several reasons, including the fact that deficits in the induction of LTP have been observed in this region, Rett syndrome mouse models display severe motor impairments, and we observed significant decreases in $mGlu_7$ expression in our human tissue samples from this brain region (Moretti et al., 2006). Taken together, these data provide a strong rationale to investigate not only the role of $mGlu_7$ in normal induction of LTP in this region but also whether

$mGlu_7$ PAMs can improve motor abnormalities and synaptic plasticity deficits in Rett syndrome as well.

In summary, we have identified a critical role for $mGlu_7$ in the induction of LTP at the SC-CA1 synapse in the hippocampus and have identified *GRM7* as the first metabotropic glutamate receptor directly regulated by MeCP2, **Chapters III and IV** (Klar et al., 2015). Additionally, we have determined that potentiation of $mGlu_7$ both *ex vivo* and *in vivo* is sufficient to rescue LTP deficits and improve learning and memory behavior in Mecp2 KO animals. Taken together, our results provide a novel, important, role for $mGlu_7$ in the control of a process critical to learning and memory. These findings are exciting because they provide insight for the first time into the function of $mGlu_7$ in a native system, which has for many years remained elusive due to a lack of subtype-selective compounds without complex pharmacology. Now, with the identification of ADX71743, a selective $mGlu_7$ NAM that as both *in vitro* and *in vivo* efficacy, we now have the ability to selectively probe $mGlu_7$ function in different brain regions that also express other members of the group III mGlu receptor family. It will be important to determine if the role of $mGlu_7$ in mediating frequency-induced changes in synaptic strength extends beyond the hippocampus into other brain regions and other forms of learning and plasticity. Because of its ability to respond to changes in the level of glutamate at the synapse, $mGlu_7$ may indeed be a sensor of alterations in synaptic firing that makes the difference between potentiation and depression of future responses at a given synapse. Additionally, due to its unique expression on both glutamatergic and GABAergic terminals and its ability to negatively regulate the release of both neurotransmitters, $mGlu_7$ is perfectly poised to regulate the balance between the main

excitatory and inhibitory neurons in the brain and affect one of the most important neurological functions, cognition.

REFERENCES

Abe T, Sugihara H, Nawa H, Shigemoto R, Mizuno N, Nakanishi S (1992) Molecular characterization of a novel metabotropic glutamate receptor mGluR5 coupled to inositol phosphate/Ca2+ signal transduction. J Biol Chem 267:13361-13368.

Acsady L, Kamondi A, Sik A, Freund T, Buzsaki G (1998) GABAergic cells are the major postsynaptic targets of mossy fibers in the rat hippocampus. J Neurosci 18:3386-3403.

Aiba A, Chen C, Herrup K, Rosenmund C, Stevens CF, Tonegawa S (1994) Reduced hippocampal long-term potentiation and context-specific deficit in associative learning in mGluR1 mutant mice. Cell 79:365-375.

Altinbilek B, Manahan-Vaughan D (2007) Antagonism of group III metabotropic glutamate receptors results in impairment of LTD but not LTP in the hippocampal CA1 region, and prevents long-term spatial memory. Eur J Neurosci 26:1166-1172.

Amir RE, Van den Veyver IB, Wan M, Tran CQ, Francke U, Zoghbi HY (1999) Rett syndrome is caused by mutations in X-linked MECP2, encoding methyl-CpG-binding protein 2. Nat Genet 23:185-188.

Andersen P (2007) The hippocampus book. Oxford ; New York: Oxford University Press.

Armstrong DD (2001) Rett syndrome neuropathology review 2000. Brain Dev 23 Suppl 1:S72-76.

Asaka Y, Jugloff DG, Zhang L, Eubanks JH, Fitzsimonds RM (2006) Hippocampal synaptic plasticity is impaired in the Mecp2-null mouse model of Rett syndrome. Neurobiol Dis 21:217-227.

Ayala JE, Niswender CM, Luo Q, Banko JL, Conn PJ (2008) Group III mGluR regulation of synaptic transmission at the SC-CA1 synapse is developmentally regulated. Neuropharmacology 54:804-814.

Ayala JE, Chen Y, Banko JL, Sheffler DJ, Williams R, Telk AN, Watson NL, Xiang Z, Zhang Y, Jones PJ, Lindsley CW, Olive MF, Conn PJ (2009) mGluR5 positive allosteric modulators facilitate both hippocampal LTP and LTD and enhance spatial learning. Neuropsychopharmacology 34:2057-2071.

Baker SA, Chen L, Wilkins AD, Yu P, Lichtarge O, Zoghbi HY (2013) An AT-hook domain in MeCP2 determines the clinical course of Rett syndrome and related disorders. Cell 152:984-996.

Balschun D, Manahan-Vaughan D, Wagner T, Behnisch T, Reymann KG, Wetzel W (1999) A specific role for group I mGluRs in hippocampal LTP and hippocampus-dependent spatial learning. Learn Mem 6:138-152.

Barnes CA (1995) Involvement of LTP in memory: are we "searching under the street light"? Neuron 15:751-754.

Bartos M, Vida I, Frotscher M, Meyer A, Monyer H, Geiger JR, Jonas P (2002) Fast synaptic inhibition promotes synchronized gamma oscillations in hippocampal interneuron networks. Proc Natl Acad Sci U S A 99:13222-13227.

Baskys A, Malenka RC (1991) Agonists at metabotropic glutamate receptors presynaptically inhibit EPSCs in neonatal rat hippocampus. J Physiol 444:687-701.

Baude A, Bleasdale C, Dalezios Y, Somogyi P, Klausberger T (2007) Immunoreactivity for the GABAA receptor alpha1 subunit, somatostatin and Connexin36 distinguishes axoaxonic, basket, and bistratified interneurons of the rat hippocampus. Cereb Cortex 17:2094-2107.

Bedogni F, Cobolli Gigli C, Pozzi D, Rossi RL, Scaramuzza L, Rossetti G, Pagani M, Kilstrup-Nielsen C, Matteoli M, Landsberger N (2015) Defects During Mecp2 Null Embryonic Cortex Development Precede the Onset of Overt Neurological Symptoms. Cereb Cortex.

Ben-Shachar S, Chahrour M, Thaller C, Shaw CA, Zoghbi HY (2009) Mouse models of MeCP2 disorders share gene expression changes in the cerebellum and hypothalamus. Hum Mol Genet 18:2431-2442.

Bessis AS, Rondard P, Gaven F, Brabet I, Triballeau N, Prezeau L, Acher F, Pin JP (2002) Closure of the Venus flytrap module of mGlu8 receptor and the activation process: Insights from mutations converting antagonists into agonists. Proc Natl Acad Sci U S A 99:11097-11102.

Bianchi R, Young SR, Wong RK (1999) Group I mGluR activation causes voltage-dependent and -independent Ca2+ rises in hippocampal pyramidal cells. J Neurophysiol 81:2903-2913.

Bienvenu T, Chelly J (2006) Molecular genetics of Rett syndrome: when DNA methylation goes unrecognized. Nat Rev Genet 7:415-426.

Bliss TV, Lomo T (1973) Long-lasting potentiation of synaptic transmission in the dentate area of the anaesthetized rabbit following stimulation of the perforant path. J Physiol 232:331-356.

Bradley SR, Levey AI, Hersch SM, Conn PJ (1996) Immunocytochemical localization of group III metabotropic glutamate receptors in the hippocampus with subtype-specific antibodies. J Neurosci 16:2044-2056.

Bradley SR, Rees HD, Yi H, Levey AI, Conn PJ (1998) Distribution and developmental regulation of metabotropic glutamate receptor 7a in rat brain. J Neurochem 71:636-645.

Breakwell NA, Rowan MJ, Anwyl R (1998) (+)-MCPG blocks induction of LTP in CA1 of rat hippocampus via agonist action at an mGluR group II receptor. J Neurophysiol 79:1270-1276.

Bubser M et al. (2014) Selective activation of M4 muscarinic acetylcholine receptors reverses MK-801-induced behavioral impairments and enhances associative learning in rodents. ACS Chem Neurosci 5:920-942.

Bushell TJ, Sansig G, Collett VJ, van der Putten H, Collingridge GL (2002) Altered short-term synaptic plasticity in mice lacking the metabotropic glutamate receptor mGlu7. ScientificWorldJournal 2:730-737.

Cajal Ry (1894) The Croonian Lecture: The Minute Structure of the Nervous Centres. Br Med J 1:543.

Calfa G, Hablitz JJ, Pozzo-Miller L (2011) Network hyperexcitability in hippocampal slices from Mecp2 mutant mice revealed by voltage-sensitive dye imaging. J Neurophysiol 105:1768-1784.

Calfa G, Li W, Rutherford JM, Pozzo-Miller L (2015) Excitation/inhibition imbalance and impaired synaptic inhibition in hippocampal area CA3 of Mecp2 knockout mice. Hippocampus 25:159-168.

Callaerts-Vegh Z, Beckers T, Ball SM, Baeyens F, Callaerts PF, Cryan JF, Molnar E, D'Hooge R (2006) Concomitant deficits in working memory and fear extinction are functionally dissociated from reduced anxiety in metabotropic glutamate receptor 7-deficient mice. J Neurosci 26:6573-6582.

Chahrour M, Zoghbi HY (2007) The story of Rett syndrome: from clinic to neurobiology. Neuron 56:422-437.

Chahrour M, Jung SY, Shaw C, Zhou X, Wong ST, Qin J, Zoghbi HY (2008) MeCP2, a key contributor to neurological disease, activates and represses transcription. Science 320:1224-1229.

Chao HT, Chen H, Samaco RC, Xue M, Chahrour M, Yoo J, Neul JL, Gong S, Lu HC, Heintz N, Ekker M, Rubenstein JL, Noebels JL, Rosenmund C, Zoghbi HY (2010) Dysfunction in GABA signalling mediates autism-like stereotypies and Rett syndrome phenotypes. Nature 468:263-269.

Chen C, Kim JJ, Thompson RF, Tonegawa S (1996) Hippocampal lesions impair contextual fear conditioning in two strains of mice. Behav Neurosci 110:1177-1180.

Chen L, Chen K, Lavery LA, Baker SA, Shaw CA, Li W, Zoghbi HY (2015) MeCP2 binds to non-CG methylated DNA as neurons mature, influencing transcription and the timing of onset for Rett syndrome. Proc Natl Acad Sci U S A 112:5509-5514.

Chen RZ, Akbarian S, Tudor M, Jaenisch R (2001) Deficiency of methyl-CpG binding protein-2 in CNS neurons results in a Rett-like phenotype in mice. Nat Genet 27:327-331.

Chen WG, Chang Q, Lin Y, Meissner A, West AE, Griffith EC, Jaenisch R, Greenberg ME (2003) Derepression of BDNF transcription involves calcium-dependent phosphorylation of MeCP2. Science 302:885-889.

Chevaleyre V, Castillo PE (2003) Heterosynaptic LTD of hippocampal GABAergic synapses: a novel role of endocannabinoids in regulating excitability. Neuron 38:461-472.

Chevaleyre V, Castillo PE (2004) Endocannabinoid-mediated metaplasticity in the hippocampus. Neuron 43:871-881.

Christodoulou J, Grimm A, Maher T, Bennetts B (2003) RettBASE: The IRSA MECP2 variation database-a new mutation database in evolution. Hum Mutat 21:466-472.

Cohen AS, Abraham WC (1996) Facilitation of long-term potentiation by prior activation of metabotropic glutamate receptors. J Neurophysiol 76:953-962.

Cohen SJ, Munchow AH, Rios LM, Zhang G, Asgeirsdottir HN, Stackman RW, Jr. (2013) The rodent hippocampus is essential for nonspatial object memory. Curr Biol 23:1685-1690.

Collingridge GL, Kehl SJ, McLennan H (1983) Excitatory amino acids in synaptic transmission in the Schaffer collateral-commissural pathway of the rat hippocampus. J Physiol 334:33-46.

Collingridge GL, Herron CE, Lester RA (1988) Frequency-dependent N-methyl-D-aspartate receptor-mediated synaptic transmission in rat hippocampus. J Physiol 399:301-312.

Collins AL, Levenson JM, Vilaythong AP, Richman R, Armstrong DL, Noebels JL, David Sweatt J, Zoghbi HY (2004) Mild overexpression of MeCP2 causes a progressive neurological disorder in mice. Hum Mol Genet 13:2679-2689.

Conn PJ, Lindsley CW, Meiler J, Niswender CM (2014) Opportunities and challenges in the discovery of allosteric modulators of GPCRs for treating CNS disorders. Nat Rev Drug Discov 13:692-708.

Conquet F, Bashir ZI, Davies CH, Daniel H, Ferraguti F, Bordi F, Franz-Bacon K, Reggiani A, Matarese V, Conde F, et al. (1994) Motor deficit and impairment of synaptic plasticity in mice lacking mGluR1. Nature 372:237-243.

Corti C, Restituito S, Rimland JM, Brabet I, Corsi M, Pin JP, Ferraguti F (1998) Cloning and characterization of alternative mRNA forms for the rat metabotropic glutamate receptors mGluR7 and mGluR8. Eur J Neurosci 10:3629-3641.

Cosgrove KE, Galvan EJ, Barrionuevo G, Meriney SD (2011) mGluRs modulate strength and timing of excitatory transmission in hippocampal area CA3. Mol Neurobiol 44:93-101.

Dalezios Y, Lujan R, Shigemoto R, Roberts JD, Somogyi P (2002) Enrichment of mGluR7a in the presynaptic active zones of GABAergic and non-GABAergic terminals on interneurons in the rat somatosensory cortex. Cereb Cortex 12:961-974.

Davis S, Butcher SP, Morris RG (1992) The NMDA receptor antagonist D-2-amino-5-phosphonopentanoate (D-AP5) impairs spatial learning and LTP in vivo at intracerebral concentrations comparable to those that block LTP in vitro. J Neurosci 12:21-34.

Deadwyler SA, Dunwiddie T, Lynch G (1987) A critical level of protein synthesis is required for long-term potentiation. Synapse 1:90-95.

Debray C, Diabira D, Gaiarsa JL, Ben-Ari Y, Gozlan H (1997) Contributions of AMPA and GABA(A) receptors to the induction of NMDAR-dependent LTP in CA1. Neurosci Lett 238:119-122.

Diana G, Domenici MR, Scotti de Carolis A, Loizzo A, Sagratella S (1995) Reduced hippocampal CA1 Ca(2+)-induced long-term potentiation is associated with age-dependent impairment of spatial learning. Brain Res 686:107-110.

Doherty JJ, Alagarsamy S, Bough KJ, Conn PJ, Dingledine R, Mott DD (2004) Metabotropic glutamate receptors modulate feedback inhibition in a developmentally regulated manner in rat dentate gyrus. J Physiol 561:395-401.

Dragich J, Houwink-Manville I, Schanen C (2000) Rett syndrome: a surprising result of mutation in MECP2. Hum Mol Genet 9:2365-2375.

Dudek SM, Bear MF (1992) Homosynaptic long-term depression in area CA1 of hippocampus and effects of N-methyl-D-aspartate receptor blockade. Proc Natl Acad Sci U S A 89:4363-4367.

Dunwiddie T, Lynch G (1978) Long-term potentiation and depression of synaptic responses in the rat hippocampus: localization and frequency dependency. J Physiol 276:353-367.

Ellison KA, Fill CP, Terwilliger J, DeGennaro LJ, Martin-Gallardo A, Anvret M, Percy AK, Ott J, Zoghbi H (1992) Examination of X chromosome markers in Rett syndrome: exclusion mapping with a novel variation on multilocus linkage analysis. Am J Hum Genet 50:278-287.

Felts AS, Rodriguez AL, Morrison RD, Venable DF, Manka JT, Bates BS, Blobaum AL, Byers FW, Daniels JS, Niswender CM, Jones CK, Conn PJ, Lindsley CW, Emmitte KA (2013) Discovery of VU0409106: A negative allosteric modulator of mGlu5 with activity in a mouse model of anxiety. Bioorg Med Chem Lett 23:5779-5785.

Ferraguti F, Shigemoto R (2006) Metabotropic glutamate receptors. Cell Tissue Res 326:483-504.

Ferraguti F, Conquet F, Corti C, Grandes P, Kuhn R, Knopfel T (1998) Immunohistochemical localization of the mGluR1beta metabotropic glutamate receptor in the adult rodent forebrain: evidence for a differential distribution of mGluR1 splice variants. J Comp Neurol 400:391-407.

Fitzjohn SM, Kingston AE, Lodge D, Collingridge GL (1999) DHPG-induced LTD in area CA1 of juvenile rat hippocampus; characterisation and sensitivity to novel mGlu receptor antagonists. Neuropharmacology 38:1577-1583.

Fitzjohn SM, Palmer MJ, May JE, Neeson A, Morris SA, Collingridge GL (2001) A characterisation of long-term depression induced by metabotropic glutamate receptor activation in the rat hippocampus in vitro. J Physiol 537:421-430.

Flor PJ, Van Der Putten H, Ruegg D, Lukic S, Leonhardt T, Bence M, Sansig G, Knopfel T, Kuhn R (1997) A novel splice variant of a metabotropic glutamate receptor, human mGluR7b. Neuropharmacology 36:153-159.

Francesconi W, Cammalleri M, Sanna PP (2004) The metabotropic glutamate receptor 5 is necessary for late-phase long-term potentiation in the hippocampal CA1 region. Brain Res 1022:12-18.

Frey U, Krug M, Reymann KG, Matthies H (1988) Anisomycin, an inhibitor of protein synthesis, blocks late phases of LTP phenomena in the hippocampal CA1 region in vitro. Brain Res 452:57-65.

Fyffe SL, Neul JL, Samaco RC, Chao HT, Ben-Shachar S, Moretti P, McGill BE, Goulding EH, Sullivan E, Tecott LH, Zoghbi HY (2008) Deletion of Mecp2 in Sim1-expressing neurons reveals a critical role for MeCP2 in feeding behavior, aggression, and the response to stress. Neuron 59:947-958.

Ganda C, Schwab SG, Amir N, Heriani H, Irmansyah I, Kusumawardhani A, Nasrun M, Widyawati I, Maier W, Wildenauer DB (2009) A family-based association study of DNA sequence variants in GRM7 with schizophrenia in an Indonesian population. Int J Neuropsychopharmacol 12:1283-1289.

Gee CE, Peterlik D, Neuhauser C, Bouhelal R, Kaupmann K, Laue G, Uschold-Schmidt N, Feuerbach D, Zimmermann K, Ofner S, Cryan JF, van der Putten H, Fendt M, Vranesic I, Glatthar R, Flor PJ (2014) Blocking metabotropic glutamate receptor subtype 7 (mGlu7) via the Venus flytrap domain (VFTD) inhibits amygdala plasticity, stress, and anxiety-related behavior. J Biol Chem 289:10975-10987.

Gemelli T, Berton O, Nelson ED, Perrotti LI, Jaenisch R, Monteggia LM (2006) Postnatal loss of methyl-CpG binding protein 2 in the forebrain is sufficient to mediate behavioral aspects of Rett syndrome in mice. Biol Psychiatry 59:468-476.

Gereau RWt, Conn PJ (1994) Potentiation of cAMP responses by metabotropic glutamate receptors depresses excitatory synaptic transmission by a kinase-independent mechanism. Neuron 12:1121-1129.

Gereau RWt, Conn PJ (1995a) Roles of specific metabotropic glutamate receptor subtypes in regulation of hippocampal CA1 pyramidal cell excitability. J Neurophysiol 74:122-129.

Gereau RWt, Conn PJ (1995b) Multiple presynaptic metabotropic glutamate receptors modulate excitatory and inhibitory synaptic transmission in hippocampal area CA1. J Neurosci 15:6879-6889.

Gereau RWt, Winder DG, Conn PJ (1995) Pharmacological differentiation of the effects of co-activation of beta-adrenergic and metabotropic glutamate receptors in rat hippocampus. Neurosci Lett 186:119-122.

Goddyn H, Callaerts-Vegh Z, Stroobants S, Dirikx T, Vansteenwegen D, Hermans D, van der Putten H, D'Hooge R (2008) Deficits in acquisition and extinction of conditioned responses in mGluR7 knockout mice. Neurobiol Learn Mem 90:103-111.

Goffin D, Allen M, Zhang L, Amorim M, Wang IT, Reyes AR, Mercado-Berton A, Ong C, Cohen S, Hu L, Blendy JA, Carlson GC, Siegel SJ, Greenberg ME, Zhou Z (2012) Rett syndrome mutation MeCP2 T158A disrupts DNA binding, protein stability and ERP responses. Nat Neurosci 15:274-283.

Goudet C, Vilar B, Courtiol T, Deltheil T, Bessiron T, Brabet I, Oueslati N, Rigault D, Bertrand HO, McLean H, Daniel H, Amalric M, Acher F, Pin JP (2012) A novel selective metabotropic glutamate receptor 4 agonist reveals new possibilities for developing subtype selective ligands with therapeutic potential. FASEB J 26:1682-1693.

Granger AJ, Nicoll RA (2014) Expression mechanisms underlying long-term potentiation: a postsynaptic view, 10 years on. Philos Trans R Soc Lond B Biol Sci 369:20130136.

Guy J, Cheval H, Selfridge J, Bird A (2011) The role of MeCP2 in the brain. Annu Rev Cell Dev Biol 27:631-652.

Guy J, Hendrich B, Holmes M, Martin JE, Bird A (2001) A mouse Mecp2-null mutation causes neurological symptoms that mimic Rett syndrome. Nat Genet 27:322-326.

Guy J, Gan J, Selfridge J, Cobb S, Bird A (2007) Reversal of neurological defects in a mouse model of Rett syndrome. Science 315:1143-1147.

Hagberg B (1985) Rett's syndrome: prevalence and impact on progressive severe mental retardation in girls. Acta Paediatr Scand 74:405-408.

Hagberg B, Aicardi J, Dias K, Ramos O (1983) A progressive syndrome of autism, dementia, ataxia, and loss of purposeful hand use in girls: Rett's syndrome: report of 35 cases. Ann Neurol 14:471-479.

Hagberg G, Stenbom Y, Engerstrom IW (2001) Head growth in Rett syndrome. Brain Dev 23 Suppl 1:S227-229.

Holscher C, Schmid S, Pilz PK, Sansig G, van der Putten H, Plappert CF (2004) Lack of the metabotropic glutamate receptor subtype 7 selectively impairs short-term working memory but not long-term memory. Behav Brain Res 154:473-481.

Holscher C, Schmid S, Pilz PK, Sansig G, van der Putten H, Plappert CF (2005) Lack of the metabotropic glutamate receptor subtype 7 selectively modulates Theta rhythm and working memory. Learn Mem 12:450-455.

Hampson DR, Huang XP, Pekhletski R, Peltekova V, Hornby G, Thomsen C, Thogersen H (1999) Probing the ligand-binding domain of the mGluR4 subtype of metabotropic glutamate receptor. J Biol Chem 274:33488-33495.

Han G, Hampson DR (1999) Ligand binding to the amino-terminal domain of the mGluR4 subtype of metabotropic glutamate receptor. J Biol Chem 274:10008-10013.

Harris KM, Teyler TJ (1984) Developmental onset of long-term potentiation in area CA1 of the rat hippocampus. J Physiol 346:27-48.

Henze DA, Urban NN, Barrionuevo G (2000) The multifarious hippocampal mossy fiber pathway: a review. Neuroscience 98:407-427.

Hermans E, Challiss RA (2001) Structural, signalling and regulatory properties of the group I metabotropic glutamate receptors: prototypic family C G-protein-coupled receptors. Biochem J 359:465-484.

Hikichi H, Murai T, Okuda S, Maehara S, Satow A, Ise S, Nishino M, Suzuki G, Takehana H, Hata M, Ohta H (2010) Effects of a novel metabotropic glutamate receptor 7 negative allosteric modulator, 6-(4-methoxyphenyl)-5-methyl-3-pyridin-4-ylisoxazonolo[4,5-c]pyridin-4(5H)-one (MMPIP), on the central nervous system in rodents. Eur J Pharmacol 639:106-114.

Holscher C, Schmid S, Pilz PK, Sansig G, van der Putten H, Plappert CF (2004) Lack of the metabotropic glutamate receptor subtype 7 selectively impairs short-term working memory but not long-term memory. Behav Brain Res 154:473-481.

Holscher C, Schmid S, Pilz PK, Sansig G, van der Putten H, Plappert CF (2005) Lack of the metabotropic glutamate receptor subtype 7 selectively modulates Theta rhythm and working memory. Learn Mem 12:450-455.

Horike S, Cai S, Miyano M, Cheng JF, Kohwi-Shigematsu T (2005) Loss of silent-chromatin looping and impaired imprinting of DLX5 in Rett syndrome. Nat Genet 37:31-40.

Hou L, Klann E (2004) Activation of the phosphoinositide 3-kinase-Akt-mammalian target of rapamycin signaling pathway is required for metabotropic glutamate receptor-dependent long-term depression. J Neurosci 24:6352-6361.

Huber KM, Kayser MS, Bear MF (2000) Role for rapid dendritic protein synthesis in hippocampal mGluR-dependent long-term depression. Science 288:1254-1257.

Huber KM, Roder JC, Bear MF (2001) Chemical induction of mGluR5- and protein synthesis--dependent long-term depression in hippocampal area CA1. J Neurophysiol 86:321-325.

Huber KM, Gallagher SM, Warren ST, Bear MF (2002) Altered synaptic plasticity in a mouse model of fragile X mental retardation. Proc Natl Acad Sci U S A 99:7746-7750.

Iacovelli L, Bruno V, Salvatore L, Melchiorri D, Gradini R, Caricasole A, Barletta E, De Blasi A, Nicoletti F (2002) Native group-III metabotropic glutamate receptors are coupled to the mitogen-activated protein kinase/phosphatidylinositol-3-kinase pathways. J Neurochem 82:216-223.

Jalan-Sakrikar N et al. (2014) Identification of positive allosteric modulators VU0155094 (ML397) and VU0422288 (ML396) reveals new insights into the biology of metabotropic glutamate receptor 7. ACS Chem Neurosci 5:1221-1237.

Jensen AA, Fahlke C, Bjorn-Yoshimoto WE, Bunch L (2015) Excitatory amino acid transporters: recent insights into molecular mechanisms, novel modes of modulation and new therapeutic possibilities. Curr Opin Pharmacol 20:116-123.

Jentarra GM, Olfers SL, Rice SG, Srivastava N, Homanics GE, Blue M, Naidu S, Narayanan V (2010) Abnormalities of cell packing density and dendritic complexity in the MeCP2 A140V mouse model of Rett syndrome/X-linked mental retardation. BMC Neurosci 11:19.

Jia Z, Lu Y, Henderson J, Taverna F, Romano C, Abramow-Newerly W, Wojtowicz JM, Roder J (1998) Selective abolition of the NMDA component of long-term potentiation in mice lacking mGluR5. Learn Mem 5:331-343.

Jingami H, Nakanishi S, Morikawa K (2003) Structure of the metabotropic glutamate receptor. Curr Opin Neurobiol 13:271-278.

Johnson KA, Niswender CM, Conn PJ, Xiang Z (2011) Activation of group II metabotropic glutamate receptors induces long-term depression of excitatory synaptic transmission in the substantia nigra pars reticulata. Neurosci Lett 504:102-106.

Jones PL, Veenstra GJ, Wade PA, Vermaak D, Kass SU, Landsberger N, Strouboulis J, Wolffe AP (1998) Methylated DNA and MeCP2 recruit histone deacetylase to repress transcription. Nat Genet 19:187-191.

Kalinichev M, Rouillier M, Girard F, Royer-Urios I, Bournique B, Finn T, Charvin D, Campo B, Le Poul E, Mutel V, Poli S, Neale SA, Salt TE, Lutjens R (2013) ADX71743, a potent and selective negative allosteric modulator of metabotropic glutamate receptor 7: in vitro and in vivo characterization. J Pharmacol Exp Ther 344:624-636.

Kandel ER, Schwartz JH, Jessell TM (1991) Principles of Neural Science.

Katona I, Sperlagh B, Sik A, Kafalvi A, Vizi ES, Mackie K, Freund TF (1999) Presynaptically located CB1 cannabinoid receptors regulate GABA release from axon terminals of specific hippocampal interneurons. J Neurosci 19:4544-4558.

Katz DM (2014) Brain-derived neurotrophic factor and Rett syndrome. Handb Exp Pharmacol 220:481-495.

Kawaguchi Y, Katsumaru H, Kosaka T, Heizmann CW, Hama K (1987) Fast spiking cells in rat hippocampus (CA1 region) contain the calcium-binding protein parvalbumin. Brain Res 416:369-374.

Kemp N, Bashir ZI (1997) NMDA receptor-dependent and -independent long-term depression in the CA1 region of the adult rat hippocampus in vitro. Neuropharmacology 36:397-399.

Kemp N, Bashir ZI (1999) Induction of LTD in the adult hippocampus by the synaptic activation of AMPA/kainate and metabotropic glutamate receptors. Neuropharmacology 38:495-504.

Kemp N, McQueen J, Faulkes S, Bashir ZI (2000) Different forms of LTD in the CA1 region of the hippocampus: role of age and stimulus protocol. Eur J Neurosci 12:360-366.

Kim SJ, Kim YS, Yuan JP, Petralia RS, Worley PF, Linden DJ (2003) Activation of the TRPC1 cation channel by metabotropic glutamate receptor mGluR1. Nature 426:285-291.

Kinde B, Gabel HW, Gilbert CS, Griffith EC, Greenberg ME (2015) Reading the unique DNA methylation landscape of the brain: Non-CpG methylation, hydroxymethylation, and MeCP2. Proc Natl Acad Sci U S A.

Kingston AE, Ornstein PL, Wright RA, Johnson BG, Mayne NG, Burnett JP, Belagaje R, Wu S, Schoepp DD (1998) LY341495 is a nanomolar potent and selective antagonist of group II metabotropic glutamate receptors. Neuropharmacology 37:1-12.

Kinoshita A, Shigemoto R, Ohishi H, van der Putten H, Mizuno N (1998) Immunohistochemical localization of metabotropic glutamate receptors, mGluR7a and mGluR7b, in the central nervous system of the adult rat and mouse: a light and electron microscopic study. J Comp Neurol 393:332-352.

Klar R, Walker AG, Ghose D, Grueter BA, Engers DW, Hopkins CR, Lindsley CW, Xiang Z, Conn PJ, Niswender CM (2015) Activation of metabotropic glutamate receptor 7 is required for induction of long-term potentiation at SC-CA1 synapses in the hippocampus. The Journal of Neuroscience 35:7600-7615.

Klausberger T, Marton LF, O'Neill J, Huck JH, Dalezios Y, Fuentealba P, Suen WY, Papp E, Kaneko T, Watanabe M, Csicsvari J, Somogyi P (2005) Complementary roles of cholecystokinin- and parvalbumin-expressing GABAergic neurons in hippocampal network oscillations. J Neurosci 25:9782-9793.

Klose RJ, Sarraf SA, Schmiedeberg L, McDermott SM, Stancheva I, Bird AP (2005) DNA binding selectivity of MeCP2 due to a requirement for A/T sequences adjacent to methyl-CpG. Mol Cell 19:667-678.

Kosinski CM, Risso Bradley S, Conn PJ, Levey AI, Landwehrmeyer GB, Penney JB, Jr., Young AB, Standaert DG (1999) Localization of metabotropic glutamate receptor 7 mRNA and mGluR7a protein in the rat basal ganglia. J Comp Neurol 415:266-284.

Kristensen P, Suzdak PD, Thomsen C (1993) Expression pattern and pharmacology of the rat type IV metabotropic glutamate receptor. Neurosci Lett 155:159-162.

Kunishima N, Shimada Y, Tsuji Y, Sato T, Yamamoto M, Kumasaka T, Nakanishi S, Jingami H, Morikawa K (2000) Structural basis of glutamate recognition by a dimeric metabotropic glutamate receptor. Nature 407:971-977.

Laeremans A, Sabanov V, Ahmed T, Nys J, Van de Plas B, Vinken K, Woolley DG, Gantois I, D'Hooge R, Arckens L, Balschun D (2014) Distinct and simultaneously active plasticity mechanisms in mouse hippocampus during different phases of Morris water maze training. Brain Struct Funct.

Lan JY, Skeberdis VA, Jover T, Zheng X, Bennett MV, Zukin RS (2001) Activation of metabotropic glutamate receptor 1 accelerates NMDA receptor trafficking. J Neurosci 21:6058-6068.

Larson J, Lynch G (1986) Induction of synaptic potentiation in hippocampus by patterned stimulation involves two events. Science 232:985-988.

Larson J, Lynch G (1988) Role of N-methyl-D-aspartate receptors in the induction of synaptic potentiation by burst stimulation patterned after the hippocampal theta-rhythm. Brain Res 441:111-118.

Larson J, Wong D, Lynch G (1986) Patterned stimulation at the theta frequency is optimal for the induction of hippocampal long-term potentiation. Brain Res 368:347-350.

Lawson-Yuen A, Liu D, Han L, Jiang ZI, Tsai GE, Basu AC, Picker J, Feng J, Coyle JT (2007) Ube3a mRNA and protein expression are not decreased in Mecp2R168X mutant mice. Brain Res 1180:1-6.

Lee O, Lee CJ, Choi S (2002) Induction mechanisms for L-LTP at thalamic input synapses to the lateral amygdala: requirement of mGluR5 activation. Neuroreport 13:685-691.

Lei S, McBain CJ (2002) Distinct NMDA receptors provide differential modes of transmission at mossy fiber-interneuron synapses. Neuron 33:921-933.

Lei S, McBain CJ (2004) Two Loci of expression for long-term depression at hippocampal mossy fiber-interneuron synapses. J Neurosci 24:2112-2121.

Lewis JD, Meehan RR, Henzel WJ, Maurer-Fogy I, Jeppesen P, Klein F, Bird A (1992) Purification, sequence, and cellular localization of a novel chromosomal protein that binds to methylated DNA. Cell 69:905-914.

Liu Y, Zhang Y, Zhao D, Dong R, Yang X, Tammimies K, Uddin M, Scherer SW, Gai Z (2015) Rare de novo deletion of metabotropic glutamate receptor 7 (GRM7) gene in a patient with autism spectrum disorder. Am J Med Genet B Neuropsychiatr Genet.

Lodge D, Tidball P, Mercier MS, Lucas SJ, Hanna L, Ceolin L, Kritikos M, Fitzjohn SM, Sherwood JL, Bannister N, Volianskis A, Jane DE, Bortolotto ZA, Collingridge GL (2013) Antagonists reversibly reverse chemical LTD induced by group I, group II and group III metabotropic glutamate receptors. Neuropharmacology 74:135-146.

Losonczy A, Somogyi P, Nusser Z (2003) Reduction of excitatory postsynaptic responses by persistently active metabotropic glutamate receptors in the hippocampus. J Neurophysiol 89:1910-1919.

Lu YM, Jia Z, Janus C, Henderson JT, Gerlai R, Wojtowicz JM, Roder JC (1997) Mice lacking metabotropic glutamate receptor 5 show impaired learning and reduced CA1 long-term potentiation (LTP) but normal CA3 LTP. J Neurosci 17:5196-5205.

Luikenhuis S, Giacometti E, Beard CF, Jaenisch R (2004) Expression of MeCP2 in postmitotic neurons rescues Rett syndrome in mice. Proc Natl Acad Sci U S A 101:6033-6038.

Lujan R, Nusser Z, Roberts JD, Shigemoto R, Somogyi P (1996) Perisynaptic location of metabotropic glutamate receptors mGluR1 and mGluR5 on dendrites and dendritic spines in the rat hippocampus. Eur J Neurosci 8:1488-1500.

Ma LY, Wu C, Jin Y, Gao M, Li GH, Turner D, Shen JX, Zhang SJ, Narayanan V, Jentarra G, Wu J (2014) Electrophysiological phenotypes of MeCP2 A140V mutant mouse model. CNS Neurosci Ther 20:420-428.

Maccaferri G, Toth K, McBain CJ (1998) Target-specific expression of presynaptic mossy fiber plasticity. Science 279:1368-1370.

Malinow R, Miller JP (1986) Postsynaptic hyperpolarization during conditioning reversibly blocks induction of long-term potentiation. Nature 320:529-530.

Manahan-Vaughan D (1997) Group 1 and 2 metabotropic glutamate receptors play differential roles in hippocampal long-term depression and long-term potentiation in freely moving rats. J Neurosci 17:3303-3311.

Manahan-Vaughan D, Braunewell KH (2005) The metabotropic glutamate receptor, mGluR5, is a key determinant of good and bad spatial learning performance and hippocampal synaptic plasticity. Cereb Cortex 15:1703-1713.

Mannaioni G, Marino MJ, Valenti O, Traynelis SF, Conn PJ (2001) Metabotropic glutamate receptors 1 and 5 differentially regulate CA1 pyramidal cell function. J Neurosci 21:5925-5934.

Maren S, De Oca B, Fanselow MS (1994) Sex differences in hippocampal long-term potentiation (LTP) and Pavlovian fear conditioning in rats: positive correlation between LTP and contextual learning. Brain Res 661:25-34.

Martinowich K, Hattori D, Wu H, Fouse S, He F, Hu Y, Fan G, Sun YE (2003) DNA methylation-related chromatin remodeling in activity-dependent BDNF gene regulation. Science 302:890-893.

Masu M, Tanabe Y, Tsuchida K, Shigemoto R, Nakanishi S (1991) Sequence and expression of a metabotropic glutamate receptor. Nature 349:760-765.

McGraw CM, Samaco RC, Zoghbi HY (2011) Adult neural function requires MeCP2. Science 333:186.

McLeod F, Ganley R, Williams L, Selfridge J, Bird A, Cobb SR (2013) Reduced seizure threshold and altered network oscillatory properties in a mouse model of Rett syndrome. Neuroscience 231:195-205.

Miles R, Wong RK (1983) Single neurones can initiate synchronized population discharge in the hippocampus. Nature 306:371-373.

Mitri C, Parmentier ML, Pin JP, Bockaert J, Grau Y (2004) Divergent evolution in metabotropic glutamate receptors. A new receptor activated by an endogenous ligand different from glutamate in insects. J Biol Chem 279:9313-9320.

Mitsukawa K, Yamamoto R, Ofner S, Nozulak J, Pescott O, Lukic S, Stoehr N, Mombereau C, Kuhn R, McAllister KH, van der Putten H, Cryan JF, Flor PJ (2005) A selective metabotropic glutamate receptor 7 agonist: activation of receptor signaling via an allosteric site modulates stress parameters in vivo. Proc Natl Acad Sci U S A 102:18712-18717.

Moretti P, Levenson JM, Battaglia F, Atkinson R, Teague R, Antalffy B, Armstrong D, Arancio O, Sweatt JD, Zoghbi HY (2006) Learning and memory and synaptic

plasticity are impaired in a mouse model of Rett syndrome. J Neurosci 26:319-327.

Morris RG, Anderson E, Lynch GS, Baudry M (1986) Selective impairment of learning and blockade of long-term potentiation by an N-methyl-D-aspartate receptor antagonist, AP5. Nature 319:774-776.

Mumby DG (2001) Perspectives on object-recognition memory following hippocampal damage: lessons from studies in rats. Behav Brain Res 127:159-181.

Muto T, Tsuchiya D, Morikawa K, Jingami H (2007) Structures of the extracellular regions of the group II/III metabotropic glutamate receptors. Proc Natl Acad Sci U S A 104:3759-3764.

Na ES, Nelson ED, Kavalali ET, Monteggia LM (2013) The impact of MeCP2 loss- or gain-of-function on synaptic plasticity. Neuropsychopharmacology 38:212-219.

Naie K, Gundimi S, Siegmund H, Heinemann U, Manahan-Vaughan D (2006) Group III metabotropic glutamate receptor-mediated, chemically induced long-term depression differentially affects cell viability in the hippocampus. Eur J Pharmacol 535:104-113.

Nakajima Y, Iwakabe H, Akazawa C, Nawa H, Shigemoto R, Mizuno N, Nakanishi S (1993) Molecular characterization of a novel retinal metabotropic glutamate receptor mGluR6 with a high agonist selectivity for L-2-amino-4-phosphonobutyrate. J Biol Chem 268:11868-11873.

Nan X, Tate P, Li E, Bird A (1996) DNA methylation specifies chromosomal localization of MeCP2. Mol Cell Biol 16:414-421.

Nelson ED, Bal M, Kavalali ET, Monteggia LM (2011) Selective impact of MeCP2 and associated histone deacetylases on the dynamics of evoked excitatory neurotransmission. J Neurophysiol 106:193-201.

Neyman S, Manahan-Vaughan D (2008) Metabotropic glutamate receptor 1 (mGluR1) and 5 (mGluR5) regulate late phases of LTP and LTD in the hippocampal CA1 region in vitro. Eur J Neurosci 27:1345-1352.

Nickols HH, Conn PJ (2014) Development of allosteric modulators of GPCRs for treatment of CNS disorders. Neurobiol Dis 61:55-71.

Nicoll RA, Schmitz D (2005) Synaptic plasticity at hippocampal mossy fibre synapses. Nature reviews Neuroscience 6:863-876.

Niswender CM, Conn PJ (2010) Metabotropic glutamate receptors: physiology, pharmacology, and disease. Annu Rev Pharmacol Toxicol 50:295-322.

Niswender CM, Johnson KA, Miller NR, Ayala JE, Luo Q, Williams R, Saleh S, Orton D, Weaver CD, Conn PJ (2010) Context-dependent pharmacology exhibited by negative allosteric modulators of metabotropic glutamate receptor 7. Mol Pharmacol 77:459-468.

Noetzel MJ, Gregory KJ, Vinson PN, Manka JT, Stauffer SR, Lindsley CW, Niswender CM, Xiang Z, Conn PJ (2013) A novel metabotropic glutamate receptor 5 positive allosteric modulator acts at a unique site and confers stimulus bias to mGlu5 signaling. Mol Pharmacol 83:835-847.

O'Connor RM, Cryan JF (2013) The effects of mGlu(7) receptor modulation in behavioural models sensitive to antidepressant action in two mouse strains. Behav Pharmacol 24:105-113.

O'Hara PJ, Sheppard PO, Thogersen H, Venezia D, Haldeman BA, McGrane V, Houamed KM, Thomsen C, Gilbert TL, Mulvihill ER (1993) The ligand-binding domain in metabotropic glutamate receptors is related to bacterial periplasmic binding proteins. Neuron 11:41-52.

Ohishi H, Shigemoto R, Nakanishi S, Mizuno N (1993a) Distribution of the messenger RNA for a metabotropic glutamate receptor, mGluR2, in the central nervous system of the rat. Neuroscience 53:1009-1018.

Ohishi H, Shigemoto R, Nakanishi S, Mizuno N (1993b) Distribution of the mRNA for a metabotropic glutamate receptor (mGluR3) in the rat brain: an in situ hybridization study. J Comp Neurol 335:252-266.

Ohishi H, Akazawa C, Shigemoto R, Nakanishi S, Mizuno N (1995a) Distributions of the mRNAs for L-2-amino-4-phosphonobutyrate-sensitive metabotropic glutamate receptors, mGluR4 and mGluR7, in the rat brain. J Comp Neurol 360:555-570.

Ohishi H, Nomura S, Ding YQ, Shigemoto R, Wada E, Kinoshita A, Li JL, Neki A, Nakanishi S, Mizuno N (1995b) Presynaptic localization of a metabotropic glutamate receptor, mGluR7, in the primary afferent neurons: an immunohistochemical study in the rat. Neurosci Lett 202:85-88.

Ohno-Shosaku T, Tsubokawa H, Mizushima I, Yoneda N, Zimmer A, Kano M (2002) Presynaptic cannabinoid sensitivity is a major determinant of depolarization-induced retrograde suppression at hippocampal synapses. J Neurosci 22:3864-3872.

Ohshima T, Ward JM, Huh CG, Longenecker G, Veeranna, Pant HC, Brady RO, Martin LJ, Kulkarni AB (1996) Targeted disruption of the cyclin-dependent kinase 5 gene results in abnormal corticogenesis, neuronal pathology and perinatal death. Proc Natl Acad Sci U S A 93:11173-11178.

Okamoto N, Hori S, Akazawa C, Hayashi Y, Shigemoto R, Mizuno N, Nakanishi S (1994) Molecular characterization of a new metabotropic glutamate receptor mGluR7 coupled to inhibitory cyclic AMP signal transduction. J Biol Chem 269:1231-1236.

Oliet SH, Malenka RC, Nicoll RA (1997) Two distinct forms of long-term depression coexist in CA1 hippocampal pyramidal cells. Neuron 18:969-982.

Ota Y, Zanetti AT, Hallock RM (2013) The role of astrocytes in the regulation of synaptic plasticity and memory formation. Neural Plast 2013:185463.

Otani S, Daniel H, Takita M, Crepel F (2002) Long-term depression induced by postsynaptic group II metabotropic glutamate receptors linked to phospholipase C and intracellular calcium rises in rat prefrontal cortex. J Neurosci 22:3434-3444.

Page G, Khidir FA, Pain S, Barrier L, Fauconneau B, Guillard O, Piriou A, Hugon J (2006) Group I metabotropic glutamate receptors activate the p70S6 kinase via both mammalian target of rapamycin (mTOR) and extracellular signal-regulated kinase (ERK 1/2) signaling pathways in rat striatal and hippocampal synaptoneurosomes. Neurochem Int 49:413-421.

Palmer MJ, Irving AJ, Seabrook GR, Jane DE, Collingridge GL (1997) The group I mGlu receptor agonist DHPG induces a novel form of LTD in the CA1 region of the hippocampus. Neuropharmacology 36:1517-1532.

Palucha-Poniewiera A, Szewczyk B, Pilc A (2014) Activation of the mTOR signaling pathway in the antidepressant-like activity of the mGlu5 antagonist MTEP and the mGlu7 agonist AMN082 in the FST in rats. Neuropharmacology 82:59-68.

Palucha A, Klak K, Branski P, van der Putten H, Flor PJ, Pilc A (2007) Activation of the mGlu7 receptor elicits antidepressant-like effects in mice. Psychopharmacology (Berl) 194:555-562.

Pancani T, Bolarinwa C, Smith Y, Lindsley CW, Conn PJ, Xiang Z (2014) M4 mAChR-mediated modulation of glutamatergic transmission at corticostriatal synapses. ACS Chem Neurosci 5:318-324.

Pelka GJ, Watson CM, Radziewic T, Hayward M, Lahooti H, Christodoulou J, Tam PP (2006) Mecp2 deficiency is associated with learning and cognitive deficits and altered gene activity in the hippocampal region of mice. Brain 129:887-898.

Pelkey KA, Lavezzari G, Racca C, Roche KW, McBain CJ (2005) mGluR7 is a metaplastic switch controlling bidirectional plasticity of feedforward inhibition. Neuron 46:89-102.

Pelkey KA, Topolnik L, Lacaille JC, McBain CJ (2006) Compartmentalized Ca(2+) channel regulation at divergent mossy-fiber release sites underlies target cell-dependent plasticity. Neuron 52:497-510.

Pelkey KA, Yuan X, Lavezzari G, Roche KW, McBain CJ (2007) mGluR7 undergoes rapid internalization in response to activation by the allosteric agonist AMN082. Neuropharmacology 52:108-117.

Pelkey KA, McBain CJ (2008) Target-cell-dependent plasticity within the mossy fibre-CA3 circuit reveals compartmentalized regulation of presynaptic function at divergent release sites. J Physiol 586:1495-1502.

Pelkey KA, Topolnik L, Yuan XQ, Lacaille JC, McBain CJ (2008) State-dependent cAMP sensitivity of presynaptic function underlies metaplasticity in a hippocampal feedforward inhibitory circuit. Neuron 60:980-987.

Pergadia ML et al. (2011) A 3p26-3p25 genetic linkage finding for DSM-IV major depression in heavy smoking families. Am J Psychiatry 168:848-852.

Phillips RG, LeDoux JE (1992) Differential contribution of amygdala and hippocampus to cued and contextual fear conditioning. Behav Neurosci 106:274-285.

Pin JP, Galvez T, Prezeau L (2003) Evolution, structure, and activation mechanism of family 3/C G-protein-coupled receptors. Pharmacol Ther 98:325-354.

Poschel B, Stanton PK (2007) Comparison of cellular mechanisms of long-term depression of synaptic strength at perforant path-granule cell and Schaffer collateral-CA1 synapses. Prog Brain Res 163:473-500.

Pozzo-Miller L, Pati S, Percy AK (2015) Rett Syndrome: Reaching for Clinical Trials. Neurotherapeutics.

Ramocki MB, Tavyev YJ, Peters SU (2010) The MECP2 duplication syndrome. Am J Med Genet A 152A:1079-1088.

Raymond CR, Thompson VL, Tate WP, Abraham WC (2000) Metabotropic glutamate receptors trigger homosynaptic protein synthesis to prolong long-term potentiation. J Neurosci 20:969-976.

Rosemond E, Wang M, Yao Y, Storjohann L, Stormann T, Johnson EC, Hampson DR (2004) Molecular basis for the differential agonist affinities of group III metabotropic glutamate receptors. Mol Pharmacol 66:834-842.

Rush LJ, Raval A, Funchain P, Johnson AJ, Smith L, Lucas DM, Bembea M, Liu TH, Heerema NA, Rassenti L, Liyanarachchi S, Davuluri R, Byrd JC, Plass C (2004)

Epigenetic profiling in chronic lymphocytic leukemia reveals novel methylation targets. Cancer Res 64:2424-2433.

Samaco RC, Mandel-Brehm C, Chao HT, Ward CS, Fyffe-Maricich SL, Ren J, Hyland K, Thaller C, Maricich SM, Humphreys P, Greer JJ, Percy A, Glaze DG, Zoghbi HY, Neul JL (2009) Loss of MeCP2 in aminergic neurons causes cell-autonomous defects in neurotransmitter synthesis and specific behavioral abnormalities. Proc Natl Acad Sci U S A 106:21966-21971.

Santschi LA, Zhang XL, Stanton PK (2006) Activation of receptors negatively coupled to adenylate cyclase is required for induction of long-term synaptic depression at Schaffer collateral-CA1 synapses. J Neurobiol 66:205-219.

Saugstad JA, Kinzie JM, Mulvihill ER, Segerson TP, Westbrook GL (1994) Cloning and expression of a new member of the L-2-amino-4-phosphonobutyric acid-sensitive class of metabotropic glutamate receptors. Mol Pharmacol 45:367-372.

Saugstad JA, Kinzie JM, Shinohara MM, Segerson TP, Westbrook GL (1997) Cloning and expression of rat metabotropic glutamate receptor 8 reveals a distinct pharmacological profile. Mol Pharmacol 51:119-125.

Schaevitz LR, Gomez NB, Zhen DP, Berger-Sweeney JE (2013) MeCP2 R168X male and female mutant mice exhibit Rett-like behavioral deficits. Genes Brain Behav 12:732-740.

Schanen C, Francke U (1998) A severely affected male born into a Rett syndrome kindred supports X-linked inheritance and allows extension of the exclusion map. Am J Hum Genet 63:267-269.

Schanen NC, Dahle EJ, Capozzoli F, Holm VA, Zoghbi HY, Francke U (1997) A new Rett syndrome family consistent with X-linked inheritance expands the X chromosome exclusion map. Am J Hum Genet 61:634-641.

Schoepp DD, Jane DE, Monn JA (1999) Pharmacological agents acting at subtypes of metabotropic glutamate receptors. Neuropharmacology 38:1431-1476.

Schoepp DD, Goldsworthy J, Johnson BG, Salhoff CR, Baker SR (1994) 3,5-dihydroxyphenylglycine is a highly selective agonist for phosphoinositide-linked metabotropic glutamate receptors in the rat hippocampus. J Neurochem 63:769-772.

Schoepp DD, Salhoff CR, Wright RA, Johnson BG, Burnett JP, Mayne NG, Belagaje R, Wu S, Monn JA (1996) The novel metabotropic glutamate receptor agonist 2R,4R-APDC potentiates stimulation of phosphoinositide hydrolysis in the rat hippocampus by 3,5-dihydroxyphenylglycine: evidence for a synergistic

interaction between group 1 and group 2 receptors. Neuropharmacology 35:1661-1672.

Schultz C, Engelhardt M (2014) Anatomy of the hippocampal formation. Front Neurol Neurosci 34:6-17.

Schwartzkroin PA, Wester K (1975) Long-lasting facilitation of a synaptic potential following tetanization in the in vitro hippocampal slice. Brain Res 89:107-119.

Selvam C, Oueslati N, Lemasson IA, Brabet I, Rigault D, Courtiol T, Cesarini S, Triballeau N, Bertrand HO, Goudet C, Pin JP, Acher FC (2010) A virtual screening hit reveals new possibilities for developing group III metabotropic glutamate receptor agonists. J Med Chem 53:2797-2813.

Shahbazian MD, Young JI, Yuva-Paylor LA, Spencer CM, Antalffy B, Noebels JL, Armstrong D, Paylor R, Zoghbi H (2002) Mice with truncated Mecp2 recapitulate many rett syndrome features and display hyperacetylation of histone h3. Neuron 35:243-254.

Shalin SC, Hernandez CM, Dougherty MK, Morrison DK, Sweatt JD (2006) Kinase suppressor of Ras1 compartmentalizes hippocampal signal transduction and subserves synaptic plasticity and memory formation. Neuron 50:765-779.

Shigemoto R, Kulik A, Roberts JD, Ohishi H, Nusser Z, Kaneko T, Somogyi P (1996) Target-cell-specific concentration of a metabotropic glutamate receptor in the presynaptic active zone. Nature 381:523-525.

Shigemoto R, Kinoshita A, Wada E, Nomura S, Ohishi H, Takada M, Flor PJ, Neki A, Abe T, Nakanishi S, Mizuno N (1997) Differential presynaptic localization of metabotropic glutamate receptor subtypes in the rat hippocampus. J Neurosci 17:7503-7522.

Skeberdis VA, Lan J, Opitz T, Zheng X, Bennett MV, Zukin RS (2001) mGluR1-mediated potentiation of NMDA receptors involves a rise in intracellular calcium and activation of protein kinase C. Neuropharmacology 40:856-865.

Skene PJ, Illingworth RS, Webb S, Kerr AR, James KD, Turner DJ, Andrews R, Bird AP (2010) Neuronal MeCP2 is expressed at near histone-octamer levels and globally alters the chromatin state. Mol Cell 37:457-468.

Sladeczek F, Pin JP, Recasens M, Bockaert J, Weiss S (1985) Glutamate stimulates inositol phosphate formation in striatal neurones. Nature 317:717-719.

Snyder EM, Philpot BD, Huber KM, Dong X, Fallon JR, Bear MF (2001) Internalization of ionotropic glutamate receptors in response to mGluR activation. Nat Neurosci 4:1079-1085.

Somogyi P, Dalezios Y, Lujan R, Roberts JD, Watanabe M, Shigemoto R (2003) High level of mGluR7 in the presynaptic active zones of select populations of GABAergic terminals innervating interneurons in the rat hippocampus. Eur J Neurosci 17:2503-2520.

Stanton PK, Sarvey JM (1984) Blockade of long-term potentiation in rat hippocampal CA1 region by inhibitors of protein synthesis. J Neurosci 4:3080-3088.

Stearns NA, Schaevitz LR, Bowling H, Nag N, Berger UV, Berger-Sweeney J (2007) Behavioral and anatomical abnormalities in Mecp2 mutant mice: a model for Rett syndrome. Neuroscience 146:907-921.

Sugiyama H, Ito I, Hirono C (1987) A new type of glutamate receptor linked to inositol phospholipid metabolism. Nature 325:531-533.

Sukoff Rizzo SJ et al. (2011) The metabotropic glutamate receptor 7 allosteric modulator AMN082: a monoaminergic agent in disguise? J Pharmacol Exp Ther 338:345-352.

Summa M, Di Prisco S, Grilli M, Usai C, Marchi M, Pittaluga A (2013) Presynaptic mGlu7 receptors control GABA release in mouse hippocampus. Neuropharmacology 66:215-224.

Suzuki G, Tsukamoto N, Fushiki H, Kawagishi A, Nakamura M, Kurihara H, Mitsuya M, Ohkubo M, Ohta H (2007) In vitro pharmacological characterization of novel isoxazolopyridone derivatives as allosteric metabotropic glutamate receptor 7 antagonists. J Pharmacol Exp Ther 323:147-156.

Tanabe Y, Masu M, Ishii T, Shigemoto R, Nakanishi S (1992) A family of metabotropic glutamate receptors. Neuron 8:169-179.

Tanabe Y, Nomura A, Masu M, Shigemoto R, Mizuno N, Nakanishi S (1993) Signal transduction, pharmacological properties, and expression patterns of two rat metabotropic glutamate receptors, mGluR3 and mGluR4. J Neurosci 13:1372-1378.

Toms NJ, Jane DE, Tse HW, Roberts PJ (1995) Characterization of metabotropic glutamate receptor-stimulated phosphoinositide hydrolysis in rat cultured cerebellar granule cells. Br J Pharmacol 116:2824-2827.

Trappe R, Laccone F, Cobilanschi J, Meins M, Huppke P, Hanefeld F, Engel W (2001) MECP2 mutations in sporadic cases of Rett syndrome are almost exclusively of paternal origin. Am J Hum Genet 68:1093-1101.

Traynelis SF, Wollmuth LP, McBain CJ, Menniti FS, Vance KM, Ogden KK, Hansen KB, Yuan H, Myers SJ, Dingledine R (2010) Glutamate receptor ion channels: structure, regulation, and function. Pharmacol Rev 62:405-496.

Traynor J, Agarwal P, Lazzeroni L, Francke U (2002) Gene expression patterns vary in clonal cell cultures from Rett syndrome females with eight different MECP2 mutations. BMC Med Genet 3:12.

Tsou K, Mackie K, Sanudo-Pena MC, Walker JM (1999) Cannabinoid CB1 receptors are localized primarily on cholecystokinin-containing GABAergic interneurons in the rat hippocampal formation. Neuroscience 93:969-975.

Tsuchiya D, Kunishima N, Kamiya N, Jingami H, Morikawa K (2002) Structural views of the ligand-binding cores of a metabotropic glutamate receptor complexed with an antagonist and both glutamate and Gd3+. Proc Natl Acad Sci U S A 99:2660-2665.

Tudor M, Akbarian S, Chen RZ, Jaenisch R (2002) Transcriptional profiling of a mouse model for Rett syndrome reveals subtle transcriptional changes in the brain. Proc Natl Acad Sci U S A 99:15536-15541.

Uyama Y, Ishida M, Shinozaki H (1997) DCG-IV, a potent metabotropic glutamate receptor agonist, as an NMDA receptor agonist in the rat cortical slice. Brain Res 752:327-330.

Varma N, Carlson GC, Ledent C, Alger BE (2001) Metabotropic glutamate receptors drive the endocannabinoid system in hippocampus. J Neurosci 21:RC188.

Vyklicky V, Korinek M, Smejkalova T, Balik A, Krausova B, Kaniakova M, Lichnerova K, Cerny J, Krusek J, Dittert I, Horak M, Vyklicky L (2014) Structure, function, and pharmacology of NMDA receptor channels. Physiol Res 63 Suppl 1:S191-203.

Walker AG, Wenthur CJ, Xiang Z, Rook JM, Emmitte KA, Niswender CM, Lindsley CW, Conn PJ (2015) Metabotropic glutamate receptor 3 activation is required for long-term depression in medial prefrontal cortex and fear extinction. Proc Natl Acad Sci U S A.

Wan M, Lee SS, Zhang X, Houwink-Manville I, Song HR, Amir RE, Budden S, Naidu S, Pereira JL, Lo IF, Zoghbi HY, Schanen NC, Francke U (1999) Rett syndrome and beyond: recurrent spontaneous and familial MECP2 mutations at CpG hotspots. Am J Hum Genet 65:1520-1529.

Wegener E, Brendel C, Fischer A, Hulsmann S, Gartner J, Huppke P (2014) Characterization of the MeCP2R168X knockin mouse model for Rett syndrome. PLoS One 9:e115444.

Weng SM, Bailey ME, Cobb SR (2011a) Rett syndrome: from bed to bench. Pediatr Neonatol 52:309-316.

Weng SM, McLeod F, Bailey ME, Cobb SR (2011b) Synaptic plasticity deficits in an experimental model of rett syndrome: long-term potentiation saturation and its pharmacological reversal. Neuroscience 180:314-321.

Wenthur CJ, Morrison R, Felts AS, Smith KA, Engers JL, Byers FW, Daniels JS, Emmitte KA, Conn PJ, Lindsley CW (2013) Discovery of (R)-(2-fluoro-4-((-4-methoxyphenyl)ethynyl)phenyl) (3-hydroxypiperidin-1-yl)methanone (ML337), an mGlu3 selective and CNS penetrant negative allosteric modulator (NAM). J Med Chem 56:5208-5212.

Whitlock JR, Heynen AJ, Shuler MG, Bear MF (2006) Learning induces long-term potentiation in the hippocampus. Science 313:1093-1097.

Wilsch VW, Pidoplichko VI, Opitz T, Shinozaki H, Reymann KG (1994) Metabotropic glutamate receptor agonist DCG-IV as NMDA receptor agonist in immature rat hippocampal neurons. Eur J Pharmacol 262:287-291.

Winder DG, Conn PJ (1996) Roles of metabotropic glutamate receptors in glial function and glial-neuronal communication. J Neurosci Res 46:131-137.

Winder DG, Ritch PS, Gereau RWt, Conn PJ (1996) Novel glial-neuronal signalling by coactivation of metabotropic glutamate and beta-adrenergic receptors in rat hippocampus. J Physiol 494 (Pt 3):743-755.

Witter MP (2007) The perforant path: projections from the entorhinal cortex to the dentate gyrus. Prog Brain Res 163:43-61.

Xu J, Antion MD, Nomura T, Kraniotis S, Zhu Y, Contractor A (2014) Hippocampal metaplasticity is required for the formation of temporal associative memories. J Neurosci 34:16762-16773.

Yamasaki T, Kumata K, Yui J, Fujinaga M, Furutsuka K, Hatori A, Xie L, Ogawa M, Nengaki N, Kawamura K, Zhang MR (2013) Synthesis and evaluation of [11C]MMPIP as a potential radioligand for imaging of metabotropic glutamate 7 receptor in the brain. EJNMMI Res 3:54.

Yang Y, Pan C (2013) Role of metabotropic glutamate receptor 7 in autism spectrum disorders: a pilot study. Life Sci 92:149-153.

Yin S, Niswender CM (2014) Progress toward advanced understanding of metabotropic glutamate receptors: structure, signaling and therapeutic indications. Cell Signal 26:2284-2297.

Young JI, Zoghbi HY (2004) X-chromosome inactivation patterns are unbalanced and affect the phenotypic outcome in a mouse model of rett syndrome. Am J Hum Genet 74:511-520.

Younts TJ, Chevaleyre V, Castillo PE (2013) CA1 pyramidal cell theta-burst firing triggers endocannabinoid-mediated long-term depression at both somatic and dendritic inhibitory synapses. J Neurosci 33:13743-13757.

Zhang L, He J, Jugloff DG, Eubanks JH (2008) The MeCP2-null mouse hippocampus displays altered basal inhibitory rhythms and is prone to hyperexcitability. Hippocampus 18:294-309.

Zoghbi H (1988) Genetic aspects of Rett syndrome. J Child Neurol 3 Suppl:S76-78.

Zoghbi HY, Percy AK, Schultz RJ, Fill C (1990) Patterns of X chromosome inactivation in the Rett syndrome. Brain Dev 12:131-135.